SENESCENCE REWIRES THE MICROENVIRONMENT SENSING PROGRAM TO FACILITATE IMMUNE SURVEILLANCE

by

Hsuan-An Chen

A Dissertation

Presented to the Faculty of the Louis V. Gerstner, Jr.

Graduate School of Biomedical Sciences,

Memorial Sloan-Kettering Cancer Center

in Partial Fulfillment of the Requirements for the Degree of

Doctor of Philosophy

New York, NY

May, 2022

_____ _____

Scott W. Lowe PhD
Dissertation mentor

Date

ABSTRACT

Cellular senescence is a stress-response program characterized by a stable cell cycle arrest and a distinctive secretory program referred to as the SASP (senescence-associated secretory phenotype). As such, cells undergoing senescence not only exhibit cell-intrinsic phenotypic changes but also remodel their tissue environment to orchestrate a diverse range of physiological and pathological processes. In the context of cancer, senescence exerts a potent tumor suppressive effect by promoting cell intrinsic growth arrest as well as cell extrinsic immune-mediated clearance of damaged, pre-malignant or cancer cells, a phenomenon termed senescence immune surveillance. When this process is impaired, senescent cells can accumulate within tissues and, paradoxically, promote cancer and other age-related diseases. However, the specific mechanisms underlying the effective immune targeting of senescent cells, and how this process is altered during cancer development, are not fully understood.

Here we aim to investigate how senescent tumor cells interact with their microenvironment. To identify mechanisms that promote and mediate anti-tumor immunity, we developed a genetic immunocompetent model of liver cancer that enables inducible and reversible suppression of the tumor suppressor gene p53 to specifically reinstate the senescence program in advanced cancer cells. We find that senescence induction in advanced liver cancers altered the immune landscape leading to potent tumor regressions via activation of adaptive and innate immunity. Through transcriptomic, proteomic and functional analyses, we uncover that, in addition to the SASP, senescent cells undergo a substantial rewiring of

their surfaceome that reprograms extracellular sensing and signaling pathways, one of which linked to IFNγ responses. We demonstrate an increased sensitivity to IFNγ is a general feature of senescent cells, and that this enhanced response to extracellular IFNγ cooperates with cell-intrinsic transcriptional changes to promote endogenous antigen presentation capacity and optimal immune surveillance.

Altogether, our results uncover an underappreciated facet of senescence involving the remodeling of surfaceome that underlies a differential tissue sensing capacity, exemplified by an augmented IFNγ response, that is necessary for their immune-mediated clearance. Thus, while senescent cells are potent remodelers of their environment via the SASP, they are in turn also shaped by microenvironmental signals.

ACKNOWLEDGEMENTS

I would like to thank Dr. Scott Lowe for giving me this opportunity to let me develop ideas and perform experiments independently for my thesis, while also giving critical scientific advice on the directions of the project and also full support and freedom to let me explore the different perspectives of this project and others. Being in a “non-immunology” lab, it is not an easy task to set up all the experimental details to navigate the immune aspects of the project, but Scott is always very open-minded letting me set up the collaboration and seeking for advice from the immune experts. I would say it is this type of training that have equipped me to be prepared for my next stage of career as a postdoc. I would like to especially thank to Dr. Direna Alonso-Curbelo, who is a supportive and caring postdoc that co-developed the ideas co-mentored me with Scott and carried out the experiments in this project. There are ups and downs during the time we worked together but in the end, I am very grateful having Direna as my “daily mentor” to walk through all these details in this project. I’ll always remember those late nights we are sitting together to discuss and brainstorm the exciting science (while I am also a bit sorry for Javi that I took quite some of her time that you can spend together!) I would also like to thank Dr. Yu-Jui Ho for his crucial contribution in those bioinformatic analysis. Without him, all the beautiful charts and graphs won’t be completed! I would like to thank Dr. Ronald Hendrickson and GSK student Ryan Smolkin for providing critical technical support performing the key experiments for this project in proteomic analysis and flow cytometry respectively. I would like to thank Drs. Riccardo Mezzadra and Changyu Zhu in our lab for their tremendous help in

setting up the in vitro co-culture system and also sharing knowledge in T cells and macrophages field. I would like to thank my collaborators in Cold Spring Harbor Laboratory, Dr. Mikala Egeblad and also Jose Adrover, for setting up all the tissue clearing technology experiment and providing valuable input for interpreting the data. I would like to give a special thanks to Wei Luan and Alexandra Wuest, and also other lab technicians, who had performed necessary help to make all the experiments possible. In addition, I would also like to thank to Drs. Kaloyan Tsanov, Francisco Sanchez-Rivera and Zeda Zhang for setting up the shRNA library screen pipeline and performing the experiments together. Lastly, I would like to thank my committee members Drs. Joseph Sun and Charles Sawyers for giving me invaluable insight on the directions of the project and also support for my future career.

Besides those who have directly contributed to the projects, I would like to thank to Direna, Riccardo above mentioned but also Drs. Bryan Ngo and Varun Narendra for reviewing my thesis and giving me constructive comments on contents and writing style. Last but not least, I would like to thank all the Lowe lab members, both postdocs and students, for cultivating such a vibrant and friendly environment for discussing exciting science and ideas and making the lab just feel like a second home. Without all your support, my PhD life would not be as colorful and fun!

Contributions of the study

Study supervision: co-mentored by Scott W. Lowe and Direna Alonso-Curbelo

Conception and design: Hsuan-An Chen, Direna Alonso-Curbelo and Scott W. Lowe

Development of methodology: Hsuan-An Chen and Direna Alonso-Curbelo for the majority of the experiment. Jose Adrover for tissue clearing technology. Riccardo Mezzadra and Changyu Zhu for in vitro co-culture system setup. Ryan Smolkin for technical support of immunophenotyping protocol.

Acquisition of data: Hsuan-An Chen, Direna Alonso-Curbelo, Jose Adrover, Wei Luan and Alexandra Wuest

Analysis and interpretation of data: Hsuan-An Chen, Direna Alonso-Curbelo, Yu-Jui Ho, Jose Adrover, Mikala Egeblad, Riccardo Mezzadra and Changyu Zhu

TABLE OF CONTENTS

LIST OF FIGURES

LIST OF ABBREVIATIONS

DNA damage response	DDR
Therapy-induced senescence	TIS
Oncogene-induced senescence	OIS
Senescence-associated β-galactosidase	SA-β-gal
Reactive oxygen species	ROS
Senescence-associated secretory phenotype	SASP
Senescence-associated heterochromatin foci	SAHF
Histone deacetylase inhibitor	HDACi
Cytosolic chromatin fragments	CCF
Cyclic GMP-AMP synthase	cGAS
Stimulator of interferon genes	STING
Extracellular matrix	ECM
Nuclear factor-κB	NF-κB
CCAAT/enhancer-binding protein-β	C/EBPβ
Bromodomain-containing protein 4	BRD4
Polycomb repressor complex 2	PRC2
IFN regulatory factor 3	IRF3
Interferons	IFN
Chimeric antigen receptor T cells	CAR-T
Nonalcoholic steatohepatitis	NASH
Plasma membrane	PM

INTRODUCTION

First characterized by Leonard Hayflick and Paul Moorhead 60 years ago, senescence remains a poorly understood cellular phenomenon characterized by (1) a robust irreversible cell cycle arrest and (2) distinct molecular, metabolic and epigenetic alterations (1). Despite its elusive features, senescence has since broad relevance in multiple physiological and pathological contexts including cancer, aging and tissue homeostasis and repair.

Cellular senescence is triggered by different stress-inducing stimuli. In cultured primary fibroblasts senescence was found to result from telomere shortening, also known as replicative exhaustion (2). Significant shortening of telomeres after several rounds of cell replication leads to one-ended double strand breaks that trigger a DNA damage response (DDR) and subsequent cell cycle arrest (2,3). In addition to telomere attrition, other cellular stress stimuli have been identified to trigger senescence, such as non-telomeric DNA damage and aberrant oncogene expression (4,5). For instance, chemotherapy or ionizing radiation, both of which cause extensive DNA damage, induce senescence and is known therapy-induced senescence (TIS) (6). On the other hand, oncogenic mutations, which cause accumulating DNA damage in normal cells as they undergo abnormal DNA replication through multiple firing at the replication fork and creating replication stress, can also lead to premature senescence, a process termed “oncogene-induced senescence (OIS)” (4,7,8).

The DDR activates downstream signaling kinases including ATM, ATR, CHK1 and CHK2 as checkpoints to inhibit cells from re-entering cell cycle before

DNA damages are resolved. If the DDR signaling pathway is inhibited, cells won't exit cell cycle to establish senescence (4,7,8). At the bottom of signaling cascade, it converges to activate tumor suppress gene p53, the target of ATM and ATR, to drive the expression of cyclin-dependent kinase inhibitor p21 for cell cycle arrest. Another critical player for enforcing senescence is p16, an inhibitor of CDK4 and CDK6, which activates downstream tumor suppressor, Rb, to stop cell cycle progression. Taken together, a persistent DDR signaling, downstream of replicative or oncogenic stress, is considered a major driver of senescence (9).

The Hallmarks of Senescence

Biomarkers of senescence

Senescent cells acquire several unique characteristics that distinguish them from normal cells. Here we describe several hallmark features of senescent cells (Fig. 1).

Morphologically, senescent cells are flattened and much bigger than proliferating or quiescent cells, and often acquire irregular shapes (1). Previously it has been deemed that the cell volume change results from the establishment of senescence; however, recent reports suggest that an increase of cytoplasm volume could also play a causative role in inducing senescence-associated growth arrest (10). Senescent cells also accumulate lysosomes in their cytoplasm, which have high β-galactosidase activity that catalyze the hydrolysis of β-galactosides into monosaccharides resulting in blue staining. This trait is also known as senescence-associated β-galactosidase (SA-β-gal), one of the most widely used senescence marker (11). This marker is generally not found in quiescent or

transformed cells, although it may still present in serum-starved or overconfluent cells in tissue culture (12). Senescent cells also have enlarged yet dysfunctional mitochondria, which may be linked to the alteration of cellular metabolism and the increase in reactive oxygen species (ROS) that accompanies the establishment of the senescent state (13).

Transcriptionally, senescent cells display widely altered gene expression programs. Consistent with the cell cycle arrest, they often strongly upregulate cyclin-dependent kinase inhibitors such as p21 and p16 (14,15). As the expression of p21 and p16 are essential for the establishment and maintenance of senescence-associated growth arrest in otherwise normal cells, they are often used as markers to identify senescent cells in vitro and in vivo. Another obvious feature of senescence is the lack of DNA replication, shown by the loss of proliferation marker, Ki-67 and decreased incorporation of nucleoside analogous, such as BrdU. However, this alone cannot distinguish the senescent cells from quiescent or postmitotic cells.

Beyond these molecular traits linked to the cell cycle arrest, senescent cells exhibit an active expression of a variety of secreted factors, also known as senescence-associated secretory phenotype (SASP) (16). While SASP has been well described in the senescence field, it is more as a general concept that senescent cells could generate a pro-inflammatory milieu rather than a definitive marker due to the heterogeneity of the SASP factors and also the fact that some of those factors could be secreted by non-senescent cells. Of note, SASP is not universally present as p16 overexpression-induced senescence does not

necessarily have altered SASP transcriptional program (17). Regardless, the SASP is known to exert a broad spectrum of biological effects on both senescent cells themselves and neighboring cells (discussed below).

Functionally, senescent cells are resistant to apoptosis-mediated cell death. This is mediated through the upregulation of anti-apoptotic Bcl-2 family proteins (18). Intriguingly, both senescence and apoptosis program are linked to the activation of p53 pathway. What determines stressed cells to undergo a certain route over the other is still unclear; but it is likely a context-dependent outcome dictated by the intensity and type of the stimuli as well as the cell type (19). Although senescent cells are generally more resistant to apoptosis, there are still several ways to eliminate senescent cells, including exploiting our immune system to kill senescent cells in Fas ligand- or perforin/granzyme-dependent manner and the development of “senolytics” by antagonizing the anti-apoptotic pathways in senescent cells (20,21).

Mechanistically, the establishment of senescence is also often accompanied with chromatin changes, that have also been used as markers of this state. For example, senescence-associated heterochromatin foci (SAHF) are spatially organized heterochromatic domains that can be detected as dense DAPI-positive structures in the nucleus (22,23). However, SAHF is not a universal senescent marker but more restricted to the senescence program induced by aberrant oncogene activation. Functionally, SAHF formation compact the chromatin to restrain extensive DDR signaling (23). Treatment of oncogene-induced senescent cells with histone deacetylase inhibitors (HDACi) causes

heterochromatin relaxation and increases DDR, resulting in apoptosis and thus acting as a class of senolytic drug (24).

Another chromatin-related feature of senescence is the appearance of cytosolic chromatin fragments (CCF). It has been observed that senescent cells have disrupted nuclear envelope and breakdown of nuclear lamina due to the loss of Lamin B1 through autophagic degradation, causing the release of cytosolic CCF in the cytoplasm (25,26). Importantly, CCF activates cyclic GMP-AMP synthase (cGAS) and the adaptor stimulator of interferon genes (STING) pathway and further the downstream type I interferon responses, which can activate innate immunity (27-29).

Despite these distinct features, however, in the senescence field, there is still not a single, universal marker that can be simply applied to define senescence. Often, it requires a combination of several markers to discriminate the senescent cells from their proliferative, quiescent or differentiated counterparts. This may be due to the heterogenous phenotype of senescence affected by the triggers, cell types and the surrounding environment (30). It is also noteworthy that most of the senescence markers are best characterized in vitro. Whether senescent cells in vivo presenting the same or different markers is under intense investigation.

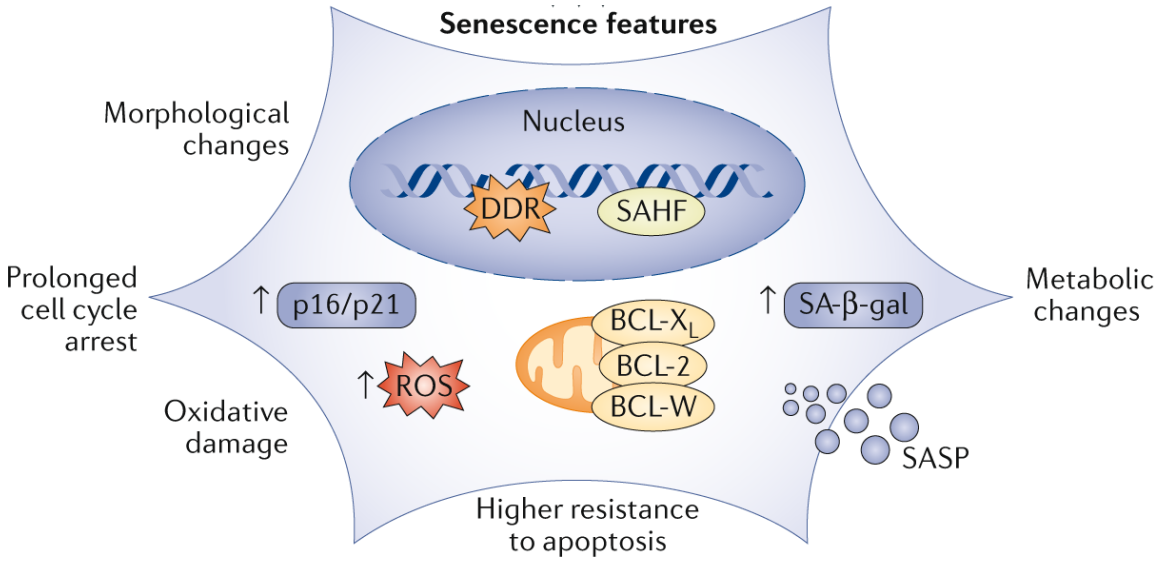

Figure 1. Hallmarks of cellular senescence Senescent cells exhibit several distinct features, including morphological, transcriptional, epigenetic and metabolic changes, that distinguish them from the proliferating or quiescent counterparts. However, so far there is not a universal specific marker but rather it requires multiple ones to define senescent cells. Of note, while most of the senescent markers are well characterized in vitro, it remains to unclear if the same criteria can be applied to identify senescent cells in vivo or whether they may present different markers.

Reprinted by permission from Springer Nature Customer Service Centre GmbH: Springer Nature, Nature Reviews Molecular Cell Biology, Cellular senescence in ageing: from mechanisms totherapeutic opportunities, Raffaella Di Micco et al, 2020

Non-Cell-autonomous effects of senescence: the SASP

Although senescent cells are non-proliferative, they are not biologically neutral, as their secretory nature affects the behavior of neighboring cells. For example, it has been demonstrated that IGFBP7 act as a critical secretory factor to reinforce the growth arrest phenotype via an autocrine/paracrine manner in oncogenic BRAF-induced senescence in melanocytes (31). Moreover, SASP not only acts locally but also extend its effect to potentially to the whole organism (32).

The SASP factors comprise a broad range of proinflammatory cytokines and chemokines, extracellular matrix (ECM) degrading enzymes, and growth factors (16). IL-6 and IL-8 and CCL2 are perhaps the most commonly identified factors in SASP but dozens if not hundreds of other less-characterized bioactive factors may be present in SASP as well (33). Notably, the full development of the SASP is not an immediate process and the spectrum of SASP factors is also highly context dependent (34,35). The mechanistic underpinnings of the dynamic feature and diversity of SASP is an active area of investigation in the field, yet it is thought to be dictated by a combination of different factors including cell types, senescent stimuli, as well as the temporal factor (34).

Several studies have identified various master regulators controlling SASP mainly at the transcriptional level. For example, transcription factors Nuclear factor-κB (NF-κB) and CCAAT/enhancer-binding protein-β (C/EBPβ) bind to the promoter of SASP genes and regulate their activation (36,37).

Chromatin changes during senescence has also been linked to the development of SASP. The epigenetic reader bromodomain-containing protein 4

(BRD4), which recognizes and accumulates at the H3K27 acetylated histone mark defining the super-enhancer region, cooperates with multiple transcription factors to promote gene transcription. Newly formed super-enhancer regions have been observed closely adjacent to SASP genes in senescent cells and, as such, the inhibition of BRD4 abrogates the expression of SASP genes in a OIS model (38). On the other hand, polycomb repressor complex 2 (PRC2), which methylates the same H3K27 histone residue for transcriptional repression, competes with BRD4 to suppress the SASP. Indeed, EZH2, a core component of PRC2 complex, is repressed in senescent cells and the overexpression of EZH2 prevents entry of OIS and also abrogates the development of SASP (39).

Activation of DDR signaling is not only required for the induction and maintenance of senescence but also the SASP (40). However, it is still not well understood how DDR is specifically linked to the secretory phenotype. The cytosolic DNA sensing pathway, cGAS-STING, is a critical mediator linking cytosolic DNA fragments such as CCF and DNA pieces to the SASP (27,29,41). The activation of these pathway drives the production of inflammatory cytokines and type I interferons (IFN). Deletion of cGAS-STING pathway components reduces the proinflammatory SASP and limits the activation of senescence surveillance by the immune system. Additionally, recent findings have demonstrated that at the late stage of senescence (deep senescence), the retrotransposon elements are derepressed and transcribed into cytosolic cDNA, activating type-I IFN responses (42,43). Together, these findings suggest the

cGAS-STING sensor pathway is a critical regulator of SASP during senescence induction, as well for the cell-intrinsic activation of the type I IFN responses.

While the SASP is a critical mediator of senescent cell-microenvironment interactions, its role is still poorly characterized. Indeed, the non-cell-autonomous effect of SASP cannot be simply explained by a single factor but most likely through a combination of many acting together. Moreover, the bidirectional crosstalk between senescent cells and microenvironment may also create a feedback loop to increase the diversity and complex of SASP, highlighting the challenges to study the versatile facets of senescence in different contexts.

Biological outputs: Senescence as a double-edge sword

Beneficial effects of senescence

Senescence plays a pivotal and beneficial role in developmental patterning and tissue repair (44). During embryonic development, senescence acts as a normal programmed mechanism parallel to apoptosis to instruct morphogenesis and tissue remodeling (45,46). Another setting in which senescence plays a crucial physiological role is tissue repair, in which the SASP has been shown to facilitate fibrosis resolution and wound healing to maintain tissue homeostasis. Specifically, fibrosis has been associated with an aberrant accumulation of ECM within tissues that limits their normal function and leads to long-term tissue scaring. In an experimental model of liver fibrosis triggered by CCl4, senescence restrains the proliferation and expansion of ECM-producing activated hepatic stellate cells to curb the progression of the pathology following liver damage. The SASP of these senescent hepatic stellate cells also recruits macrophages and reprograms them

into an M1 phenotype leading to immune-mediated clearance of those ECM-producing cells (47,48). In the context of cutaneous wound healing, damaged fibroblasts and endothelial cells undergo senescence and secrete SASP factors that promote myofibroblast differentiation to accelerate wound closure (49). The requirement of senescent cells in instructing these would healing processes has been further supported by a genetic mouse model (p16-3MR (49)), which showed that specific depletion of p16-positive (including senescent) cells through the administration of ganciclovir slowed down the wound healing process.

Given its growth arrest characteristic, senescence has been extensively studied in the context of cancer, where it has been shown to act as a potent barrier to tumorigenesis and cancer progression. For example, senescence induced by oncogenic signaling restrains the transformation of premalignant cells. Moreover, TIS promotes cell cycle arrest and immune-mediated elimination of cancer cells (6,8). In both contexts, the tumor suppressive role of senescence has been linked to both cell-intrinsic and cell-extrinsic mechanisms. As such, beyond the growth arrest phenotype, the SASP can reinforce the senescence state in an autocrine and also lead to senescence immune surveillance through paracrine effects in non-tumor cells of the tissue environment. Specifically, in the premalignant setting, the SASP can induce a senescence-like arrest in normal neighboring cells, such as fibroblasts or melanocytes, to reinforce growth arrest in the preneoplastic lesions (31,50). In the OIS model, aberrant activation of oncogenic RAS in hepatocytes triggers senescence which in turn drives recruitment of macrophages and CD4 T cells for their immune-mediated elimination, in a SASP-dependent manner (51).

Moreover, a pioneering study from our lab showed that triggering senescence in cancer cells through restoration of endogenous tumor suppressor gene, p53, leads to the recruitment and activation of innate immune cells that can then kill senescent tumor cells and drive potent tumor regressions, also in a SASP-dependent manner (52). This report provided proof of concept that inducing senescence in cancer cells can elicit potent anti-tumor immune responses.

Building upon these findings, several studies have shown that therapy-induced senescence could mimic the effects of restoring endogenous TSG in driving anti-tumor immunity through SASP-mediated mobilization and activation of NK and CD8 T cells into the tumor microenvironment, and remodeling the vasculature to increase the accessibility of drug and immune cells (53,54). Importantly, the abrogation of SASP in both premalignant or full-blown cancer cells triggered to senesce impairs recruitment of immune cells, resulting in an aberrant accumulation of senescent cells *in vivo* (38,53). As detailed below, such aberrant accumulation of senescent cells can promote tumor initiation and/or outgrowth, suggesting that a dynamic balance between the induction and elimination of senescent cells is key for promoting its beneficial effects in vivo (Fig. 2).

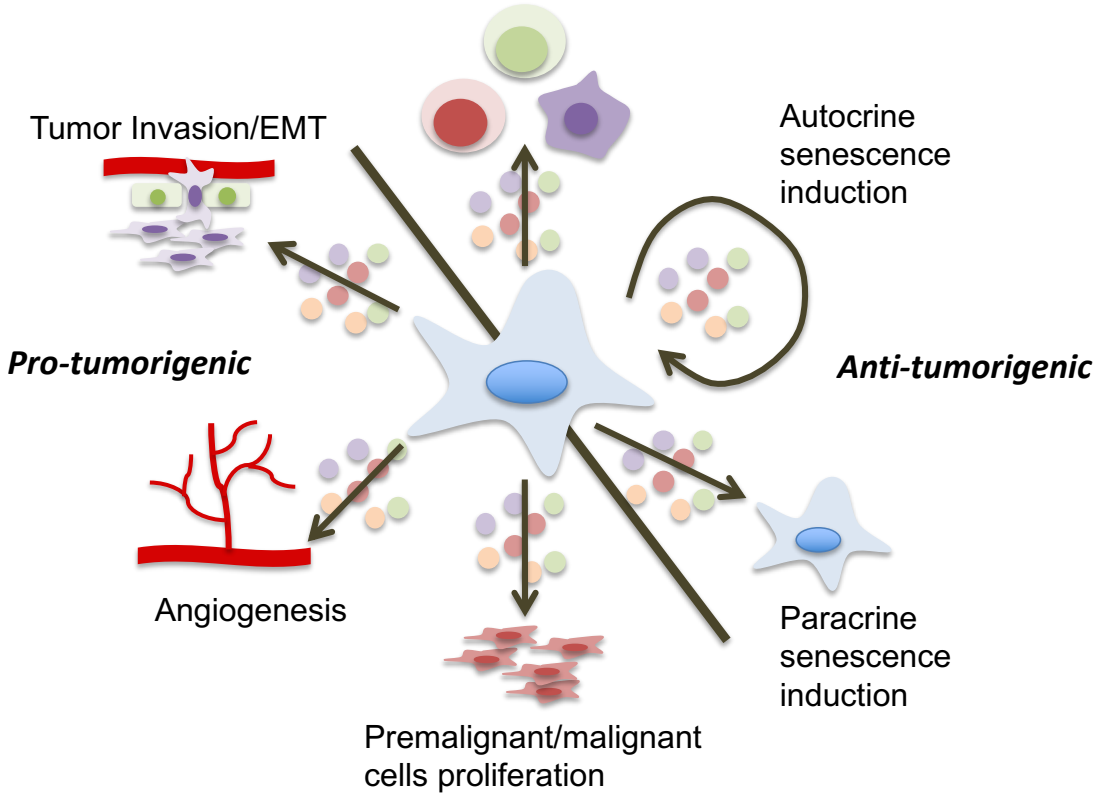

Figure 2. The pleiotropic effects of the SASP. SASP can exert both anti- and pro-tumorigenic roles depending on the context. It's most likely that senescence and the accompanying SASP exerts its beneficial effect to prevent tumorigenesis and cancer progression if it is resolved in a timely manner, whereas its chronic presence could elicit the undesirable adverse effects that disrupt the original barrier and promote cancer development.

Detrimental effects of senescence

Although senescence likely evolved as a protective mechanism for maintaining tissue homeostasis and preventing tumorigenesis, it can also have a dark side mainly conferred by the pleiotropic effect of the SASP when senescent cells accumulate within tissues. Multiple proinflammatory factors, including IL-6 and IL-1RA, are secreted from senescent cells and promote sterile chronic inflammation. These signals lead to several age-related diseases, including cardiovascular diseases, tissue dysfunction and paradoxically, cancer (55).

An example of a senescence-associated pathology are atherosclerotic plaques, which have been shown to accumulate SA-β-Gal- and p16-positive endothelial cells, vascular smooth muscle cells and macrophages, suggesting senescent cells play a critical role in their pathogenesis (56). In addition, senescent cells might affect tissue regeneration by exhausting stem cells or progenitors in a paracrine manner (57). While autocrine senescence may be beneficial for self-amplifying the senescent phenotype and limiting tumorigenesis, the same proinflammatory factors including IL-6, GROα and TGF-β, either are directly secreted by senescent cells and/or indirectly secreted from SASP-recruited immune cells in the microenvironment, could contribute to the spread of senescence in tissues through circulation and lead to tissue and organismal dysfunction. There is an accumulating evidence suggesting that senescent cells aberrantly accumulate in different tissues during ageing and also are responsible for age-associated pathologies (58). These phenotypes have been proposed to link to the high circulating levels of inflammatory molecules secreted by senescent

cells, also known as inflammaging (59). It is manifested at an organismal level including weight loss, muscle loss and weakness and chronic inflammation. By removing senescent cells through the genetic approach, it showed an improvement in the activity and health index in both prematurely and naturally aged mice and also extend lifespan (60,61). However, it still remains unclear whether it is the elimination of senescent cells or abrogating the accompanying SASP contributing to the effect.

In the context of cancer, SASP plays a dual role which can be either tumor-suppressive or tumor-promoting depending on the context (62,63). For example, it has been demonstrated in a liver model where senescent cells present along with the pre-malignant and malignant cells, the inflammatory cytokines and growth factors will enhance the tumor cell proliferation and lead to the cancer progression (64). SASP can also create an immune suppressive environment to promote tumorigenesis by recruiting immune suppressive immature myeloid cells that inhibit T cells function in the premalignant senescent prostate cancer lesions (65). Moreover, SASP is also linked to the adverse effect of chemotherapy and increased the risk of cancer relapse. As SASP also contains ECM-degrading enzymes, it is involved in ECM remodeling through factors such as matrix metalloproteinases, which can expose a variety of nutrients and mitogens to the cancer cells thereby increasing their proliferation (66). It has also been demonstrated that SASP promotes the invasiveness of tumor cells by facilitating the angiogenesis and also cell-intrinsic ability to metastasize (67).

Altogether, both senescence and the SASP has both positive and negative effects that appear to be highly context-dependent, influenced by a poorly understood interplay between the nature of the senescence inducer, the cell types undergoing this process, the timing and dynamics of senescence response, and the environment in which it takes place. It is mostly likely that in an acute manner, senescence and the accompanying SASP favors proper tissue development, tissue repair and recruitment of immune cells to preserve tissue homeostasis. Nevertheless, a persistent presence of senescent cells can lead to chronic inflammation and contribute to ageing-related pathologies including cancer (Fig. 2). This highlights the importance of understanding the mechanisms of senescence immunosurveillance in relevant models that can capture both its cell-intrinsic and cell-extrinsic effects, and also developing methods to favor the elimination of senescent cells in vivo.

Selective elimination of senescent cells for therapeutics

The accumulation of senescent cells in the tissue can promote chronic inflammation and lead to an increased risk of developing age-related diseases including tissue dysfunction and cancer. Therefore, in an effort to extend the healthspan and lifespan, the development of senolytic strategies to specifically eliminate senescent cells has received increasing attention. Genetic elimination of p16 positive cells, a marker of senescent cells, significantly increases the healthspan and lifespan of the mice in several mouse models (p16-3MR (49) and INK-ATTAC (60)). Conversely, an interesting study demonstrated that transplanting a small number of senescent adipocytes into young mice could have

a systemic effect on the organism that leads to deteriorating tissue function and also shorter lifespan (32). Consistent with this notion, chemotherapy-induced senescence in primary normal cells has been associated with an increased risk of blood clotting and cancer relapse (68,69). This phenotype is mitigated by the depletion of p16 positive senescent cells in the p16-3MR mice, suggesting senescence functionally contributes to these deleterious effects. Thus, a proliferating body of evidence supports the idea that aberrant accumulation of senescent cells can compromise the beneficial role of senescence and leave undesirable outcomes. To selectively eliminate senescent cells, there are currently two major strategies that have been currently explored: the development of pharmacological agents termed “senolytics” and harnessing the immune system, either in its natural form or in a synthetic one.

Senolytics

As many senescence triggers are also potent inducers of apoptosis, senescent cells have been shown to be primed to this form of cell death yet avoid it often by the upregulation of anti-apoptotic Bcl2 family proteins in mitochondria (18). Therefore, inhibition of those proteins (Bcl-2, Bcl-XL, Bcl-W) is a feasible approach to antagonize the pro-survival machinery of senescent cells. ABT-737 and ABT-263 (also known as navitoclax) are drugs inhibiting the activity of Bcl-2 family to selectively initiate apoptosis in senescent cells (18,21). Another commonly used senolytics is the combination of dasatinib (D), a pan-tyrosine kinase inhibitor, plus quercetin (Q), a natural flavonoid that affect PI3K pathway, to inhibit pro-survival signaling (70). This combination can reduce p16 positive cells

in vivo and extend survival in mice and is currently under clinical trial now (71); however, whether the effect is conferred by the specific elimination of senescent cells or including other non-senescent p16-positive remains obscure. Other class of drugs have been identified in phenotypic screens to eliminate senescent cells, including heat shock protein (Hsp90) inhibitors (72) and HDAC inhibitors (24). Interestingly, a recent concept termed “one-two punch approach” has been proposed to exploit senolytics in cancer therapy, with a first drug inducing senescence in cancer cells followed by second drug triggering selective elimination of those cells (73,74). This synthetic lethal approach may provide extra specificity of targeting malignant cells and spare normal cells during cancer treatments.

Senescence immunosurveillance

A different approach to selectively target senescent cells is using the natural role of immune system in recognizing and eliminating stressed, damaged cells. As an example, our lab has demonstrated that combinatorial treatment of KRAS-mutated lung cancer cells with CDK4/6 and MEK inhibitors trigger senescence and elicits a potent NK cell response to eliminate senescent tumor cells (53). The same combination therapy has also shown efficacy in treating pancreatic cancer where in this case, senescence induces vascular remodeling that favors infiltration of immune cells, especially CD8 T cells. Though the intratumoral T cells showed exhausted phenotype, the combination of CDK4/6 and MEK inhibition with blockade of immune checkpoints restores the cytotoxicity to kill the senescent cells and extend the survival in mice (54). One the other hand, a recent study shows that by engineering senescence-specific chimeric antigen receptor T cells (CAR-

T), it can be used as a cellular therapy to target senescent cells (75). The identification of relative specific senescent cell surface marker, uPAR, has enabled the development of CAR-T cells, which showed potent senolytic effect in two different senescent models, liver fibrosis and nonalcoholic steatohepatitis (NASH). This methodology has also opened a new route to eliminate senescent cells by developing agents such as bispecific antibodies or antibodies conjugated with toxic ligands that can recognize unique senescent cell surface markers.

Together, these approaches show several parallel paths to eliminate senescent cells in vitro and in vivo. However, considering the highly heterogeneous nature of senescence in vivo, there may not be a universal way to target all types of senescent cells. Instead, different contexts, such as aging, atherosclerosis and cancer, may require a specific strategy for alleviating the downside of senescence.

Liver cancer as a clinical challenge and model to study senescence

Liver cancer is not only a leading cause of cancer-related deaths globally but also one of a few cancer types with a rising trend of annual rates of death in the past two decades. Thus, there is a need to develop novel strategies to treat this deadly cancer (76). The initiation and progression of liver cancer is highly related to chronic inflammation and repetitive tissue damage/repair. Consistent with the tumor suppressive role of cellular senescence, aberrant activation of oncogenes, such as mutant Nras, in hepatocytes can induce OIS and restrain liver tumorigenesis (51). In addition, senescence can limit liver fibrosis and cancer in a non-cell-autonomous manner, with tissue damage induced-senescence of hepatic

stellate cells enabling tissue repair in a p53-dependent manner (47,48). Moreover, a seminal discovery from our lab demonstrated that restoration of p53 in established murine liver cancer cells can trigger them to undergo cellular senescence and thereby activate the innate immune system, including NK cells and macrophages, to drive rapid tumor regressions (52). However, some technical limitations from the study should also be noted, it relied on transplantation liver cancer model into nude mice which are not fully immunocompetent, thus limiting the interpretation for the contribution of the adaptive immune system and associated cellular networks. In addition, it used liver progenitor cells as the cell of origin for liver tumor transformation, which do not fully recapitulate the natural development of liver tumors, formed by transformation of adult hepatocytes (77).

Circumventing these limitations, the development of hydrodynamic tail vein injection technique has enabled somatic genetic engineering of adult hepatocytes more feasible (78). Through this technique, hepatocytes specifically uptake DNA constructs for the expression of oncogenes and inactivation of tumor suppressor genes, without affecting other cell types. As such, it can be used to generate a syngeneic murine liver tumor with different combination of genetic alterations found in human liver cancer in a completely immunocompetent background. Together, the senescence-associated features of liver pathology and the availability of flexible approaches for its in vivo genetic manipulation make liver cancer an attractive disease setting to study senescence and anti-tumor immunity in vivo.

OBJECTIVES

Despite the well-established roles of senescence in physiopathological processes including wound healing, host immunity and tumor suppression, the molecular mechanisms underlying these processes are poorly understood. Moreover, as the senescence state has been predominantly studied in *in vitro* cultured cells, how this alters the state, behavior and fate of tumor cells *in vivo* is still incompletely understood. Understanding these fundamental aspects of senescence is important, as the aberrant accumulation of senescent cells within tissues increases the risk of developing age-related diseases including organ dysfunction and cancer, hence the increasing interest in developing immune- or drug-based senolytics.

To address these questions, the first part of my thesis aims to ***elucidate the mechanisms whereby cellular senescence elicits effective anti-tumor immune responses*** against liver cancer in vivo, with the ultimate goal of identifying new strategies to pharmacologically mimic or enhance these effects. To do so, we developed up a ***genetically-controlled in vivo system to study senescence in an novel immunocompetent mouse model of liver cancer***. There are two unique features of this senescence-inducible model that distinguishes from other approaches (eg. therapy-induced senescence): 1) it allows for selective perturbation of the epithelial compartment, avoiding confounding effects of inducing senescence systemically in immune, stromal cells and other normal cells in the tumor microenvironment (79,80); 2) it enables synchronous and ubiquitous engagement of senescence program controlled by a

genetic switch, thus avoiding potential penetrance issues of pharmacologic senescence inducers. These features thus allow us to interrogate the biology of senescence *in vivo*, in a spatiotemporally-controlled manner.

The specific objectives are:

- To develop an immunocompetent senescence-inducible liver cancer mouse model.
- To characterize tumor cell-intrinsic changes of senescence and their effects in the tumor microenvironment.
- To identify pathways/factors critical for the interaction between senescent tumor cells and the tumor microenvironment that triggers effective anti-tumor surveillance.

During my thesis, we have also developed an optimized pipeline for high-throughput functional genomic screens to identify factors sustaining the senescent cell state that could serve as ***novel senolytic targets***. This work is still at the early stage and will be included in the Appendix.

The specific objectives are as followed:

- To generate an optimized-shRNA library targeting cell-surface factors selectively expressed by senescent cells
- To identify putative senolytic targets to eliminate senescent liver cancer cells.

MATERIALS AND METHODS

Cell Culture and drug treatment

p53-inducbble mouse liver cancer cell lines were cultured in DMEM supplemented with 10% FBS and penicillin and streptomycin (GIBCO) on the collagen-coated plates (PurCol, Advanced Biomatrix, 0.1 mg/ml) and maintain by the addition of 1 μg/ml doxycycline to suppress p53 expression. To trigger the senescence response, the cells were removed from doxycycline treatment and the cells became senescent around 6 days. For human liver cell lines, HepG2 and SK-Hep1 were cultured with EMEM dish and SNU447 was cultured in RPMI-1640, all supplemented with 10% FBS and penicillin and streptomycin, in non-coated, tissue culture treated vessels. The concentration and regimen of drug treatment in cancer cell lines were as followed. For JQ1 treatments, cells were treated with 500 nM of JQ1 for 48 hours prior to harvest. For trametinib (25nM), palbociclib (500nM), nutlin (10 uM) and cisplatin (1uM) treatment, cells were treated for 7 days prior to harvest. The concentration of DMSO corresponded to the drug treatment and does not exceed 1:3,000 of dilution, which shown no discernable toxicity to the cultured cells. Indicated dose of mouse and human recombinant IFNγ was administrated to the murine and human lines respectively after 24 hours of cell seeding and the cells were harvest after 24 hr treatment.

Primary Liver tumor generation and isolation of liver cell lines

C57BL/6N female mice aged 8-9 weeks old were injected via hydrodynamic injection with a sterile 2 ml (or 1/10 of mouse body weight) 0.9% NaCl solution

containing 5 μg of NrasG12D-IRES-rtTA (or NrasG12D-IRES-rtTA-IRES-Luc) and 20 ug of TRE-tRFP-shp53 each transposon vector together with 5ug CMV-SB13 Transposase (5:1 ratio) via the lateral tail vein. Doxycycline was administered to mice via 625 mg/kg doxycycline-containing food pellets (Harlan Teklad) at least 4 days before injection. The tumor was harvested at 5-7 weeks after injection for cell line isolation or bulk RNA-seq analysis. To derive cancer cell lines from primary liver tumor, tumors were minced and digested with 1 mg/ml collagenase IV (C5138, Sigma-Aldrich) and 0.3% Dispase II (Roche 04942078001) in DEME at 37 °C for a maximum of 30 mins. The cells were spun down to remove the supernatant and plated on collagen-coated plate. The cells were passaged at least 7-8 passages to remove the fibroblasts and obtain homogenous population.

Animal study

C57BL/6 mice were predominantly used for the animal study for the HTVI tumor generation and orthotopic liver injection experiments in the immunocompetent setting. C57BL/6N strain was mainly used except for the matching control strain with IFNG KO mice that was in the C57BL/6J background. However, we didn't observe any difference in terms of the tumor growth or senescence surveillance phenotype between C57BL/6N and J strain. The female mice were used in the experiment for the convenience of cage separation. Nonetheless, there was no observed sex and age (between 8-13 weeks) difference for the aforementioned phenotypes, and we managed to match the control and experimental group with the same sex and age of mice. For the orthotopic liver tumor injection, the cells

were prepared in 20 ul with 1:1 ratio of DMEM and Matrigel and injected using 31-gauge needle to the left lobe of the mouse liver following the standard surgery practice at MSKCC. Due to a varied degree of immunodeficiency in C57BL/6, Nude and R2G2 (Envigo) mice, different amount of mouse liver tumor cells was injected to the mouse liver and the mice were kept on dox feed. In details, 500,000, 100,000 and 50,000 cells were injected respectively to have comparable tumor size at 2 weeks after injection. The mice were then randomized for the subsequent experimental design.

Lentiviral and retroviral production and infection

Lentivirus was generated by co-transfection of viral vectors with packaging plasmids psPAX2 and pCMV-VSVG (Addgene) into 293T cells. Retroviruses were generated by co-transfection of viral vectors with pCMV-VSVG (Addgene) into 293GP cells. Polyethylenimine (PEI) is added during co-transfection with a ratio of total DNA:PEI = 1:3 to facilitate the binding of the plasmid to the cell surface. Viral containing supernatants were cleared of cellular debris by 0.45 μM filtration and mixed with 4 μg/ml polybrene. Target cells were exposed to viral supernatants for overnight before being washed, grown for 24 h in fresh media, then subjected to antibiotic selection or fluorescence-based cell sorting.

Genetic manipulation of cell line using CRISPR/Cas9

To knock out specific gene in the mouse and human liver tumor cell line, plasmid pX458 that contain the individual sgRNA was used for transient PEI transfection.

Cells were subsequently sorted by GFP positivity with flow cytometry 36-48 h post-transfection. For Ifngr1 and B2m KO experiment, cells were first stained with IFNGR1 and MHC-I antibody respectively and sorted through flow cytometry to enrich the negative population with mean fluorescence intensity comparable to IgG control. The sorted population were further tested with IFNγ to examine if MHC-I expression is still inducible or present in those KO cells. For p53 KO in human cell lines, transfected cells were first sorted based on GFP positivity to enrich the population then selected through Nutlin treatment (10 uM) for 5-7 days until the cells are not responsive to Nutlin-induced growth arrest.

Co-culture killing assays

CD8 T cells were isolated from spleens of female OT-1 mice (Jackson laboratory), mechanically disrupted by passing them through a 70 μm cell strainer, and centrifuged at 1500 rpm x 5 minutes. Red blood cells were lysed with ACK lysis buffer (Quality Biological) for 5 minutes. Total splenocytes or CD8+ T cells FACS sorted on a Sony MA900 were then activated with CD3/CD28 Dynabeads (one bead/T cell, Thermo Fisher) and cultured in presence of IL-2 (2 ng/ml; Biolegend), IL-7 (2.5 ng/ml; Peprotech) and IL-15 (50 ng/ml; Peprotech) in complete RPMI media supplemented with 10% FBS and 100 IU/ml penicillin/streptomycin for four to six days prior to co-culture assays with mouse liver tumor cells. For Kupffer cells isolation, the mice were first subjected to liver perfusion as previously described (81). After perfusion, the liver was removed and homogenized and then digested with protease solution (0.5 mg/ml type XIV protease, Sigma, P5147) supplemented

with DNAseI (0.2 ug/ml, Roche, 10104159001) for 15 minutes at 37C with constant stiring. This suspension was then centrifuged at 50 xg for 3 minutes to remove the sedated hepatocytes. The supernatant was then transferred and centrifuged 580xg for 5 minutes at 4C. The pellet was then washed with HBSS to remove residual protease solution and centrifuged at 580xg for 5 minutes at 4C to pellet the cells again. The pellet is then resuspended with FACS buffer and subjected to α-F4/80 isolation according to the manufacturer instruction (Miltenyi Biotec, 130-110-443). After isolation, the purity of Kupffer cells was confirmed with F4/80 staining through flow cytometry.

Murine liver tumor cells were transduced with retrovirus expressing PresentER-SIINFEKL construct (Addgene #102944) to present OVA on the cell surface. The construct conatin a puromycin selection marker and also GFP for cell visualization. The transduced cells were further selected against puromycin to obtain > 95% GFP positivity. Then the tumor cells were kept ± dox to induce senescence (p53 restored for 6 days). To set up the co-culture assay, proliferating and senescent tumor cells were first plated in the individual well of a 96 well collagen-coated plate (the cell number ratio is 1:2 to have similar amount of the cells next day). Kupffer cells were isolated at the same day and plated with indicated ratio about 7 hours after. If only T cells and tumor cells co-culture was performed, the step of Kupffer cells can be skipped. After 24 hours of initial plating, OT-I T cells were added at the indicated ratio. Co-cultures were imaged over time using an INCell 6000 high-content imager (GE Healthcare Life Sciences), with the 488 nm and 633 nm laser excitation, using a 10× objective. The correct focal plane was maintained by the

use of the INCell laser–based focus system at each time point, which maintains a focal plane relative to the bottom of the well. Images were captured at indicated time points, starting after the seeding of T cells onto liver cancer cells/Kupffer cells co-cultures. Images for each channel were saved during the experiment and subsequently analyzed using Columbus image analysis software. GFP+ tumor cells were identified and segmented from background using an intensity-based threshold method. T cells labeled with the CellTracker Deep Red Dye were identified using the same threshold method as the tumor cells. The number of the GFP+ tumor cells was quantified and normalized to the untreated control to calculate the killing index.

Senescence *in vitro* and *in vivo* assays

For colony formation assays, 2,500 mouse liver cancer cells were plated in each well of a 6-well plate. Cells were cultured for 6 days, then fixed with 4% formaldehyde, and stained with crystal violet. Detection of SA-β-gal activity in mouse tissues was performed as described (36). Population doubling curves were generated as follows. Cells were washed with PBS, trypsinized, and 100,000 cells were initially plated in triplicate in 6 well dishes off and on dox. Every 48 h cell number was recorded and same number of cells was replated. Population doublings for each 48 h period were calculated by dividing the final cell number to initial cell number. For in vivo SA-b-gal staining, fresh frozen tissue sections were fixed with 0.5% glutaraldehyde in phosphate-buffered saline (PBS) for 15 min, washed with PBS supplemented with 1 mM $MgCl_2$ and stained for 5–8 h in PBS

containing 1 mM $MgCl_2$, 1mg ml^{-1} X-gal, 5 mM potassium ferricyanide and 5 mM potassium ferrocyanide. Tissue sections were counterstained with eosin.

Whole mount immunostaining and tissue clearing

To determine the abundance of T-cells and neutrophils and their spatial relation in the livers of mice injected with 500,000 murine liver tumor cells, we performed whole mount immunostaining and tissue clearing of excised tumors as previously described (82). For these experiments, mice were euthanized with CO_2 to harvest proliferating and senescent liver tumors 10 days or where indicated after randomization point. Mice were then the livers were collected in PBS with 4% PFA and were fixed at 4ºC overnight. After three washes with PBS for 1 h each at room temperature, tissues were permeabilized in methanol (MetOH) gradients in PBS (PBS > MetOH 50% > MetOH 80% > MetOH 100%, for 30 min in each solution). Then, tissues were bleached with Dent's bleach (15% H_2O_2, 16.7% Dimethyl sulfoxide [DMSO] in MetOH) for 1h at room temperature and rehydrated through descending methanol gradients in PBS (MetOH 80% > MetOH 50% > PBS, 30 min in each solution). Then tissues were incubated with blocking buffer containing PBS with 0.3% Triton X100, 0.2% BSA, 5% DMSO, 0.1% azide and 25% FBS for 24h at 4ºC with shaking. Afterwards, lungs were stained with antibodies against CD3 (rat anti CD3, clone 17A2, cat 100202, Biolegend), MPO (goat, Human/Mouse Myeloperoxidase/MPO Antibody, R&D Systems) and CD31 (Hamster anti human/mouse-CD31, 2H8, MA3105, Thermo Fisher), all 1:200 in blocking buffer for 3 days at 4ºC and shaking. After washing for 24 h in washing buffer (PBS with

0.2% Triton X100 and 3% NaCl), the tissues were stained with secondary antibodies donkey-anti-Rat-AF488 (A212008, Invitrogen) and donkey-anti-goat AF647 (A21447, Invitrogen) 1:400 for 2 days at 4ºC, shaking. Then, tissues were washed for 24 h in washing buffer and thereafter stained with goat-anti-hamster-AF568 (Goat anti-Hamster IgG (H+L) Cross-Adsorbed Secondary Antibody, Alexa Fluor 568, A21112, Thermo Fisher) 1:400 and DAPI (1:1000) for 2 days at 4ºC, shaking. Finally, tissues were washed for 24 h in washing buffer and thereafter dehydrated in MetOH gradients in dH_20 using glass containers (MetOH 50% > MetOH 70% > MetOH 90% > 3x MetOH 100%, 30 min for each step). Then, tissues were cleared for 30 min in 50% MetOH and 50% benzyl alcohol, benzyl benzoate (BABB, mixed 1:2) and 1 h in 100% BABB, and finally, imaged on an SP8 Microscope (Leica). Quantification was performed with Imaris software (Bitplane). In some experiments we quantified the endogenous signal of the IFNγ sensing reporter in the liver tumor cells. In these experiments, we employed a different clearing technique that maintains the endogenous fluorescence (83). Tissues were excised and fixed as stated above, and then were soaked in CUBIC-I in a 15 ml conical tube container. CUBIC-I was prepared mixing 108 ml of ddH_2O with 75g of Urea (Sigma, U5128), 75g of N,N,N',N'-Tetrakis(2-Hydroxypropyl)ethylenediamine (Sigma, 122262) and 42ml of Triton X-100 (Sigma, X100). Samples were maintained at 37ºC and shaking for 7 days, changing the media every other day, until clear. Then, the samples were counterstained for DAPI in CUBIC-1 (1:1000) for 24h and washed in CUBIC-I overnight. Images were acquired and analyzed the same as above.

Western blotting

Cell lysates were extracted using RIPA buffer supplemented with phosphatase and protease inhibitor (5872, Cell Signaling Technology) and protein concentration was determined by BCA assay. Samples were boiled for 5 minutes and 20 to 30 µg of protein were separated by SDS-PAGE, transferred to polyvinylidene difluoride (PVDF) membranes (Millipore) according to standard protocols and probed with the relevant primary antibody overnight at 4°C. Membranes were then incubated with horseradish peroxide (HRP)-conjugated) anti-rabbit IgG or anti-mouse IgG secondary antibodies (1:10,000, GE Healthcare Life Science) at room temperature and proteins were detected using Pierce ECL Western Blotting Substrate (34095, Thermo Fisher Scientific). Antibodies were diluted as follows: p53 (CM5) (1:500, NCL-L-p53-CM5p, Leica Biosystems), p21 (F-5) (1:500, sc-6246, Santa Cruz Biotechnology), Phospho-Stat1 (Tyr701) (1:500, #9167, Cell Signaling Technology), Stat1 (1:1,000, #14994, Cell Signaling Technology). Protein loading was measured using a monoclonal β-actin antibody directly conjugated to horseradish peroxidase (1:20,000; AC-15, Sigma-Aldrich) and vinculin (1:2,000, ab129002, Abcam). ECL developed blots were imaged using a FluorChem M system (Protein Simple).

Cytokine array

Conditioned media samples (collected in complete DMEM) from proliferating or senescent in mouse liver cancer cell lines (plated in duplicate) were normalized

based on cell number by diluting with complete DMEM. Aliquots (50 µl) of the conditioned media were analyzed using multiplex immunoassays designed for mouse (Mouse Cytokine/Chemokine Array 31-Plex) from Eve Technologies. Biological replicates were averaged to determine cytokine levels. Heatmaps display relative cytokine expression values normalized to geometric means from both proliferating and senescent samples.

Plasma membrane-enriched mass spectrometry

To capture potential post-transcriptional changes altering the cell surface proteome induced by senescence induction, we enriched for cell surface proteins of proliferating or senescent cells through biotin-based labeling followed by pull-down purification. We adapted the protocol from previous published study (84) and followed the manufacturer instruction (Pierce Cell Surface Protein Isolation Kit #89881). In brief, we plated the proliferating and senescent cells (p53 restored 6 days) and collected the 2 days later. Before harvesting the cells, cells were incubated with biotin solution for 30 minutes at 4C to allow the surface protein labeling. Cells were then washed and lysed followed by column purification to enriched plamsa membrane proteins. The proteins were then digested in situ in the column overnight using trypsin at 37C on a rotor. Digested proteins were subjected to liquid chromatography–mass spectrometry (LC-MS/MS) according to established protocols. Non-biotinylated cell lysates were also included and served as background controls.

High throughput RNA-sequencing (RNA-seq) analysis

For in vitro liver cell lines RNA preparation, total RNA was extracted using using TRIzol (Thermo Fisher Scientific) following the manufacturer's instructions. For in vivo bulk tumor RNA-seq, proliferating tumor was harvested 7-10 day after randomization point and senescent tumor was harvested 12 days after p53 restoration. To extract tissue RNA, freshly isolated tumor chunk was first stored in RNA-later solution (AM7024, Thermo Scientific) to preserve RNA integrity until extraction and RNeasy kit (74106, Quiagen) was used to purified tissue RNA following the instructions. Purified polyA mRNA was subsequently fragmented, and first and second strand cDNA synthesis performed using standard Illumina mRNA TruSeq library preparation protocols. Double stranded cDNA was subsequently processed for TruSeq dual-index Illumina library generation. For sequencing, pooled multiplexed libraries were run on a HiSeq 2500 machine on RAPID mode. Approximately 10 million 76bp single-end reads were retrieved per replicate condition. Resulting RNA-Seq data was analyzed by removing adaptor sequences using Trimmomatic (85), aligning sequencing data to GRCm38 – mm10 with STAR (86), and genome wide transcript counting using HTSeq (87) to generate a RPKM matrix of transcript counts. Genes were identified as differentially expressed using R package DESeq2 with a cutoff of absolute log2FoldChange ≥ 1 and adjusted p value < 0.05 between experimental conditions (88). Functional enrichments of these differential expressed genes were performed with enrichment analysis tool Enrichr (89). Gene expressions of RNA-Seq data were clustered using hierarchical clustering based on one minus pearson

correlation test. For pathway enrichment analysis, the weighted GSEA Preranked mode was used on a set of curated signatures in the molecular signatures database (MSigDB v6.2) (https://www.broadinstitute.org/gsea/msigdb/index.jsp). From 17,810 signatures, signatures with 15-500 genes were only considered for the further analyses. From the results, enriched signatures with an adjusted p value less than 0.05 were considered as statistically significant.

Quantitative PCR with reverse transcription

Total RNA was isolated from mouse liver tumor cell line using TRIzol (Thermo Fisher Scientific) following the manufacturer's instructions. cDNA was obtained from 500 ng RNA using the Transcriptor First Strand cDNA Synthesis Kit (Roche) after treatment with DNase I (18068015, Thermo Fisher Scientific) following the manufacturer's instructions. The following primer sets for mouse sequences were used: Tap1_F 5'-GGACTTGCCTTGTTCCGAGAG-3', Tap1_R 5'-GCTGCCACATAACTGATAGCGA-3', Psmb8_F 5'-ATGGCGTTACTGGATCTGTGC-3', Psmb8_R 5'-CGCGGAGAAACTGTAGTGTCC-3', Nlrc5_F 5'-CCTGCGTCCCAGTCATTC-3', Nlrc5_R 5'-CTGCTGGTCAGTGATGGAGA-3', Hprt_F 5′-TCAGTCAACGGGGGACATAAA-3′, Hprt_R 5′-GGGGCTGTACTGCTTAACCAG-3′, Rplp0_F 5′-GCTCCAAGCAGATGCAGCA-3′, Rplp0_R 5′-CCGGATGTGAGGCAGCAG-3′, Quantitative PCR with reverse transcription (qRT–PCR) was carried out in triplicate (10 cDNA ng per reaction) using SYBR Green PCR Master Mix (Applied Biosystems) on the ViiA 7 Real-Time

PCR System (Life technologies). Hprt, Rplp0 (also known as 36b4) served as endogenous normalization controls.

Tumor measurement by ultrasound and bioluminescence imaging

High-contrast ultrasound imaging was performed on a Vevo 2100 System with a MS250 13- to 24-MHz scanhead (VisualSonics) to stage and quantify liver tumor burden. Tumor volume was analyzed using Vevo LAB software. Bioluminescence imaging was used to track luciferase expression in orthotopically injected liver tumor cells expressing a LUC-GFP reporter as well as primary HTVI tumor harboring luciferase construct. Mice were injected IP with luciferin (5 mg/mouse; Gold Technologies) and then imaged on a Xenogen IVIS Spectrum imager (PerkinElmer) 10 minutes later. Quantification of luciferase signaling was analyzed using Living Image software (Caliper Life Sciences).

Flow cytometry

For *in vivo* sample preparation, orthotopically injected liver tumors were isolated by removing the adjacent normal tissue, and allocated for 10% formalin fixation, OCT frozen blocks, snap frozen tissue, and flow cytometry analysis. To prepare single cell suspensions for flow cytometry analysi, liver tumor was mechanically disrupted to a single cell suspension using a 150 μm metal mesh and glass pestle in ice-cold 3% FCS/HBSS and passed through a 70 μm strainer. The liver homogenate was spun down at 400 g × 5 minutes at 4°C, and the pellet was resuspended in 15ml 3% FCS/HBSS, 500ul (500U) heparin, and 8ml Percoll (GE),

mixed by inversion, and spun at 500 g × 10 min at 4°C. After removal of supernatant, cells were resuspended in PBS supplemented with 2% FBS. Samples were blocked with anti-CD16/32 (FC block, BD Pharmigen) for 20 minutes and then incubated with the following antibodies for 30 minutes on ice: CD45 (30-F11), NK1.1 (PK136), CD3 (17A2), CD19 (1D3), CD4 (RM4-5), Gr-1 (RB6-8C5), CD44 (IM7), CD11b (M1/70) (BD Biosciences); MHC-I (H-2k^{b}; AF6-88.5.5.3), CD119 (2E2, biotin), Armenian Hamster IgG isotype (eBio299Arm, biotin) (Invitrogen); Streptavidin, F4/80 (BM8), CD8 (53-6.7), Ly6C (HK1.4), CD11c (N418), Ly6G (1A8), CD69 (H1.2F3), CD106 (MVCAM.A), CD62L (MEL-14), PD-1 (29F.1A12) (Biolegend); Tigit (1G9) (Tonbo). For human antibody HLA-A,B,C (W6/32) (BD Biosciences). To distinguish live/dead cells, DAPI and Ghost dye violet 510 (Tonbo) were used depending on whether the cells are fixed. Flow cytometry was performed on an LSRFortessa or Guava flow cytometer (Luminex Corporation) where indicated, and data were analyzed using FlowJo (TreeStar).

Neutralizing antibody and liposomal clodronate studies

To determine the specific immune cell dependency of senescence surveillance, depleting antibodies or drugs were administrated to the mice the day after doxycycline withdrawal. For NK cell depletion, mice were injected intraperitoneally (IP) with an α-NK1.1 antibody (250 μg; PK136, BioXcell) twice per week. For T cell depletion, mice were injected IP with either an α-CD4 (200 μg; GK1.5, BioXcell) or α-CD8 antibody (200 μg; 2.43, BioXcell) twice per week. Depletion of NK, CD4+, and CD8+ T cells was confirmed by flow cytometric of liver tumor tissue. For

neutrophil/myeloid-derived suppressive cells depletion, mice were injected intraperitoneally with an α-Gr-1 (200 µg; RB6-8C5, BioXcell) twice per week. For control, isotype control antibody (200 µg; LTF-2, BioXcell) was IP twice per week. For macrophage depletion, mice were injected intravenously (IV) with clodronate liposomes (10 gram/kg of mouse weight; ClodronateLiposomes.com) twice per week. PBS was used as a control.

Immunofluorescence and immunohistochemistry

Tissues were fixed overnight in 10% neutral buffered formalin (Richard-Allan Scientific), embedded in paraffin and cut into 5 µm sections. Sections were deparaffinized and rehydrated with a histoclear/alcohol series and subjected to antigen retrieval by boiling in citrate antigen retrieval buffer (Vector). Slides were then blocked in PBS/0.1% Triton X-100 containing 1% BSA. Primary antibodies were incubated overnight at 4°C in blocking buffer. The following primary antibodies were used: GFP (ab13970, Abcam, 1:500), Ki67 (550609, BD Biosciences, 1:200), CD8 (4SM15, eBioscience, 1:200), CD45 (70257, Cell Signaling Technology, 1:100), F4/80 (70076, Cell Signaling Technology, 1:200). For immunohistochemistry, Vector ImmPress HRP kits and ImmPact DAB (Vector Laboratories) were used for secondary detection. For immunofluorescence, the following secondary antibodies were used: goat anti-chicken AF488 (A11039, Invitrogen, 1:500), donkey anti-rabbit AF594 (A21207, Invitrogen, 1:500), goat anti-rabbit AF594 (A11037, Thermo Fisher Scientific, 1:500). All secondary antibodies were diluted in blocking buffer and incubated for 1 h at room

temperature. Subsequently, slides were washed and nuclei were counterstained with PBS containing DAPI, and mounted under cover slips with ProLong Gold (LifeTechnologies). Images were acquired with a Zeiss AxioImager microscope using Axiovision software.

Public dataset transcriptomic analyses

Signature of different human liver cancer subtype was obtained from previous study (90). In brief, the top 200 upregulated and downregulated genes were selected as the signature for each subtype. Transcriptomic data of senescent human tumor cell lines was used according to the previously published study (43) and obtained from the website https://ccb.nki.nl/publications/cancer-senescence/. The expression of selected genes was compared between senescent and the corresponding proliferating cells among individual cell lines and normalized to determine the fold change. Another dataset reporting surface proteomic changes in the senescent cells was used and transcriptomic data was obtained from accession numbers GSE72404, GSE72407 and GSE72409. Differential expression analysis was then applied using the DESeq2 package (88) to define DEGs between proliferating and senescent samples, using fold change > 2 and an adjusted P value < 0.05 cut-off.

Generation of IFNγ sensing (IGS) reporter

We have adapted the construct design from the previously described paper (91). In brief, we have crafted a 5x Interferon Gamma-activated sequence (GAS) inserted in front of a mini promoter followed by ZsGreen1 reporter. The construct

also contains RFP driven by the PGK promoter to have constitutive RFP expression for cell visualization. The cells were transduced with virus and sorted through flow cytometry with high RFP level for stable expression of the construct in the cells.

Statistical analyses

Statistical analyses were performed using unpaired two-tailed Student's t-test in GraphPad Prism. Graphs display means ± s.e.m of independent biological replicates (mice).

RESULTS

A p53-restorable liver cancer model uncovers a cancer immune evasion-to-immune recognition switch

To study the specific effect of senescence on tumor cells and how senescence shapes the tumor microenvironment, we generated a senescence-inducible liver cancer model controlled by a restorable p53 short-hairpin RNA (shRNA). Specifically, we utilized the hydrodynamic tail vein injection (HTVI) technique (78) to transfect two transposon constructs (encoding NrasG12D-IRES-rtTA and TRE-tRFP-shp53, respectively) and a sleeping beauty SB13 transposase plasmid into adult liver hepatocytes of Bl/6 mice. In this Tet-On system, endogenous p53 is suppressed in the presence of doxycycline (Dox) via an inducible shRNA (Fig. 3A). As expected, the cooperation of oncogenic Ras and suppression of p53 leads to the transformation of hepatocytes. Mice develop tumors with poorly differentiated features 5-8 weeks after HTVI. To assess whether resulting tumors recapitulate molecular features of human liver cancer, we performed RNA-seq analysis in bulk tumor samples and compared our results with publicly available transcriptional profiles of human hepatocellular carcinoma (HCC) (90). As shown in Fig 3.1, our model resembles the 'Proliferation Class' of HCC, which is enriched in mutations of *TP53* and cell proliferation signaling pathways (such as PI3K/AKT and RAS/MAPK cascades) and has the worst prognosis amongst HCC genetic subtypes (92).

Exploiting the reversible nature of shRNA-mediated p53 suppression of this model, we were then able to restore endogenous p53 through doxycycline

withdrawal. Consistent with prior work from our lab demonstrating the addiction of cancer cells to sustained p53 loss (52,93) p53 restoration triggered tumor cells to undergo cellular senescence, as shown by the lack of proliferation marker Ki67 and the acquisition of positive SA-b-gal cell staining (Fig. 3B). This cell state switch triggered by p53 restoration translated into an extended survival of tumor bearing-mice (Fig. 3.2A).

To dissect the molecular and cellular mechanisms underlying the anti-tumor effects of senescence induction in advanced liver cancers, we derived 3 independent primary cell lines from on-dox tumors in which p53 is constantly suppressed and cell line NSP3 was predominantly used in this study. In line with our *in vivo* phenotype, tumor cells with restored p53 expression after doxycycline withdrawn exhibited upregulation of the downstream p53 target p21, which translated into a decreased proliferation rate and colony forming capacity and a robust SA-b-gal staining, further supporting the establishment of senescence (Fig. 3.2B-E). Importantly, injection of these (on dox) primary cell lines back into the liver of secondary recipient 'on dox' mice generated focal liver cancers in 3 weeks in a synchronized manner. Furthermore, these tumors rapidly regressed upon p53 restoration, consistent with the primary HTVI setting, as shown by longitudinal measurement of tumor volumes via ultrasound (Fig. 3D; Fig. 3.2F). Strikingly, liver tumors regressed extensively in size, up to an average of 80% within 3 weeks after p53 restoration, regardless of their initial size. This effect was further quantified through bioluminescence imaging of tumor cells expressing a GFP-luciferase (GFP-Luc) construct, in both HTVI and orthotopic injection models (Fig. 3.2G and

H). Given the comparable phenotypes observed between HTVI and orthotopic models, we exploited the latter as it enabled flexible molecular and functional characterization in both in vivo and in vitro contexts.

Given that the p53 restoration-induced senescence led to cell cycle arrest *in vitro* but potent tumor regressions *in vivo*, we hypothesized that senescence rewired interactions between tumor cells and their immune environment and that these interactions contribute to tumor control. To specifically assess a potential contribution of the immune system, we injected on-dox tumor cells into different mouse strains with varying degrees of immunodeficiency (Fig. 3.2B). Comparison of tumor volume changes upon p53 reactivation between Bl/6, Nude and $Rag2^{-/-}$ $Il2rg^{-/-}$ (R2G2) mice (a comparable equivalent to NSG mice) showed that tumor regressions were significantly impaired in Nude mice and entirely blunted in R2G2, indicating the requirement of innate and adaptive cell immunity for senescence surveillance (Fig. 3E-G; Fig. 3.2I and J). Of note, these phenotypes were independent of doxycycline administration, as (i) similar liver tumor regressions were observed with the Tet-Off system where the administration of doxycycline turns off the p53 hairpin (Fig. 3.2K), and (ii) tumor growth of liver tumors with constitutive suppression of p53 was comparable in the presence or absence of doxycycline (Fig 3.2L). Finally, regressions were comparable in both parental lines and those transduced with the GFP-Luc construct, ruling out a contribution from immunogenicity of exogenous proteins underlying these potent anti-tumor effects (Fig. 3.2M). Together, these data indicate that p53 reactivation triggers cancer

cells into a senescence response that is able to elicit potent immune mediated-tumor regressions in a physiologically accurate model of liver cancer in vivo.

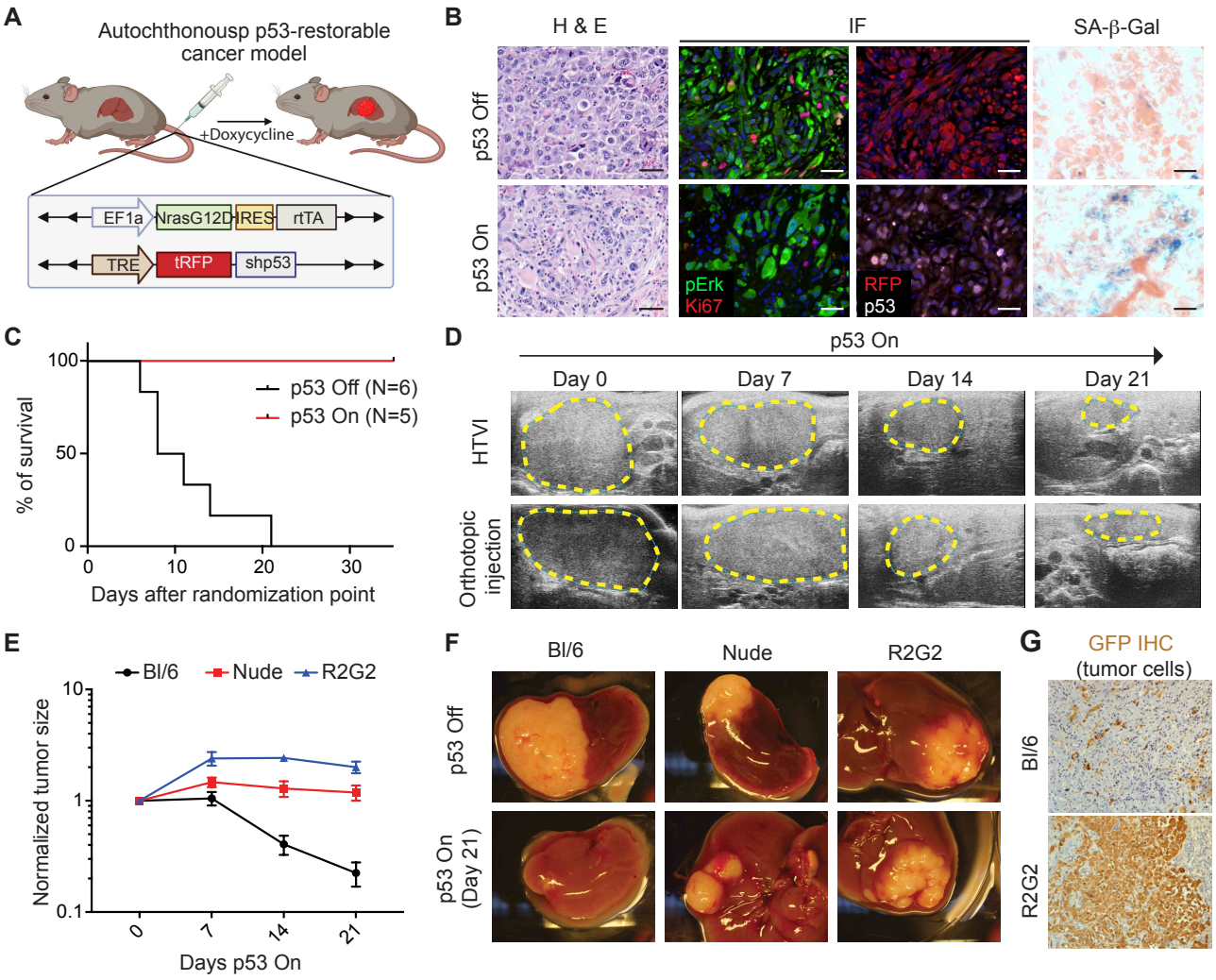
A
Autochthonousp p53-restorable cancer model
+Doxycycline
EF1a
NrasG12D
IRES
rtTA
TRE
tRFP
shp53
B
H & E
IF
SA-β-Gal
p53 Off
p53 On
pErk
Ki67
RFP
p53
C
% of survival
100
50
0
0
10
20
30
Days after randomization point
p53 Off (N=6)
p53 On (N=5)
D
p53 On
Day 0
Day 7
Day 14
Day 21
HTVI
Orthotopic injection
E
Bl/6
Nude
R2G2
Normalized tumor size
10
1
0.1
0
7
14
21
Days p53 On
F
Bl/6
Nude
R2G2
p53 Off
p53 On (Day 21)
G
GFP IHC
(tumor cells)
Bl/6
R2G2

Figure 3. A p53-restorable liver cancer model uncovers a cancer immune evasion-to-immune recognition switch.

A, generation of the p53-restoratable mouse liver cancer model using hydrodynamic tail vein injection (HTVI). **B**, representative haematoxylin and eosin (H&E), immunofluorescence (IF) and senescence-associated β-Gal (SA-β-Gal) staining of p53-suppressed (p53 Off) and -restored (p53 On for 14 days) tumor sections generated from HTVI model. Scale bar, 50 mm. **C**, survival analysis of mice orthotopically injected with NSP3 liver tumor cells. **D,** representative time-lapsed ultrasonogram of HTVI and orthotopic injection liver cancer model after p53 restoration. **E**, tumor size change measured by ultrasound upon p53 restoration in different immune background mouse strains. R2G2, Rag2-Il2rg double knockout mouse. Data are presented as mean ± s.e.m. At least N=9 for each strain. **F**, representative images of p53 Off and p53 On tumor in different immune background mouse strains. **G**, representative immunohistochemistry (IHC) staining of GFP-harboring tumor cells at day 21 upon p53 restoration.

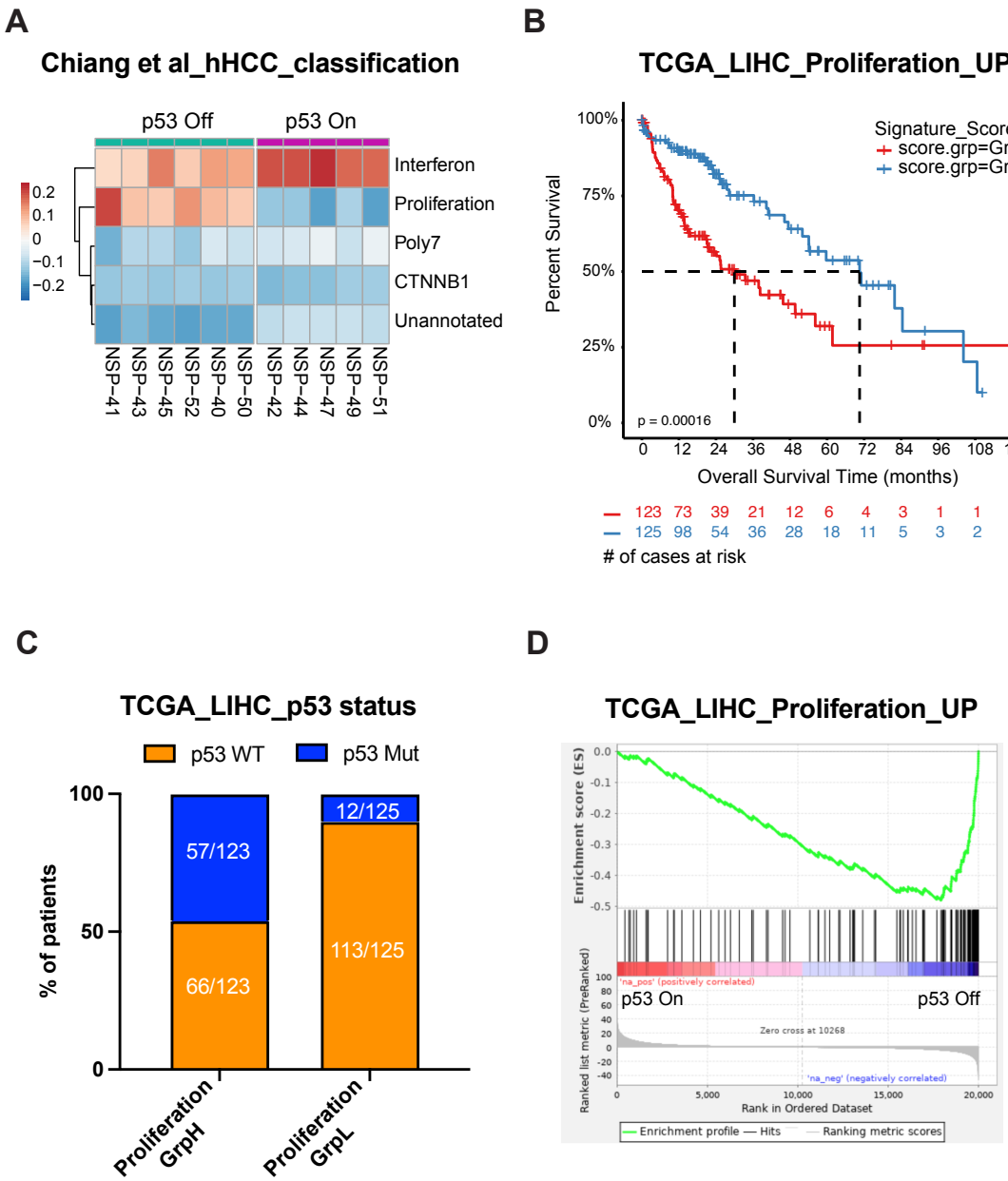
A
Chiang et al_hHCC_classification
p53 Off
p53 On
Interferon
Proliferation
Poly7
CTNNB1
Unannotated
0.2
0.1
0
−0.1
−0.2
NSP−41
NSP−43
NSP−45
NSP−52
NSP−40
NSP−50
NSP−42
NSP−44
NSP−47
NSP−49
NSP−51
B
TCGA_LIHC_Proliferation_UP
Signature_Score
score.grp=GrpH
score.grp=GrpL
Percent Survival
100%
75%
50%
25%
0%
p = 0.00016
0 12 24 36 48 60 72 84 96 108 120
Overall Survival Time (months)
123 73 39 21 12 6 4 3 1 1 1
125 98 54 36 28 18 11 5 3 2 0
# of cases at risk
C
TCGA_LIHC_p53 status
p53 WT
p53 Mut
% of patients
100
50
0
57/123
66/123
12/125
113/125
Proliferation GrpH
Proliferation GrpL
D
TCGA_LIHC_Proliferation_UP
Enrichment score (ES)
0.0
-0.1
-0.2
-0.3
-0.4
-0.5
'na_pos' (positively correlated)
p53 On
p53 Off
Zero cross at 10268
'na_neg' (negatively correlated)
Ranked list metric (PreRanked)
100
80
60
40
20
0
-20
-40
0
5,000
10,000
15,000
20,000
Rank in Ordered Dataset
Enrichment profile — Hits
Ranking metric scores

Figure 3.1. The Nras-p53 liver tumor model resembles proliferation class in human hepatocellular carcinoma.

A, in vivo HTVI liver tumor RNA-seq revealed that p53 off tumors resembles “Proliferation Class” while p53 on tumor resembles “Interferon Class”. **B,** TCGA data of liver cancer patients were stratified with Proliferation signature score and grouped into top and bottom 33%. **C,** p53 mutation status of patients grouped by high or low Proliferation signature score. **D,** Gene Set Enrichment Analysis between p53 on and p53 Off tumor using Proliferation Class signature.

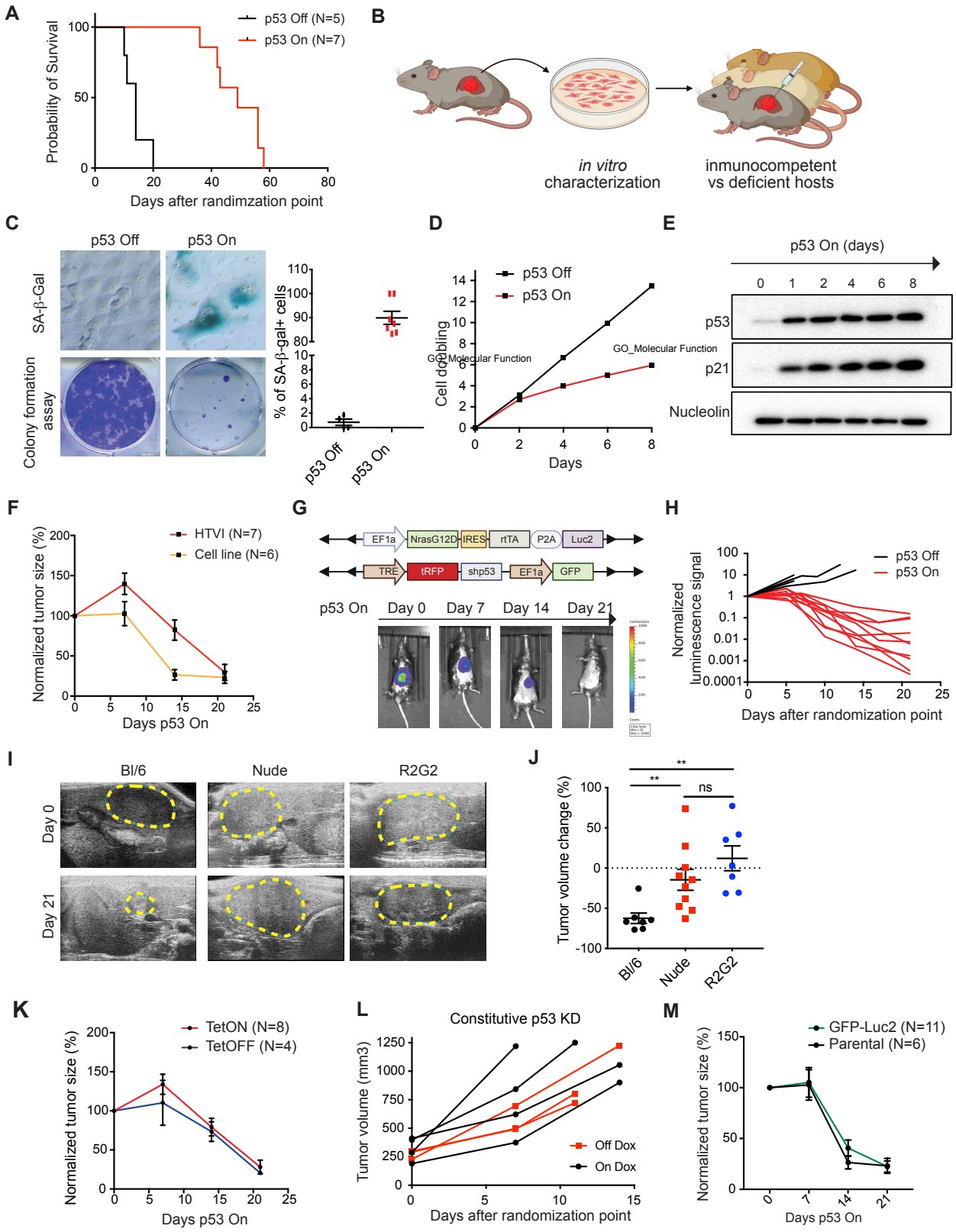
A
Probability of Survival
p53 Off (N=5)
p53 On (N=7)
Days after randimzation point
B
in vitro
characterization
inmunocompetent
vs deficient hosts
C
p53 Off
p53 On
SA-β-Gal
Colony formation assay
% of SA-β-gal+ cells
D
p53 Off
p53 On
Cell doubling
GO_Molecular Function
Days
E
p53 On (days)
0 1 2 4 6 8
p53
p21
Nucleolin
F
HTVI (N=7)
Cell line (N=6)
Normalized tumor size (%)
Days p53 On
G
EF1a
NrasG12D
IRES
rtTA
P2A
Luc2
TRE
tRFP
shp53
EF1a
GFP
p53 On
Day 0
Day 7
Day 14
Day 21
H
p53 Off
p53 On
Normalized luminescence signal
Days after randomization point
I
Bl/6
Nude
R2G2
Day 0
Day 21
J
Tumor volume change (%)
ns
Bl/6
Nude
R2G2
K
TetON (N=8)
TetOFF (N=4)
Normalized tumor size (%)
Days p53 On
L
Constitutive p53 KD
Tumor volume (mm3)
Off Dox
On Dox
Days after randomization point
M
GFP-Luc2 (N=11)
Parental (N=6)
Normalized tumor size (%)
Days p53 On

Figure 3.2. Establishment of a genetically controlled tumor-specific senescence mouse model

A, survival analysis of mice from HTVI model. **B**, graphic illustration of cell lines generation from HTVI model and subsequent in vivo orthotopic tumor cells injection experiment. **C**, in vitro characterization of p53-restorable NSP3 liver cancer cell line by colony formation assay and SA-β-Gal staining. **D**, comparison of the cell doubling in p53-restored (p53 On) and p53-suppressed (p53 Off) cells. **E**, immunoblot analysis of p53 and p21 upon doxycycline withdrawal in *in vitro* NSP3 cells. **F**, comparison of tumor regression phenotype between HTVI and orthotopic tumor cell injection model measured by ultrasound. **G**, representative bioluminescence images of tumor regression upon p53 restoration in HTVI model. **H**, tumor regression monitored by bioluminescence imaging in orthotopic injection model with cells transduced with GFP-luciferase construct. **I** and **J**, representative time-lapsed ultrasonogram of the tumor between different immune background mice (**I**). Quantification of tumor volume change between day 7 and 14 in those mice (**J**). Data presents as mean ± s.e.m. **K**, comparison tumor regression phenotype between TetOn and TetOff system HTVI model. **L**, p53 constitutive suppressed tumor growth in the presence or absence of doxycycline treatment. **M**, comparison of tumor regression phenotype between parental and GFP-luciferase transduced liver tumor cells.

Senescence induction remodels the immune landscape to trigger innate and adaptive anti-tumor immunity

We then exploited this senescence-inducible model to investigate how senescence reprograms the tumor microenvironment to elicit anti-tumor immunity. As a start, we first characterized immune infiltrate of p53-supressed (herein referred to as proliferating) and p53-reactivated (herein referred to as senescent) tumors. As shown in Fig. 4A, senescent tumors exhibited a significant increase of total CD45+ immune cells, consistent with previous reports that senescence can drive immune cell recruitment through the SASP (51,52). To obtain a more comprehensive picture of the immune landscape, we performed flow cytometry-based immunophenotyping of both proliferating and senescent tumors (the latter at 9 days after p53 restoration, i.e. the time-point in which tumor regressions start to occur). This showed an increase in the fraction of lymphocytes, including B cells and CD3 T cells, and a decrease of the Gr-1+ myeloid-derived suppressor cells/neutrophils (CD11b+Gr1+Ly6C low) upon senescence induction (Fig. 4B; Fig. 4.1A). This translated into a significant increase of CD3/neutrophil ratio (Fig. 4.1B), which has been identified as a favorable prognostic factor in human liver cancer (94).

To gain spatial information, we then exploited tissue clearing technology that preserves the tissue integrity and enables visualization of the different immune cells in the tumor microenvironment. Consistent with the flow cytometry immunophenotyping data, senescent tumors showed an accumulation of CD3 T cells and a decrease in the absolute numbers of neutrophils marked by MPO (95),

in both adjacent and core tumor regions (Fig. 4C; Fig. 4.1C and D). Importantly, CD8 T cells within senescent tumors were positive for CD69 and CD44 markers, indicating an activation state. In addition, a higher percentage of PD-1+ CD8 T cells is observed, suggesting prior T cell activation and priming (96). Finally, we have also observed an increased percentage of CD44+CD62L- CD8 T cells with effector function (97) (Fig. 4D).

To functionally pinpoint the specific cell types contributing to senescence surveillance, we then performed pharmacological perturbation to deplete specific immune compartments. Blocking antibodies targeting Gr1+ (anti-neutrophils) and NK1.1+ (anti-NK cells) cells did not affect senescent tumor regression, indicating that these cell types do not play a major role in senescence surveillance. In line with the abrogated tumor regression response in Nude mice lacking adaptive immunity (Fig. 3E), depletion of CD8+ (but not CD4+) T cells impaired senescence surveillance (Fig. 4E). Lastly, targeting macrophages through liposomal clodronate (98) also delayed senescence-driven tumor regressions (Fig. 4E; Fig. 4.1E). Interestingly, immunofluorescence staining showed that CD8 T cells localized with F4/80+ macrophages within senescent tumors in the transplantable (Fig. 4F) and primary HTVI (Fig. 4.1F) models, suggesting that these two populations may cooperate for optimal senescence surveillance. Together, our results indicate that senescence induction reprograms the tissue environment to activate innate and adaptive anti-tumor immunity, resulting in tumor regressions and extended host survival.

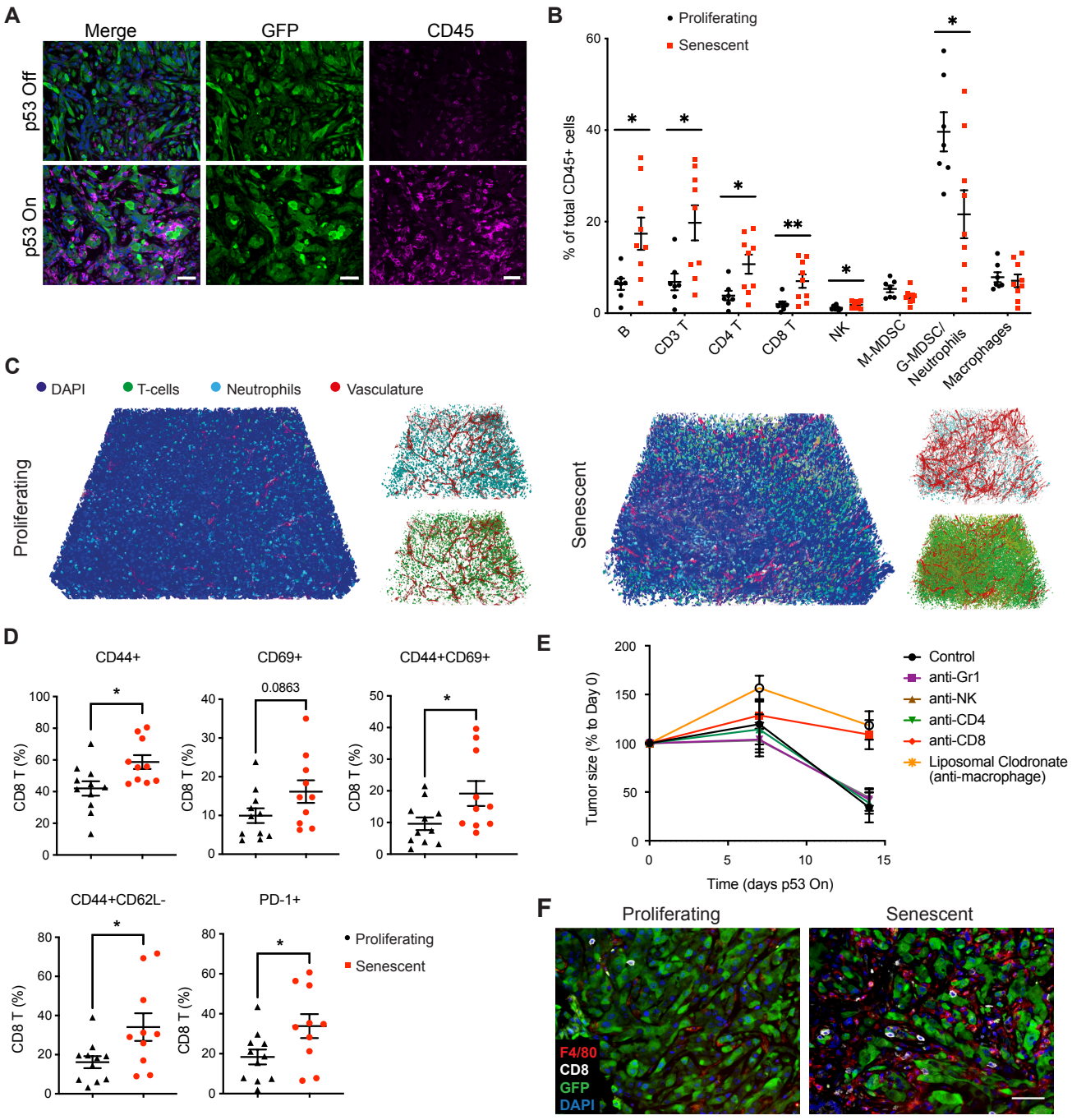
A
Merge
GFP
CD45
p53 Off
p53 On
B
Proliferating
Senescent
% of total CD45+ cells
B
CD3 T
CD4 T
CD8 T
NK
M-MDSC
G-MDSC/ Neutrophils
Macrophages
C
DAPI
T-cells
Neutrophils
Vasculature
Proliferating
Senescent
D
CD44+
CD69+
CD44+CD69+
0.0863
CD8 T (%)
CD44+CD62L-
PD-1+
Proliferating
Senescent
E
Tumor size (% to Day 0)
Time (days p53 On)
Control
anti-Gr1
anti-NK
anti-CD4
anti-CD8
Liposomal Clodronate (anti-macrophage)
F
Proliferating
Senescent
F4/80
CD8
GFP
DAPI

Figure 4. Senescence induction remodels immune landscape to trigger innate and adaptive anti-tumor immunity.

A, representative immunofluorescence images of CD45 and GFP staining marking immune cells and tumor cells respectively in proliferating and senescent tumor (7 days after p53 restored). **B**, flow cytometry analysis of immune landscape from proliferating and senescent tumor. Data are pooled from 3 independent experiments with total n=7 for proliferating tumor and n=9 for senescent tumor. **C**, Representation tissue clearing images from the orthotopically injected liver tumor. T cells are marked with CD3 staining. Neutrophils are marked with MPO staining. Vasculature is marked with CD31 staining. **D**, flow cytometry analysis of activation and effector markers of CD8 T cells. Data are pooled from 2 independent experiments with total n=11 for proliferating tumor and n=10 for senescent tumor. **E**, relative tumor volume measurement upon specific immune cells depletion. **F**, representative immunofluorescence images of CD8 T cells and F4/80 positive macrophages staining in the liver tumor.

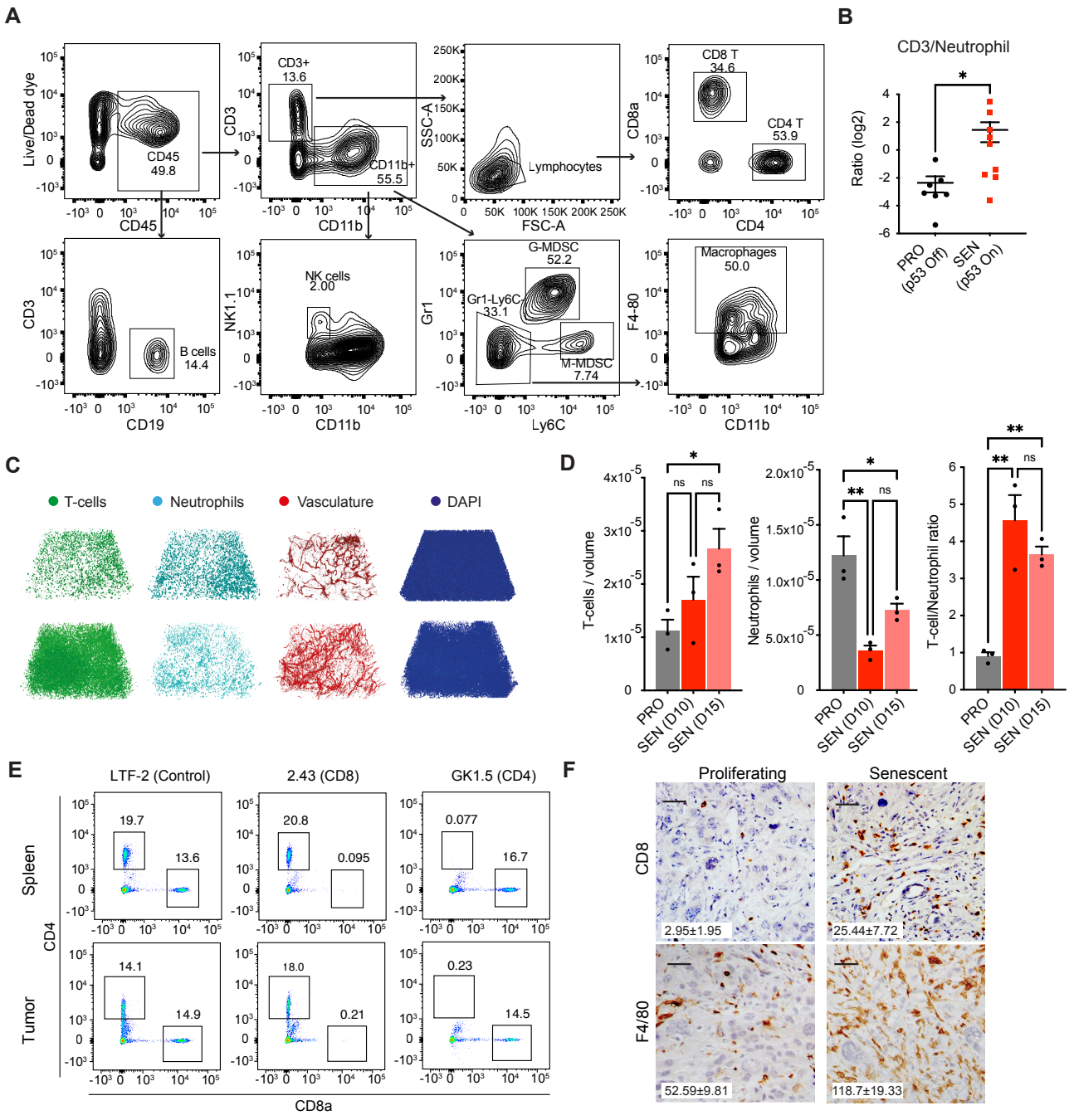
A
Live/Dead dye
CD45
49.8
CD45
CD3
CD3+
13.6
CD11b+
55.5
CD11b
SSC-A
Lymphocytes
FSC-A
CD8a
CD8 T
34.6
CD4 T
53.9
CD4
CD3
B cells
14.4
CD19
NK1.1
NK cells
2.00
CD11b
Gr1
G-MDSC
52.2
Gr1-Ly6C
33.1
M-MDSC
7.74
Ly6C
F4-80
Macrophages
50.0
CD11b
B
CD3/Neutrophil
Ratio (log2)
PRO
(p53 Off)
SEN
(p53 On)
C
T-cells
Neutrophils
Vasculature
DAPI
D
T-cells / volume
Neutrophils / volume
T-cell/Neutrophil ratio
PRO
SEN (D10)
SEN (D15)
ns
E
LTF-2 (Control)
2.43 (CD8)
GK1.5 (CD4)
Spleen
Tumor
CD4
CD8a
19.7
13.6
20.8
0.095
0.077
16.7
14.1
14.9
18.0
0.21
0.23
14.5
F
Proliferating
Senescent
CD8
F4/80
2.95±1.95
25.44±7.72
52.59±9.81
118.7±19.33

Figure 4.1 Senescence engagement reverts from immune-suppressive to immune-activated tumor microenvironment.

A, gating strategy for immunophenotyping. Related to **Fig. 4B**. **B**, CD3 to neutrophil ratio calculated from **Fig. 4B**. **C** and **D**, individual channel of tissue clearing images (**C**) and quantification of CD3 T cells and neutrophil/volume and the CD3/Neutrophil ratio at indicated time points of tumor harvest (**D**). **E**, representative flow cytometry plots of CD4 and CD8 T cells depletion through corresponding antibodies. **F**, representative immunohistochemistry images showing CD8 T cells and F4/80+ macrophages staining in the HTVI tumor. Number of CD8 T cells/field is quantified and presented as mean ± s.e.m. 3 independent fields from each mouse were selected and for N=4 for both proliferating and senescent tumor (p53 restoration for 14 days).

Remodeling of secretome and surfaceome rewires cell-cell communication pathways in senescent cells

In order to identify senescence effector programs underlying immune-mediated tumor control, we performed transcriptomic analysis comparing *in vitro* proliferating versus senescent NSP3 tumor cells, 8 days after p53 induction, a time-point when the senescence state is fully established (Fig. 3.1C). Among those changes, Gene Set Enrichment Analysis (GSEA) showed senescent cells upregulate genes mediating immune responses while downregulating genes related to cell cycle, consistent with their growth arrest feature and SASP (Fig. 5A). In line with the previously described secretory phenotype (Fig. 5B), categorization of the differentially expressed genes (DEGs) by subcellular compartments of encoded proteins also showed a significant enrichment of the genes encoding for extracellular (EC) factors in senescent cells, which we validated by an orthogonal cytokine array measuring several SASP factors in the conditioned media of senescent cells (Fig. 5C). Interestingly, subcellular compartmentalization analysis of DEGs revealed that a quarter of the upregulated genes encoded plasma membrane (PM) proteins, which represented an even larger fraction than the secreted factors above described (Fig. 3B). Gene Ontology analyses of these genes indicated an enrichment in pathways related to signaling transduction and cytokine receptor activity (Fig. 5D; Fig. 5.1A), suggesting that senescence triggers a major remodeling of microenvironment sensing programs.

To determine whether transcriptional rewiring of PM factors is a universal feature of senescence or an effect uniquely linked to p53 action, we treated p53-

suppressed liver cancer cells with a previously published drug combination, trametinib plus palbociclib (T+P) that inhibits CDK4/6 and MEK respectively to induce senescence in a p53-independent manner. In accordance with the p53 restoration-induced senescence results, we found that drug-induced senescence similarly triggers upregulation of genes encoding both extracellular and PM factors (Fig. 5.1B). A consistent finding is observed mining the transcriptomic data from previous study inducing senescence in IMR90 fibroblasts with different senescence triggers (Fig. 5.1C, (35)). Interestingly, similar to the activation of SASP genes, the activation of genes encoding plasma membrane factors was blunted by JQ1 treatment, (Fig. 5H), a Brd4 inhibitor impairing enhancer-mediated gene expression (38). Together, these data suggest that, in addition to the SASP, senescence triggers major remodeling of the cell surface proteome, or surfaceome.

To validate these predictions from our transcriptomic analysis, we next directly profiled surfaceome changes triggered upon senescence induction by performing PM factor-enriched mass spectrometry (MS) using a biotin-labeling based approach (84) (Fig. 5.1D) in proliferating tumor cells and senescent counterparts. Non-biotin labeled samples were included as a control group to set up background signal-to-noise thresholds. This analysis revealed 887 high-confidence hits (see methods), including a large fraction of previously annotated plasma membrane factors annotated in the Uniprot database (Fig. 5E). The comparison between transcriptomic and proteomic analyses showed high consistency of mRNA expression and protein level, as well as an increased proportion of PM factors upregulated in senescent cells (Fig. 5F; Fig. 5.1E, F). We

have also identified previously described senescence-associated markers such as CD44 (99) and many more less characterized factors (Fig. 5G). Senescence-associated surface molecule changes were further validated by flow cytometry, validating the robustness of our methodology (Fig. 5.1G).

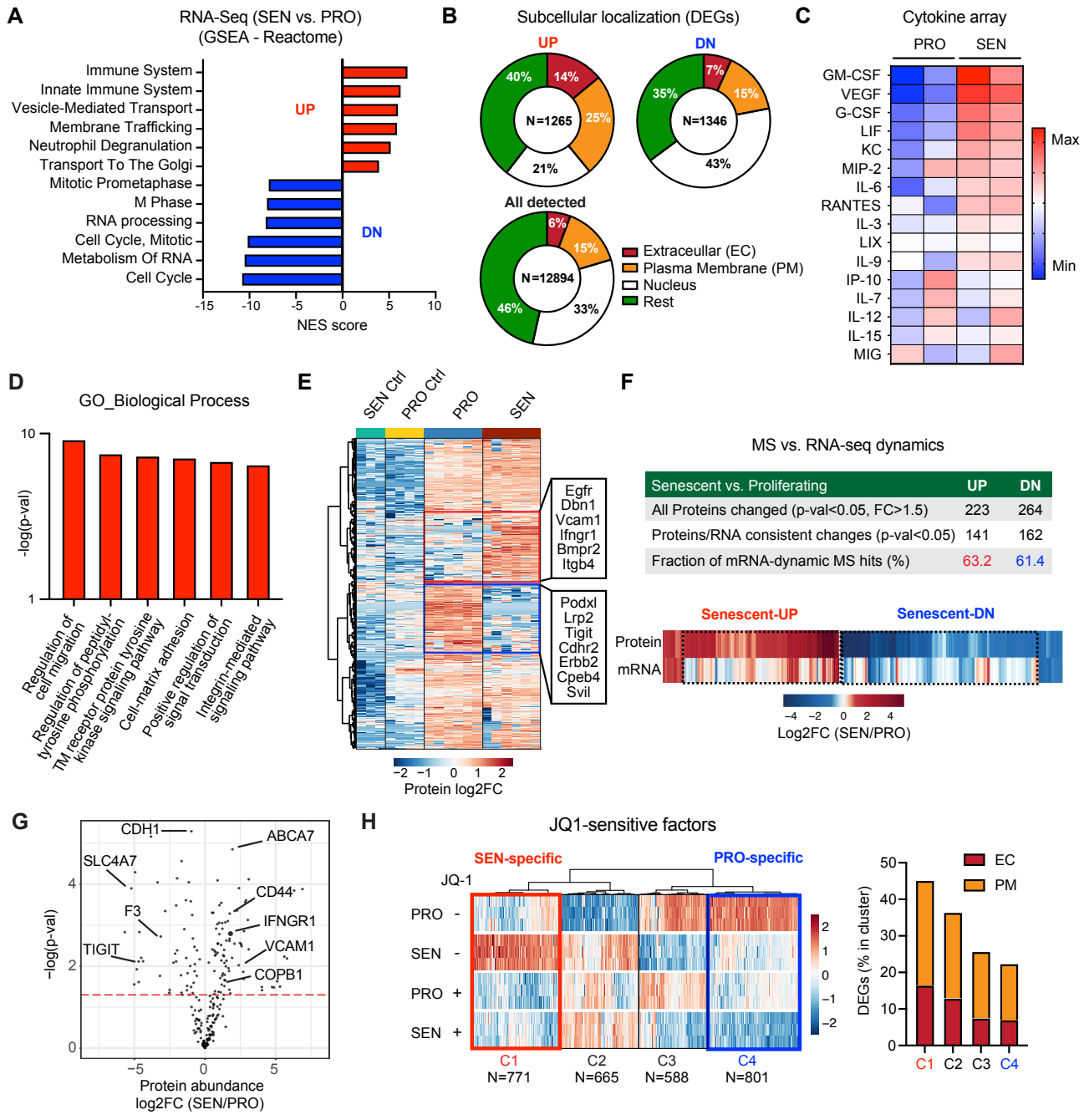
A
RNA-Seq (SEN vs. PRO)
(GSEA - Reactome)
Immune System
Innate Immune System
Vesicle-Mediated Transport
Membrane Trafficking
Neutrophil Degranulation
Transport To The Golgi
Mitotic Prometaphase
M Phase
RNA processing
Cell Cycle, Mitotic
Metabolism Of RNA
Cell Cycle
UP
DN
-15 -10 -5 0 5 10
NES score
B
Subcellular localization (DEGs)
UP
N=1265
40%
14%
25%
21%
DN
N=1346
7%
15%
35%
43%
All detected
N=12894
6%
15%
46%
33%
Extracellular (EC)
Plasma Membrane (PM)
Nucleus
Rest
C
Cytokine array
PRO
SEN
GM-CSF
VEGF
G-CSF
LIF
KC
MIP-2
IL-6
RANTES
IL-3
LIX
IL-9
IP-10
IL-7
IL-12
IL-15
MIG
Max
Min
D
GO_Biological Process
-log(p-val)
10
1
Regulation of cell migration
Regulation of peptidyl-tyrosine phosphorylation
TM receptor protein tyrosine kinase signaling pathway
Cell-matrix adhesion
Positive regulation of signal transduction
Integrin-mediated signaling pathway
E
SEN Ctrl
PRO Ctrl
PRO
SEN
Egfr
Dbn1
Vcam1
Ifngr1
Bmpr2
Itgb4
Podxl
Lrp2
Tigit
Cdhr2
Erbb2
Cpeb4
Svil
−2 −1 0 1 2
Protein log2FC
F
MS vs. RNA-seq dynamics
Senescent vs. Proliferating | UP | DN
All Proteins changed (p-val<0.05, FC>1.5) | 223 | 264
Proteins/RNA consistent changes (p-val<0.05) | 141 | 162
Fraction of mRNA-dynamic MS hits (%) | 63.2 | 61.4
Senescent-UP
Senescent-DN
Protein
mRNA
−4 −2 0 2 4
Log2FC (SEN/PRO)
G
CDH1
ABCA7
SLC4A7
CD44
F3
IFNGR1
TIGIT
VCAM1
COPB1
-log(p-val)
4
2
0
−5 0 5
Protein abundance
log2FC (SEN/PRO)
H
JQ-1
SEN-specific
PRO-specific
PRO -
SEN -
PRO +
SEN +
2
1
0
−1
−2
C1
N=771
C2
N=665
C3
N=588
C4
N=801
DEGs (% in cluster)
50
40
30
20
10
0
EC
PM
C1 C2 C3 C4

Figure 5. Remodeling of secretome and surfaceome rewires communication pathways in senescent cells.

A, GSEA of RNA-Seq data from p53 On (Senescent, SEN) vs. p53 Off (Proliferating, PRO) liver tumor cells in vitro. **B**, subcellular localization of differentially expressed genes ($p < 0.05$, FC >2) and all detected genes (TPM >1) from RNA-seq data in **A**. **C**, cytokine array of conditioned medium collected from proliferating and senescent cells (p53 On D6 to D8) in vitro. Samples are from 2 independent biological replicates. **D**, Gene Ontology (GO) analysis of upregulated plasma membrane proteins in senescent cells. **E**, mass spectrometry analysis of plasma membrane-enriched proteome in proliferating and senescent cells. Controls are the samples without biotin labeling serving as background noise. Red and blue box represent proteins enriched in senescent and proliferating cells respectively. **F**, comparison between mass spectrometry and RNA-seq of detected differentially expressed genes. **G**, Volcano plot of annotated plasma membrane factors identified from mass spectrometry. **H**, transcriptomic analysis of DEGs from proliferating and senescent cells treated with JQ1. EC, extracellular; PM, plasma membrane.

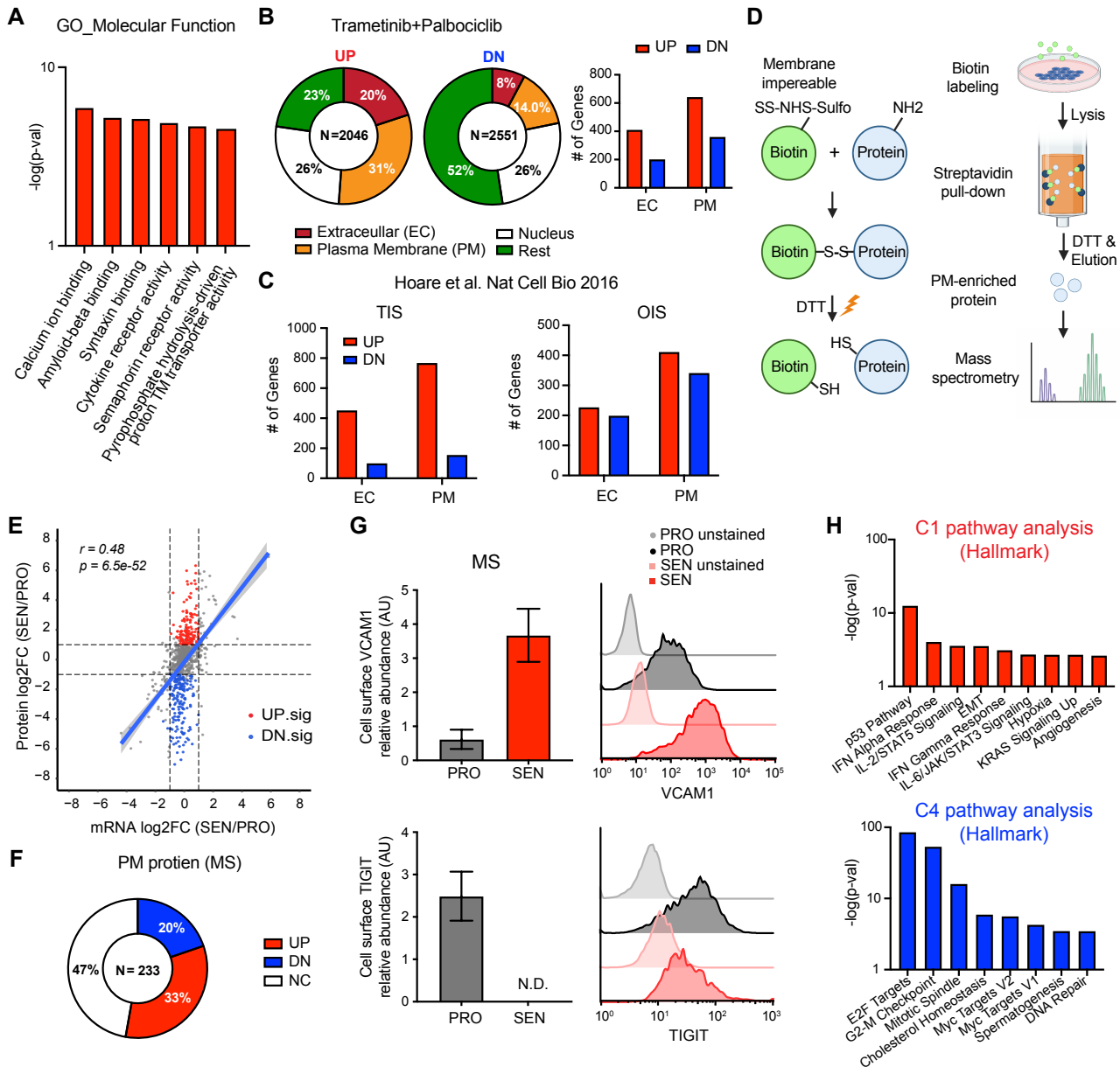
A
GO_Molecular Function
-log(p-val)
Calcium ion binding
Amyloid-beta binding
Syntaxin binding
Cytokine receptor activity
Semaphorin receptor activity
Pyrophosphate hydrolysis-driven proton transmembrane transporter activity
B
Trametinib+Palbociclib
UP
DN
N=2046
N=2551
23%
20%
26%
31%
8%
14.0%
52%
26%
UP DN
# of Genes
EC
PM
Extracellular (EC)
Plasma Membrane (PM)
Nucleus
Rest
C
Hoare et al. Nat Cell Bio 2016
TIS
OIS
UP
DN
# of Genes
EC
PM
D
Membrane impereable
SS-NHS-Sulfo
NH2
Biotin
Protein
S-S
DTT
HS
SH
Biotin labeling
Lysis
Streptavidin pull-down
DTT & Elution
PM-enriched protein
Mass spectrometry
E
r = 0.48
p = 6.5e-52
Protein log2FC (SEN/PRO)
mRNA log2FC (SEN/PRO)
UP.sig
DN.sig
F
PM protien (MS)
N= 233
20%
33%
47%
UP
DN
NC
G
MS
PRO unstained
PRO
SEN unstained
SEN
Cell surface VCAM1 relative abundance (AU)
PRO
SEN
VCAM1
Cell surface TIGIT relative abundance (AU)
N.D.
TIGIT
H
C1 pathway analysis (Hallmark)
-log(p-val)
p53 Pathway
IFN Alpha Response
IL-2/STAT5 Signaling
EMT
IFN Gamma Response
IL-6/JAK/STAT3 Signaling
Hypoxia
KRAS Signaling Up
Angiogenesis
C4 pathway analysis (Hallmark)
-log(p-val)
E2F Targets
G2-M Checkpoint
Mitotic Spindle
Cholesterol Homeostasis
Myc Targets V2
Myc Targets V1
Spermatogenesis
DNA Repair

Figure 5.1. Cell surfaceome is substantially remodeled in senescent cells.

A, GO analysis of upregulated plasma membrane proteins in senescent cells. Related to **Fig. 5D**. **B,** subcellular localization of detected DEGs (TPM > 1, p <0.05, FC >2) of trametinib (T) and palbociclib (P) treated and vehicle treated mouse liver cancer cells. **C**, transcriptomic data analysis from public dataset comparing two senescent triggers in IMR90 fibroblast. TIS, therapy-induced senescence triggered by etoposide; OIS, oncogene-induced senescence by HRasG12V. Related to **Fig. 5D**. **D**, graphic illustration of the protocol of plasma membrane-enriched mass spectrometry (MS). **E**, dynamics of the annotated plasma membrane genes compared between mass spectrometry and RNA-seq. **F**, differentially expressed Uniprot-annotated plasma membrane factors profiled by MS. **G**, validation of MS hits using flow cytometry. **H**, pathway analysis using MsigDB Hallmark genesets of cluster 1 and 4 in proliferating and senesecent cells treated with JQ1. Related to **Fig. 5H**.

Senescent cells are primed to sense and amplify IFNγ signaling

The above transcriptional and proteomic changes suggest that senescent cells sense extracellular tissue cues differently, and that these changes may be involved in the interaction between senescent cells and their environment. To examine this further, we mined DEGs and proteomic changes that may rewire signaling pathways relevant for senescence surveillance. Specifically, we searched for signaling pathways predicted to be: (i) uniquely hyper-activated in senescent cells, (ii) blunted by Brd4 inactivation, a perturbation known to blunt senescence surveillance (38), (iii) altered in human liver cancers (90). This revealed a major rewiring of interferon pathways in senescent cells (Fig. 5H; Fig. 5.1H), consistent with their higher IFNGR1 surface protein levels, and further validated by flow cytometry (Fig. 6A, B; Fig. 6.1A). Additional upregulation of several positive regulators of interferon signaling such as Irf1 (Fig. 6C) and concomitant downregulation of multiple negative regulators (Ptpn2 (100), Socs1 and Socs3) was observed (101,102), Fig. 6D). Together, these results suggest that senescence induction enhances responsiveness of tumor cells to Type II IFN (ie. IFNγ) signals.

To functionally test whether senescent cells are "primed" for sensing IFNγ, we treated proliferating and senescent cells with the same amounts of IFNγ and examined the activation of downstream IFNγ signaling transcription factor, Stat1. As shown in Fig. 6D, tumor cells triggered to senescence have much higher levels of phospho-Stat1, which is the active form of Stat1 that transcribes IFN genes. Importantly, the enhanced IFNγ sensing phenotype was consistently observed

across different genetic or pharmacologic insults (p53 restoration, trametinib plus palbociclib, and also cisplatin) (Fig. 5D; Fig. 5.1D). Consistently, human cell lines from various cancer types triggered to senesce by different drug treatments showed enhanced IFNγ sensing machinery, independent of their underlying p53 status (Fig. 6E; Fig. 6.1F-I), indicating that upregulation of IFNγ sensing may be a more general feature of senescence rather than a p53-dependent phenomenon. Of note, IFNγ is not secreted by senescent cells as part of a SASP program, excluding the possibility of IFNγ signaling may influence senescence responses in an autocrine manner.

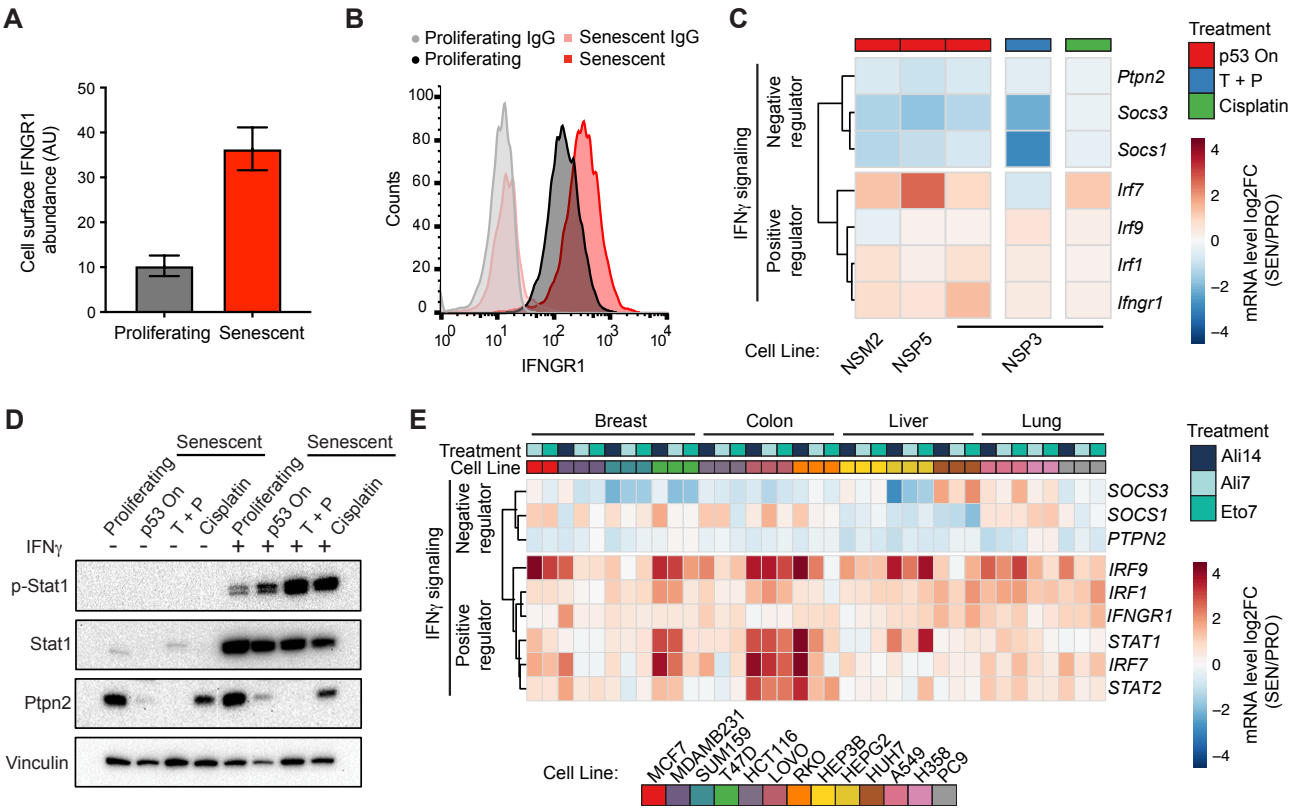
A
Cell surface IFNGR1 abundance (AU)
Proliferating
Senescent
B
Proliferating IgG
Proliferating
Senescent IgG
Senescent
Counts
IFNGR1
C
IFNγ signaling
Negative regulator
Positive regulator
Ptpn2
Socs3
Socs1
Irf7
Irf9
Irf1
Ifngr1
Cell Line:
NSM2
NSP5
NSP3
Treatment
p53 On
T + P
Cisplatin
mRNA level log2FC (SEN/PRO)
D
Senescent
Proliferating
p53 On
T + P
Cisplatin
IFNγ
p-Stat1
Stat1
Ptpn2
Vinculin
E
Breast
Colon
Liver
Lung
Treatment
Cell Line
Ali14
Ali7
Eto7
SOCS3
SOCS1
PTPN2
IRF9
IRF1
IFNGR1
STAT1
IRF7
STAT2
MCF7
MDAMB231
SUM159
T47D
HCT116
LOVO
RKO
HEP3B
HEPG2
HUH7
A549
H358
PC9

Figure 6. Senescent cells are primed to sense and amplify IFNγ signaling

A and **B**, IFNGR1 level between proliferating and senescent cells profiled from mass spectrometry and validated by flow cytometry. AU, arbitrary unit. **C**, normalized expression level (senescent/proliferating) of selected IFNγ signaling genes from RNA-seq data of 3 independent p53-restorable cell lines and also two other senescence triggers. NSP3 are the cell line predominantly used in this study. **D**, western blot analysis of IFNγ signaling genes. T+P, trametinib plus palbociclib. **E,** transcriptomic analysis from public dataset SENESCopedia. Human cells lines were treated with Ali, alisertib or Eto, etoposide for indicated days.

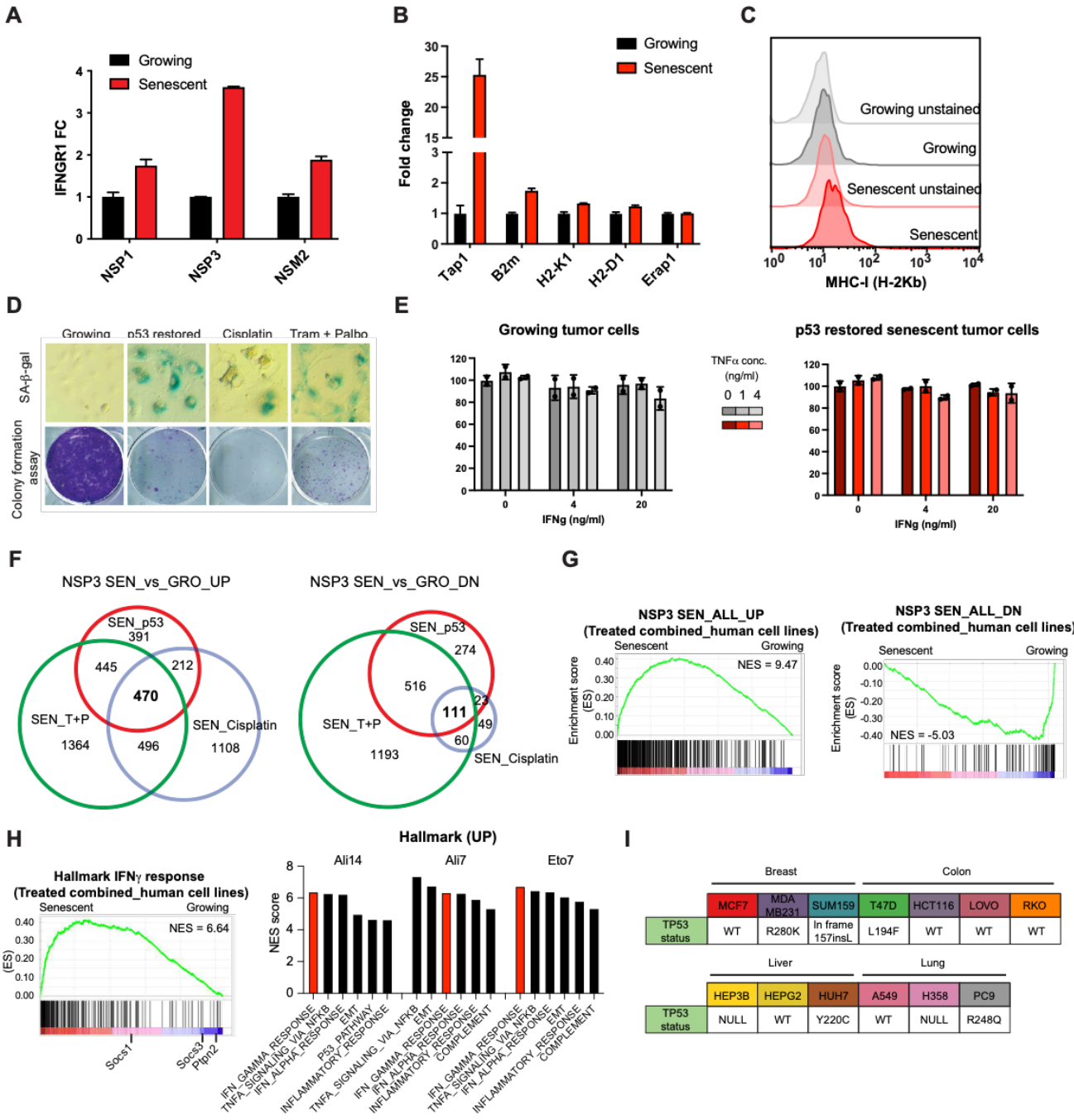
A
Growing
Senescent
IFNGR1 FC
NSP1
NSP3
NSM2
B
Growing
Senescent
Fold change
Tap1
B2m
H2-K1
H2-D1
Erap1
C
Growing unstained
Growing
Senescent unstained
Senescent
MHC-I (H-2Kb)
D
Growing
p53 restored
Cisplatin
Tram + Palbo
SA-β-gal
Colony formation assay
E
Growing tumor cells
p53 restored senescent tumor cells
TNFα conc. (ng/ml)
0 1 4
IFNg (ng/ml)
F
NSP3 SEN_vs_GRO_UP
SEN_p53
391
445
212
470
SEN_T+P
1364
496
SEN_Cisplatin
1108
NSP3 SEN_vs_GRO_DN
SEN_p53
274
516
23
111
49
SEN_T+P
60
1193
SEN_Cisplatin
G
NSP3 SEN_ALL_UP
(Treated combined_human cell lines)
Senescent
Growing
NES = 9.47
Enrichment score (ES)
NSP3 SEN_ALL_DN
(Treated combined_human cell lines)
Senescent
Growing
NES = -5.03
Enrichment score (ES)
H
Hallmark IFNγ response
(Treated combined_human cell lines)
Senescent
Growing
NES = 6.64
Enrichment score (ES)
Socs1
Socs3
Ptpn2
Hallmark (UP)
Ali14
Ali7
Eto7
NES score
IFN_GAMMA_RESPONSE
TNFA_SIGNALING_VIA_NFKB
IFN_ALPHA_RESPONSE
P53_PATHWAY
EMT
INFLAMMATORY_RESPONSE
TNFA_SIGNALING_VIA_NFKB
IFN_GAMMA_RESPONSE
IFN_ALPHA_RESPONSE
EMT
INFLAMMATORY_RESPONSE
COMPLEMENT
IFN_GAMMA_RESPONSE
TNFA_SIGNALING_VIA_NFKB
IFN_ALPHA_RESPONSE
EMT
INFLAMMATORY_RESPONSE
COMPLEMENT
I
Breast
Colon
MCF7
MDA MB231
SUM159
T47D
HCT116
LOVO
RKO
TP53 status
WT
R280K
In frame 157insL
L194F
WT
WT
WT
Liver
Lung
HEP3B
HEPG2
HUH7
A549
H358
PC9
TP53 status
NULL
WT
Y220C
WT
NULL
R248Q

Figure 6.1. Sensitization to IFNγ in senescent cells is independent of p53 status

A, IFNGR1 level validation in 3 independent cell lines. NSP3 line is predominantly used in this study. **B**, expression level of selected antigen presentation genes from RNA-seq data in proliferating and senescent cells. **C**, MHC-I level in proliferating and senescent cells measured by flow cytometry. **D**, SA-β-gal staining in NSP3 cells with different senescence triggers. **E**, IFNγ and TNFα treatment on both proliferating and senescent cells for 2 days. **F**, overlapping of DEGs comparing senescent vs. proliferating NSP3 cells treated with different senescence triggers. **G**, GSEA comparing our common senescence signature from **F** and the RNA-seq results from SENESCopedia human cell lines. **H**, GSEA revealed an enrichment in MSigDB Hallmark IFN gamma response pathway in senescent human cell lines of SENESCopedia. **I**, p53 mutation status of human cell lines used in SENESCopedia.

Senescence cooperates with IFNγ to potentiate the antigen presentation program independent of SASP regulation

To explore the downstream consequences of the enhanced Type II IFN sensing and signaling of senescent cells, we performed the RNA-seq on both proliferating and p53-restored senescent cells treated with or without IFNγ at low dose (50 pg/ml). Mining established IFNγ response gene sets, we observed that cell-intrinsic senescent cell changes cooperate with extracellular IFNγ to enhance genes expression involved in antigen presentation. Specifically, we found (i) a cluster of IFNγ response genes whose expression is downregulated in senescence even in the presence of IFNγ, containing the aforementioned negative regulators of IFNγ pathway such as Ptpn2, Socs1 and Socs3; and (ii) a cluster representing synergistic effects of IFNγ and senescence, including several critical factors mediating the antigen presentation program, such as the transcription factor Nlrc5, immunoproteaosome Psmb8, Psmb9, and also Tap1 and B2m, essential for processing and presenting the peptide on MHC-I complex (Fig. 7A). Interestingly, while many of these factors were induced by the induction of senescence alone (eg. Tap1 and B2m), these analyses uncover a cooperative effect of extracellular IFNγ in activating the antigen presenting program, independent of the SASP program, that did not further change upon IFNγ treatment (Fig. 7B). Consistently, levels of MHC-I levels and other IFNγ response genes were specifically induced in senescent exposed to IFNγ as compared to proliferating counterparts, even at higher doses of IFNγ treatment (1 ng/ml, Fig. 7C-D; Fig. 6.1B-C).

To confirm these findings in the human setting, we validated the enhancement of antigen presentation pathway in human cancer cell lines triggered to senesce (Fig. 7.1A) (43). Furthermore, we experimentally generated isogenic human liver cancer cells differing in their p53 status to selectively alter their senescence responsiveness to specific senescence-inducing perturbations such as Nutlin. Consistent with the above findings, surface HLA levels were cooperatively induced by the convergent effects of senescence induction and IFNγ treatment, in a manner that could be correlated with the senescence responsiveness across the different lines tested and that could be genetically rescued by perturbations driving senescence bypass in previously senescence-sensitive cells. (Fig. 7.1B-D). In sum, our data show that cell-intrinsic senescence-associated changes cooperate with IFNγ to further shape the transcriptome of senescent cells in a manner that enhances the antigen presentation program.

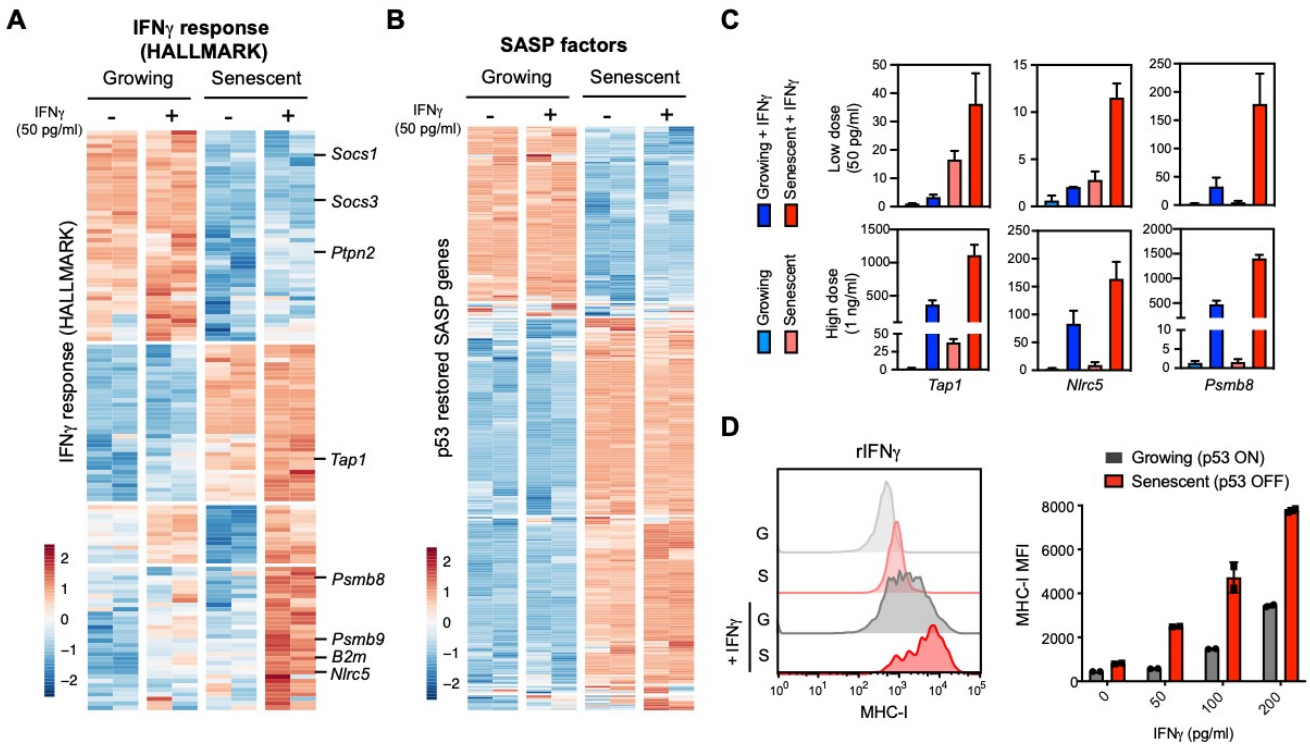
A
IFNγ response (HALLMARK)
Growing
Senescent
IFNγ (50 pg/ml)
IFNγ response (HALLMARK)
Socs1
Socs3
Ptpn2
Tap1
Psmb8
Psmb9
B2m
Nlrc5
B
SASP factors
Growing
Senescent
IFNγ (50 pg/ml)
p53 restored SASP genes
C
Growing + IFNγ
Senescent + IFNγ
Growing
Senescent
Low dose (50 pg/ml)
High dose (1 ng/ml)
Tap1
Nlrc5
Psmb8
D
rIFNγ
G
S
+ IFNγ
MHC-I
Growing (p53 ON)
Senescent (p53 OFF)
MHC-I MFI
IFNγ (pg/ml)

Figure 7. Senescence cooperates with IFNγ to potentiate the antigen presentation program independent of SASP regulation

A and **B**, RNA-seq of p53 restored senescent and proliferating cells treated with low dose of IFNγ (50 pg/ml). Genes from MSigDB Hallmark IFN gamma response were used for heatmap clustering (**A**). Differentially expressed genes comparing p53 restored senescent and proliferating cells that encode extracellular factors were selected for heatmap clustering (**B)**, **C**, RT-qPCR of selected antigen presentation pathway genes in NSP3 cells treated with low (50 p/ml) or high (1 ng/ml) dose of IFNγ. **D**, MHC-I level of proliferating and p53-restored senescent cells after IFNγ treatment measured by Guava flow cytometer.

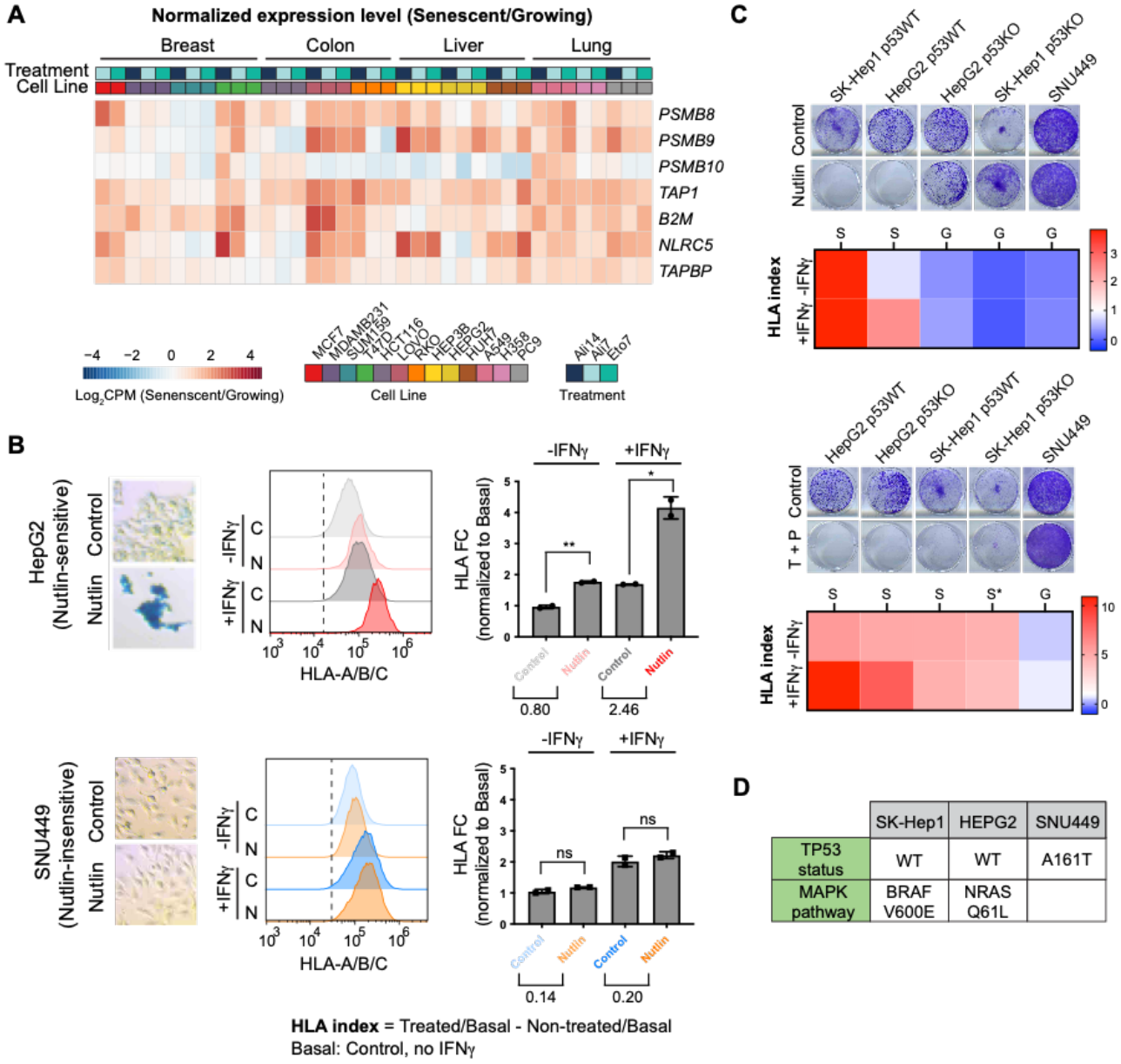

D

	SK-Hep1	HEPG2	SNU449
TP53 status	WT	WT	A161T
MAPK pathway	BRAF V600E	NRAS Q61L	

Figure 7.1. Validation of the cooperativity between senescence and IFNγ signaling in human cell lines.

A, Expression of selected genes in antigen presentation pathways comparing between senescent and proliferating from human cancer cell lines from SENESCopedia. **B** to **D**, Human liver cancer cell lines and isogenic p53 KO clones were treated with indicated drug to induce senescence. Human rIFNγ was subsequently treated in those cells and HLA was measured after 24h of treatment. “HLA-index” was determined by calculating the HLA expression level difference between drug-treated vs. untreated cells, in the presence or absence of IFNγ (**B**). The summary of 5 human cell lines (including two isogenic p53 KO clones) treated with Nutlin or trametinib + pablociclib shown by the colony formation assay after 8 days of replating and HLA-index results (**C**). p53 and RAS pathway mutation status of the human cell lines (**D**).

Senescence enhances IFNγ signaling sensitivity in vivo

As senescent cells themselves do not express IFNγ confirmed by cytokine array in our system, we hypothesized that the enhanced IFNγ sensing phenotype renders senescent cells more sensitive to signals stemming from the immune microenvironment. To examine this phenomenon *in vitro* and *in vivo*, we adapted an IFNγ sensing (IGS) reporter from a recently published study for visualization of intracellular IFNγ signaling (91). The reporter consists of a series of Interferon Gamma-activated sequence (GAS), followed by ZsGreen1 fluorescent protein sequence, and a RFP sequence driven by a constitutive promoter for visualization of cells (Fig. 8A). As expected, IGS reporter-expressing NSP3 cells showed increased ZsGreen1 signal upon treatment with recombinant IFNγ in a dose-dependent manner and, consistent with our previous results, this signal was stronger in senescent cells, across different senescence triggers, compared to their proliferating counterparts (Fig. 8B; Fig. 8.1A and B). The same finding could be also extended in the context of heterotypic cell-cell interactions, where an *in vitro* co-culture system was established by incubating OT-I T cells with antigen-matched ovalbumin (OVA)-expressing NSP3 cells (Fig. 8.1C). With this observation, we turned to an *in vivo* setup where BL/6 mice were orthotopically injected with IGS reporter-expressing tumor cells and the liver tumors were subsequently harvested after p53 reactivation or not for tissue clearing technology. This revealed a robust ZsGreen1 expression in p53-restored tumors that contrasted with the reduced patterns in the p53-suppressed counterparts (Fig. 8C

and D). Together these data suggest that senescent tumor cells in vivo also have an increased sensitivity to IFNγ.

To interrogate the functional contribution of IFNγ signaling to the interactions between senescent cells and immune cells, we first used the aforementioned *in vitro* co-culture system, which in particular, circumvents the confounding effect of immune recruitment mediated by SASP *in vivo*. Given the immune blockade phenotype as well as the spatial distribution between CD8 T cells and F4/80 macrophages in p53-restored tumor above noted, OT-I T cells and Kupffer cells, the liver resident macrophages, were added in the *in vitro* co-culture with senescent NSP3 tumor cells (Fig. 8.2A and B). In the presence of macrophages, a significant increase of IFNγ level was detected in the conditioned medium collected from this assay, which also correlates with a higher MHC-I level on the cell surface of senescent cells (Fig. 8.2F and G). Furthermore, a more prominent cell death phenotype, in an IFNγ-dependent manner, was observed when cells were cocultured with T cells and macrophage rather than with T cells alone (**Fig. 9A; Fig. 8.1C-E**). These results showed a critical heterotypic interaction between CD8 T cells and macrophages for eliminating senescent cells, supporting the previous finding *in vivo*, and suggest the intact cell-intrinsic IFNγ-sensing pathway in senescent cells is required for their effective clearance.

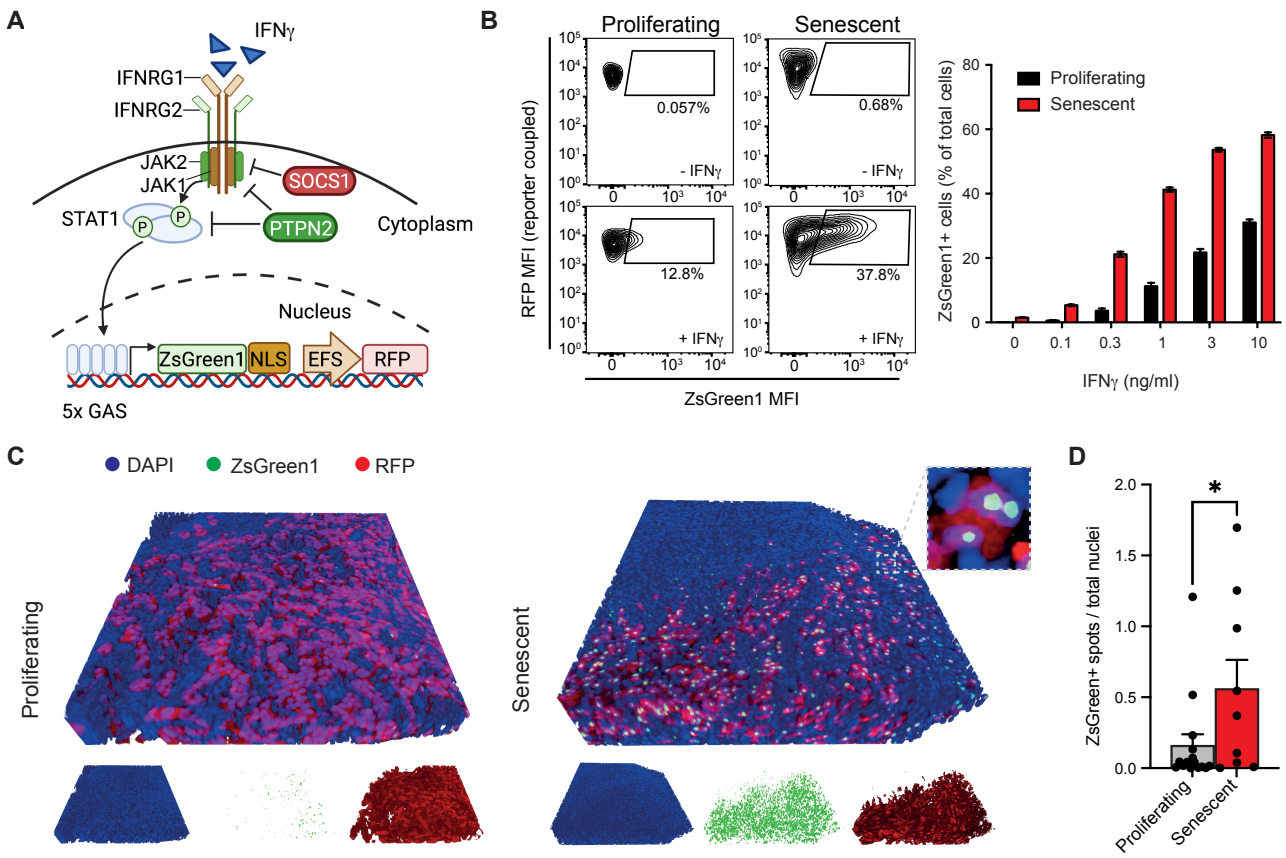
A
IFNγ
IFNRG1
IFNRG2
JAK2
JAK1
SOCS1
STAT1
P
P
PTPN2
Cytoplasm
Nucleus
ZsGreen1
NLS
EFS
RFP
5x GAS
B
Proliferating
Senescent
RFP MFI (reporter coupled)
0.057%
0.68%
- IFNγ
12.8%
37.8%
+ IFNγ
ZsGreen1 MFI
ZsGreen1+ cells (% of total cells)
Proliferating
Senescent
IFNγ (ng/ml)
C
DAPI
ZsGreen1
RFP
Proliferating
Senescent
D
ZsGreen+ spots / total nuclei
Proliferating
Senescent

Figure 8. Senescence enhances IFNγ signaling sensitivity in vivo

A, graphic illustration of IFNγ sensing (IGS) reporter. **B**, left, representative flow cytometry plots measuring ZsGreen1 signals in proliferating and senescent cells treated with 1 ng/ml IFNγ. Right, quantification of ZsGreen1 positive cells of total population upon IFNγ treatment. **C**, RepresentationTissue clearing images from the orthotopically injected liver tumor expressing IGS reporter-expressing. **D**, quantification of 3 randomly selected fields from each mouse. N=5 and N=3 for the proliferating and senescent tumor respectively.

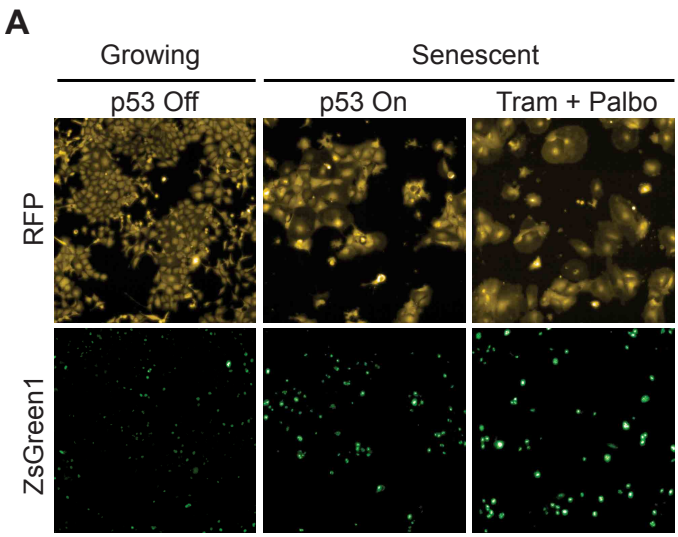
A
Growing
Senescent
p53 Off
p53 On
Tram + Palbo
RFP
ZsGreen1

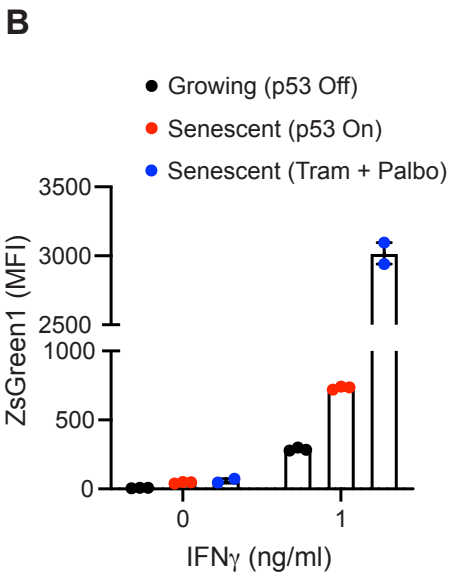
B
Growing (p53 Off)
Senescent (p53 On)
Senescent (Tram + Palbo)
ZsGreen1 (MFI)
3500
3000
2500
1000
500
0
0
1
IFNγ (ng/ml)

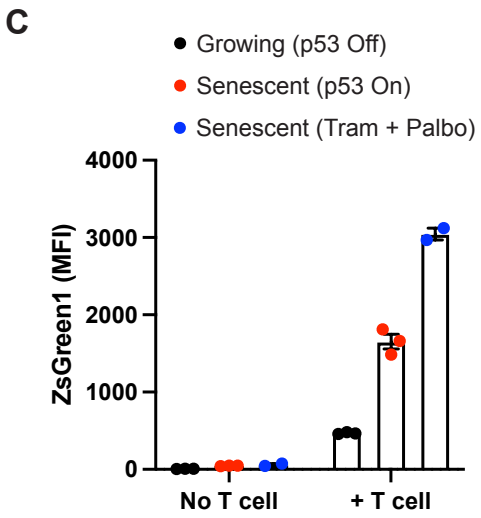
C
Growing (p53 Off)
Senescent (p53 On)
Senescent (Tram + Palbo)
ZsGreen1 (MFI)
4000
3000
2000
1000
0
No T cell
+ T cell

Figure 8.1. Increased sensitivity of IFNγ across different senescent triggers

A, representative microscopic images of IGS reporter-expressing cells treated with IFNγ under different senescent triggers. **B**, quantification of ZsGreen1 intensity from (**A**) through Guava flow cytometer. MFI, median fluorescence intensity. **C**, quantification of ZsGreen1 intensity in OT-I T cells and tumor cells co-culture experiments. Cells are trypsinized and measured after 20 hours of co-culture.

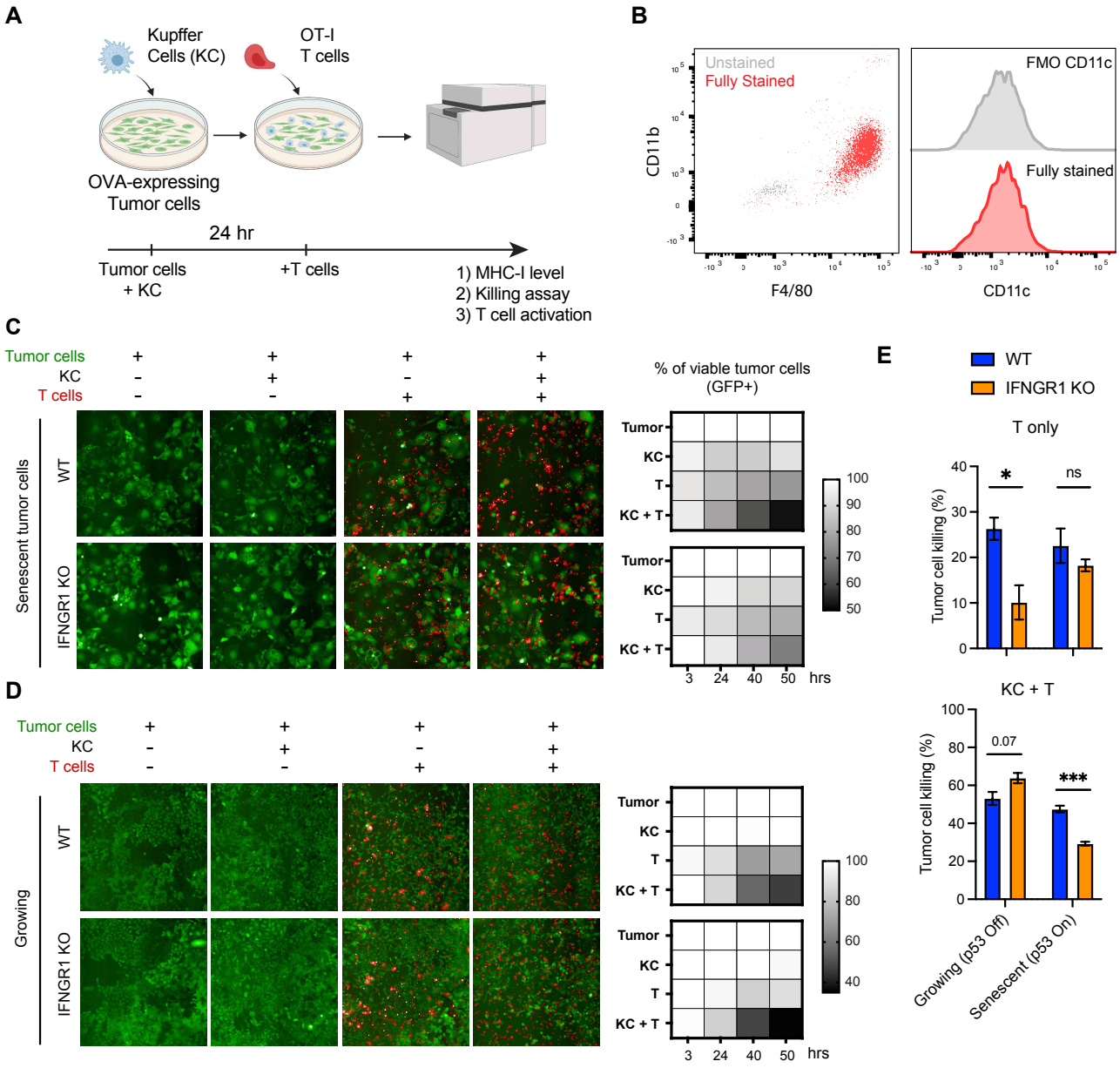
A
Kupffer Cells (KC)
OT-I T cells
OVA-expressing Tumor cells
24 hr
Tumor cells + KC
+T cells
1) MHC-I level
2) Killing assay
3) T cell activation
B
Unstained
Fully Stained
CD11b
F4/80
FMO CD11c
Fully stained
CD11c
C
Tumor cells
KC
T cells
Senescent tumor cells
WT
IFNGR1 KO
% of viable tumor cells (GFP+)
Tumor
KC
T
KC + T
3 24 40 50 hrs
100 90 80 70 60 50
D
Growing
E
WT
IFNGR1 KO
T only
Tumor cell killing (%)
*
ns
KC + T
0.07
***
Growing (p53 Off)
Senescent (p53 On)

Figure 8.2. CD8 T cells and macrophages cooperate to kill senescent cells in a IFNγ-dependent manner.

A, Schematic of triple co-culture with OT-I T cells, Kupffer cells (KC) and tumor cells. **B**, purity of KC examined by flow cytometry. **C** to **E**, time-lapsed co-culture assay images and quantification by measuring the number of GFP positive cells changes, normalized to the tumor cell only well as control. **C**, senescent cells and **D**, proliferating cells. **E**, quantification of the the final time point at 50 hours after co-culture.

IFNγ signaling is necessary for effective senescence surveillance

To interrogate the functional contribution of senescent cell-IFNγ signaling to immune-mediated surveillance, we first used CRISPR/Cas9-tools to knockout IFNGR1 in liver tumor cells and injected them into the liver of immunocompetent mice (Fig. 9A). We found that the senescence-induced regression triggered by p53 restoration was blunted in IFNGR1 KO tumors (Fig. 9B). Of note, while IFNGR1 KO did not affect basal MHC-I levels in tumor or senescent cells, it blunted MHC-I inducibility upon IFNγ treatment. In accordance, the KO of IFNGR1 mimicked effects of knockout of B2M, a critical component of MHC-I (Fig. 9.1A, B), demonstrating that intact cell-intrinsic IFNγ signaling is required for effective senescence surveillance in vivo (Fig. 9.1C).

As IFNγ is not secreted by senescent cells in vitro, we also assessed the effects of suppressing host derived IFNγ in senescent cell state and fate in vivo. To do so, we injected parental liver tumor cells into the livers of WT vs. IFNG KO mice orthotopically and assessed tumor regressions upon p53 restoration, as above. This showed that senescent tumor regressions are completely blunted (Fig. 9C, D). Strikingly, the immune infiltration phenotype is not abrogated upon senescence induction, as shown by flow cytometry results and histologic quantification of immune cells within senescent versus proliferating tumors (Fig. 7E, F; Fig. 9.1D-F), and consistent with a retained SASP response (Fig. 7B). In contrast, inactivation of host-derived IFNγ resulted in loss of MHC-I expression. This effect was specific to tumor cells, as immune cells and other normal cells still retained basal MHC-I levels (Fig. 9.1E). These data demonstrate a critical

contribution of heterotypic cell-cell interactions and tissue sensing programs of senescent cells for their effective elimination, and a decoupling from the immune recruitment mediated by SASP that is necessary but not sufficient for optimal senescence surveillance in vivo.

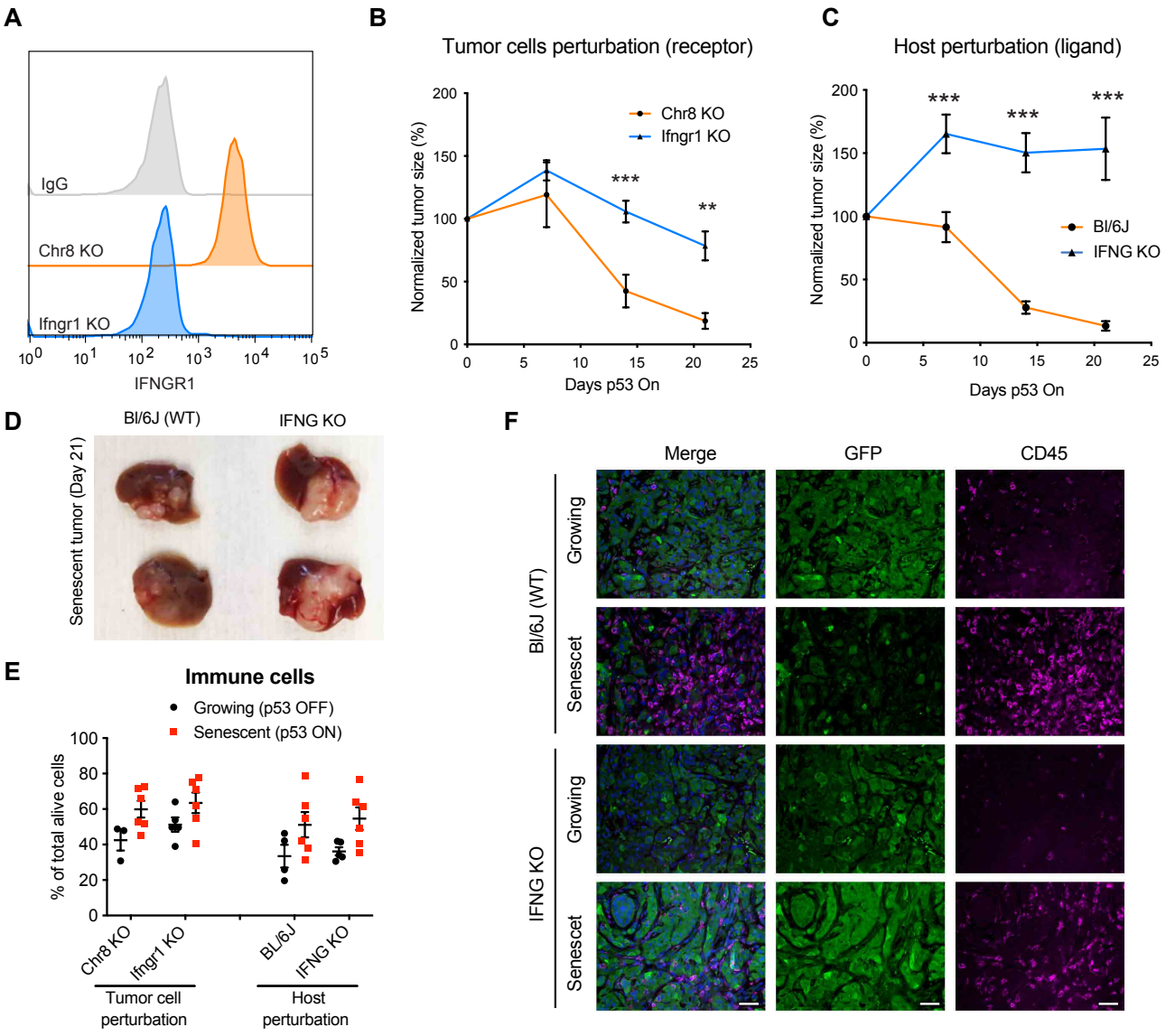
A
IgG
Chr8 KO
Ifngr1 KO
IFNGR1
B
Tumor cells perturbation (receptor)
Chr8 KO
Ifngr1 KO
Normalized tumor size (%)
Days p53 On
C
Host perturbation (ligand)
Bl/6J
IFNG KO
Normalized tumor size (%)
Days p53 On
D
Bl/6J (WT)
IFNG KO
Senescent tumor (Day 21)
E
Immune cells
Growing (p53 OFF)
Senescent (p53 ON)
% of total alive cells
Chr8 KO
Ifngr1 KO
BL/6J
IFNG KO
Tumor cell perturbation
Host perturbation
F
Merge
GFP
CD45
Bl/6J (WT)
IFNG KO
Growing
Senescet

Figure 9. IFNγ signaling is necessary for effective senescence surveillance

A, IFNGR1 knockout shown by flow cytometry. Chr8 KO serves as a neutral control. **B**, Senescent tumor regression phenotype of ifngr1 or Chr8 KO tumor cells orthotopically injected into WT Bl/6N mice. **C**, Senescent tumor regression phenotype of parental tumor cells orthotopically injected into WT or IFNG KO mice. **D**, representative macroscopic images of tumor collected at D21 from (**C**). **E**, immunophenotyping of tumor from indicated tumor cells or hosts, quantifying CD45 positive cells among total alive cells. **F**, representative immunofluorescence images of CD45 staining in proliferating and senescent tumor from indicated host.

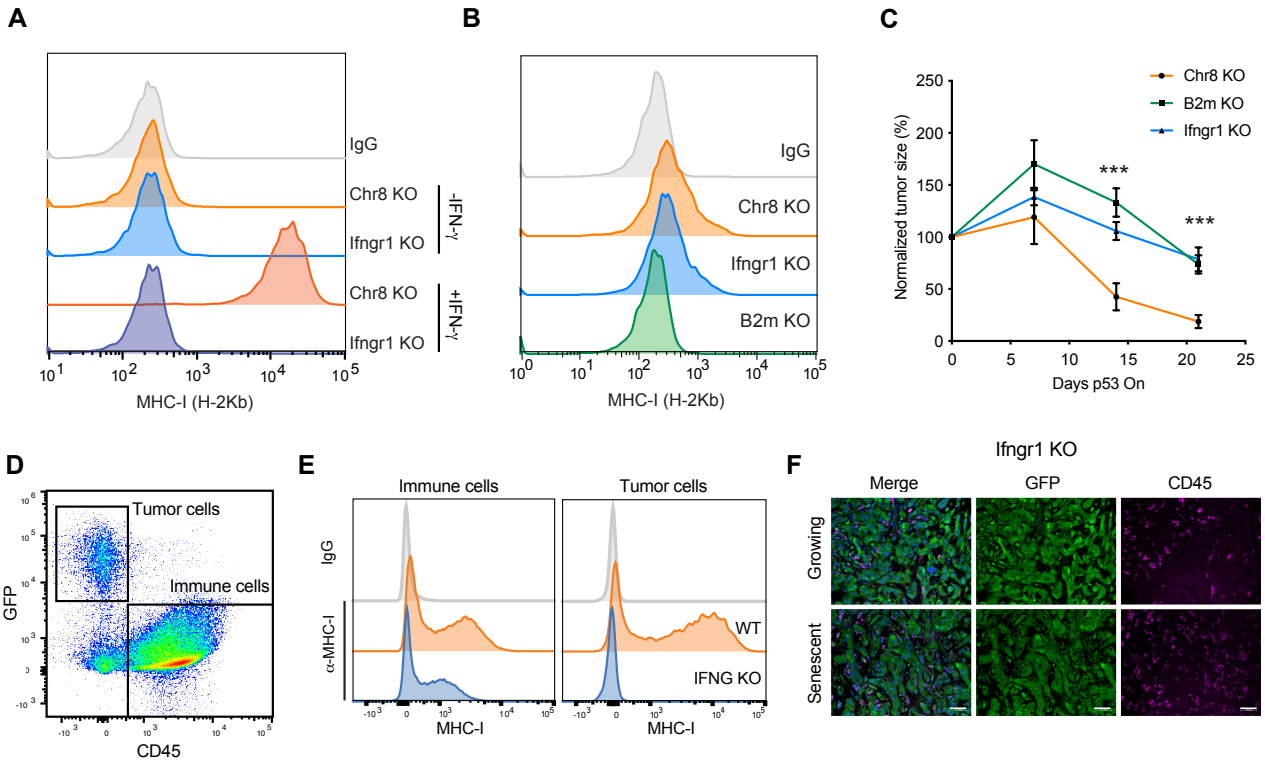
A
IgG
Chr8 KO
Ifngr1 KO
-IFN-γ
Chr8 KO
Ifngr1 KO
+IFN-γ
MHC-I (H-2Kb)
B
IgG
Chr8 KO
Ifngr1 KO
B2m KO
MHC-I (H-2Kb)
C
Chr8 KO
B2m KO
Ifngr1 KO
Normalized tumor size (%)
***
***
Days p53 On
D
Tumor cells
Immune cells
GFP
CD45
E
Immune cells
Tumor cells
IgG
α-MHC-I
WT
IFNG KO
MHC-I
MHC-I
F
Ifngr1 KO
Merge
GFP
CD45
Growing
Senescent

Figure 9.1. Blunting IFNGR1/IFNγ signaling in tumor cells phenocopies B2m knockout in senescence surveillance.

A, MHC-I level comparing Ifngr1 KO and Chr8 KO tumor cells treated with IFNg (1ng/ml). **B**, MHC-I level between Ch8r, Ifngr1 and B2m KO tumor cells. **C**, Senescent tumor regression phenotype of B2m KO comparing Ifngr1 KO and Chr8 KO. Figure was overlay with **Fig. 9B. D**, representative flow cytometry plots gating the GFP+ tumor cells and CD45+ immune cells. **E**, representative flow cytometry plots showing MHC-I level in tumor cells and immune cells from WT and IFNG KO mice. **F**, representative immunofluorescence images of CD45 staining in proliferating and senescent tumor from indicated host.

DISCUSSION

Senescence is a potent tumor suppressive program that (1) antagonizes cell cycle progression and (2) can elicit a robust immune surveillance response. However, the mechanistic basis by which senescence prevents tumor initiation can vary and is likely context dependent. In the discussion below, I will reconcile the various mechanisms of senescence described in the literature.

In contrast to the evidence provided in this thesis that demonstrates senescent cells are cleared by CD8+ T cells, it was previously reported that p53 restoration in liver tumor cells evoked a strong NK cell – dependent anti-tumor immune response (52). One explanation is that the previous study was performed in nude mice, which lack adaptive immunity, and therefore the contribution of T cells could not be investigated. Second, it is plausible that the cell of origin might influence immune recognition and clearance of senescent cells. For example, the previous studied derived senescent cells from liver progenitor cells, whereas the cells used in this study was generated from adult hepatocytes. In addition, the NK cell population in the immunocompetent liver tumor model only slightly increased upon senescence induction (1.5 -> 2.5%) (Fig. 4B), suggesting that NK cells didn't play a predominant role in senescence surveillance in our model. However, our results didn't completely contradict to the previous finding that by if we look more carefully at senescent tumor regression phenotype between nude and R2G2 mice (Fig. 3.1J), there is still a slight decrease of the tumor volume in nude mice whereas it is entirely abrogated in R2G2. This may suggest NK cells might still contribute to senescence surveillance while its effect may be masked by the presence of T cells.

In another study, senescent cells were cleared by macrophages and CD4 T cells. In this scenario, oncogenic RAS was expressed in hepatocytes directly with p53 intact. This differs from our study, whereby we restored p53 expression in RAS transformed hepatocytes to induce senescence. While senescence is the major phenotypic outcome in both experiments, these striking observations suggest that the order in which p53 is activated is critical for eliciting innate or adaptive immune surveillance programs.

One intriguinig possibility is that CD4 and CD8 T cells may mediate immune surveillance at different stages of malignancy. It was observed in mice challenged with OIS and harvested long after the premalignant hepatocytes were cleared (~3.5 months), that there was significant accumulation of CD8 T cells in the liver compared to PBS control. This observation supports the theory that CD4 and CD8 T cell mediated anti-tumor immunity may depend on the particular stage of tumorigenesis; however, such conclusions would need to be further validated experimentally.

In addition to cell-intrinsic factors, the microenvironment might also play an important role in determining what immune cell subtype may mediate the clearance of senescent cells. Two previous studies from our lab support a NK-dependent mechanism, while other studies favor a CD8 T-dependent mechanism. In support of this theory, it was observed that pancreatic cancer cells that metastasize to lung are more sensitive to NK-cell mediated clearance compared to primary tumor cells in the pancreas, which were eliminated by CD8 T cells. Furthermore, in our liver tumor model, we also also observed that senescence tumor regression response

differs between orthotopic injected liver tumor vs. subcutaneously transplanted tumor. Thus, it is plausible that the location and tissue type dictates whether senescent cells are cleared by adaptive of innate immune cells.

Although our p53 restoration senescence model is somewhat artificial given that the loss of p53 is an irreversible event during tumorigenesis, we uncovered some interesting biology that could be extended to other context of senescence beyond this model. Importantly, as our model triggered senescence in tumor cells specifically, we could therefore exclude some confounding factors that other senescence stimuli (such as drug or radiation therapy) that could also modulate the microenvironment such as activation of the immune system and stromal cells for anti-tumorigenic effect (79,80). It would be important to further validate our observation in other senescence context but a recent preprint study from Julian Downward group, who has made a similar finding of increased sensitivity towards IFNγ in Kras inhibitor treated lung cancer model, has given us some confidence in the generalizability of our findings.

Here we proposed a working model based on our findings that senescent tumor cells interact with the microenvironment in a reciprocal manner: 1) through the secreted proteins associated with SASP, recruit and activate the immune cells, particularly CD8 T cells and macrophages; 2) senescent cells remodel their surfaceome and signaling networks to receive and interpret the environmental signal differently that prime the senescent cells to environmental signals. Specially, in our model, we have demonstrated that different factors, both positively and negatively regulate the IFNγ signaling, have converged to jointly upregulate the

pathway to promote the antigen presentation program in senescent cells for appropriate immune recognition and together with SASP to achieve optimal senescence surveillance (Fig. 10).

Beyond our work demonstrating a differential sensitivity to IFNγ in senescent cells, it is conceivable that there are other sensing pathways that have been altered during senescence. Of note, calcium signaling has stood out as one of the top hits from GO analysis of differentially expressed genes encoding plasma membrane proteins. Calcium signaling has been linked to a broad range of cellular functions in several physiological contexts (103). Nonetheless, how this signaling is regulated in senescence and affects the microenvironment remains poorly understood. Moreover, the fact that other secretory factors independent of SASP could further modify senescent cells implies that the gene expression profiles we see in vitro will not fully predict what is observed in vivo, and this argues strongly for in vivo profiling studies to fully understand senescent states.

While the regulation of SASP is well understood, it has not been systemically characterized how the remodeling of surfaceome is regulated when cells are triggered to senesce. Interestingly, we found a coincidental dynamic that the genes encoding secreted factors and plasma membrane proteins seems to be jointly regulated in a Brd4-dependent manner (Fig. 5H). Brd4 is a chromatin reader that binds to the superenhencer region and recruit transcription factors to enhance gene transcription. It has been shown that Brd4 binds to the emerging superenhancer region adjacent to SASP genes during senescence to drive gene expression (38). It is intriguing to speculate that the epigenetic changes in

senescent cells lead to coordinate efforts to rewire both secretome and surfaceome simultaneously. These changes may jointly create a crosstalk feedback loop between senescent cells and neighboring cells to remodel the whole microenvironment. However, more mechanistic studies are entailed to support this hypothesis, including performing the chromatin profiling for the superenhancer changes and analysis on transcription factors driving those genes encoding PM factors to understand the underlying regulation.

Recently it has been demonstrated that type I Interferon (IFN) response is triggered at the late stage of senescence due to the de-repression of retrotransposable elements (RTEs) Those RTEs are reverse transcribed into cDNA and sensed by cGAS-STING to activate the downstream type I IFN. Interestingly, several studies from early 2000 has revealed that a great number of IFN pathway (majorly type I IFN) genes are silenced through DNA methylation during the process of immortalization in Li–Fraumeni syndrome (LFS) fibroblasts, and with the treatment of DNMT inhibitor it induced senescence in those cells and reactivated those IFN genes (104,105). The authors have concluded that IFN signaling, which have shown to exert a growth-suppressive through in a p53 and p21-dependent manner (106-108), may get silenced as an early event in acquisition to immortalization. These coinciding findings have together pointed toward a conclusion that the cell-intrinsic IFN pathway, more specifically type I IFN, is naturally evolved to be silenced during immortalization and can be reactivated during senescence induction. While most of the studies have linked senescence to type I IFN responses, less is known about the role of type II IFN (ie. IFNγ) in

senescence, probably due to the fact that IFNγ is not commonly reported as a SASP factor. Although both type I and II IFN signaling share some common downstream targets and thus they often come up together in the pathway analysis, the machinery to receive the exogenous ligand is different (109). Type I IFN pathway starts with interferons such as IFNα and IFNβ binding to common receptor IFNAR1/IFNAR2 and activating TYK2 and JAK1 respectively. It subsequently phosphorylates transcription factor STAT1 and STAT2 and leads to the formation of STAT1–STAT2–IRF9 complex to drive the transcription in the nucleus through binding to IFN-stimulated response elements (ISREs) in DNA. On the other hand, the receptor of type II IFN pathway is composed of two subunits, IFNGR1 and IFNGR2, in association with JAK1 and JAK2 respectively. Once binding to the ligand IFNγ, it activates STAT1–STAT1 homodimers that translocate to nucleus to bind to GAS for gene transcription. Notably, recent studies have identified Ptpn2 as a critical negative regulator specific to IFNγ signaling and the loss of Ptpn2 sensitized the tumor cells to CD8 T-mediated immune surveillance (100). We have found that by inducing senescence, Ptpn2 is mildly downregulated transcriptionally while more strikingly reduced at the protein level (Fig. 4C, D). The mechanisms of how Ptpn2 is downregulated in senescence requires more detailed investigation. In our study, we have demonstrated that IFNγ response is not only a hallmark of senescence as previously shown (43) but more interestingly, it is augmented in senescent cells in the presence of exogenous IFNγ comparing with their proliferating counterpart. This makes IFNγ signaling a new player to field of

senescence studies, in concert with type I IFN to jointly regulate immune responses.

It is well established that IFNγ plays a critical role in immune surveillance (110). For instance, it has been found that those non-responders to checkpoint blockade immunotherapy harboring mutations in IFNγ signaling pathway (111). However, some recent findings have also shown that the chronic exposure to IFNγ could lead to upregulation of PD-L1 expression and thus inhibit T cell activation, with the consequence of immune evasion (112,113). It has been thus proposed that whether IFNγ acting as anti- or pro-tumor role depends largely on the duration and magnitude of IFNγ signaling (112). In our case where senescence is induced in tumor cells, it could re-engage IFNγ signaling in an acute manner to facilitate the immune surveillance. However, whether senescent cells observed in other contexts (eg. senescent adipocytes and stromal cells during ageing) behave the same when receiving exogenous IFNγ signaling remains to be determined.

Finally, our study has revealed a potential mechanism of how senescence can provoke immune surveillance and also provide a rationale to use senescence-eliciting agents to further potentiate immunotherapy. Although our study primarily used liver cancer as the model for senescence, we expect our findings can be extended to other cancer contexts where senescence induction in tumor cells could synergize with immunotherapy.

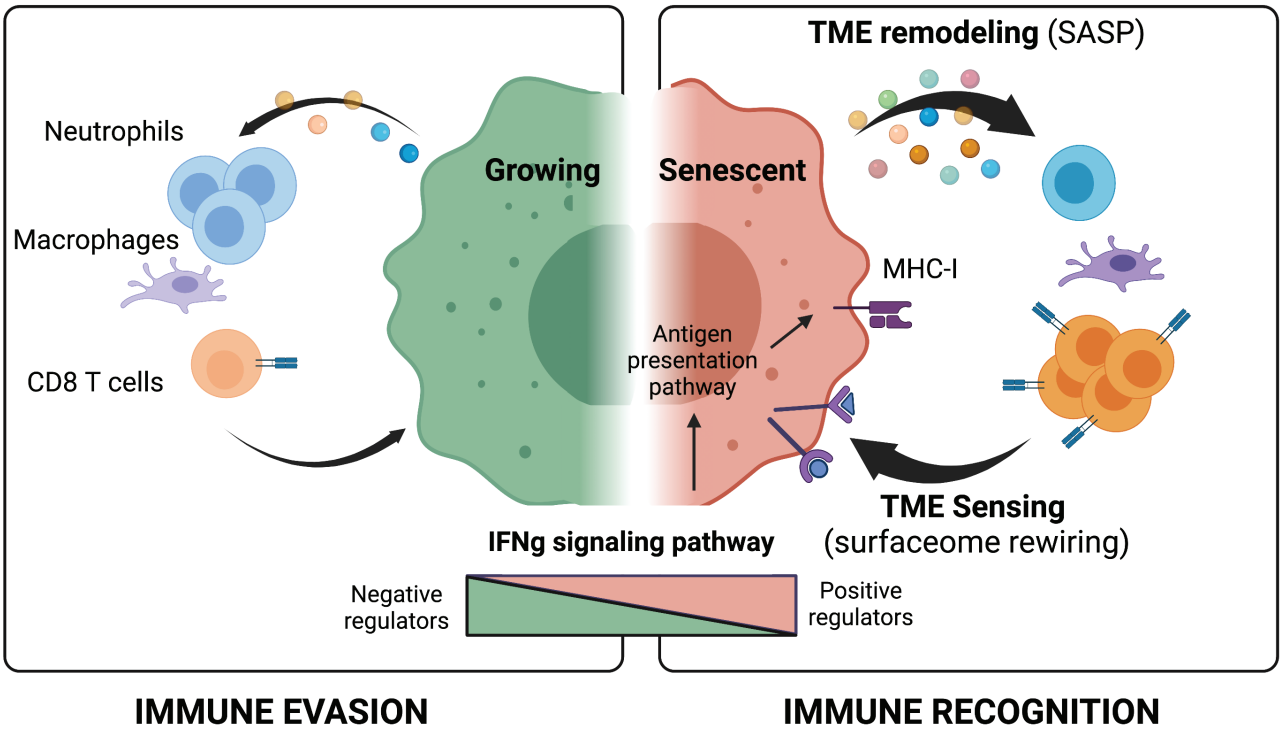

Figure 10. Senescence rewires the microenvironment sensing program to facilitate immune surveillance

FUTURE PERSPECTIVES

Advancing the first part of my thesis, we have also performed scRNA-seq analysis in both proliferating and senescent tumor on tumor, immune and stromal cells to obtain a comprehensive picture of tumor and microenvironmental changes upon senescence induction in vivo. Particularly, we would like to have more granularity on the immune cells part as it might shed some light about how CD8 T cells and macrophages interact with each other to mediate senescence surveillance in our model. In light of a recently published study in the context of HBV infection, it appears that liver macrophages, or Kupffer cells, can present viral antigens to the CD8 T cells to re-invigorate the cytotoxic activity against HBV-infected hepatocytes (114). We therefore are wondering whether macrophages help cross-present the antigens to CD8 T cells for tumor cells recognition in our model.

Transcriptomic analysis of macrophages and T cells, whether at the single cell or bulk level, should provide valuable insight into the signaling pathway that might be rewired in these two cell types. Moreover, our consistent in vitro finding that T cells and macrophages cooperate for killing senescent cells suggested that it could be also a useful assay to interrogate such interactions in a more manageable manner. Other ongoing studies are incorporating intravital microscopy to observe in real-time the interaction between immune cells and tumor cells. Here, we expect to see different waves of immune infiltration during senescence induction. Another interesting question is where those immune cells are coming from and where they might go afterwards. As our current study only

record the immune landscape at one snapshot in time, the incorporation of intravital microscopy would undoubtedly unveil additional aspects of senescence immune surveillance.

From the tumor perspective, the concept that in vitro and in vivo senescence might differ a lot is an attractive and provocative hypothesis to test. From our study, it is suggested that the tumor cells might lack of intact signaling coming from the microenvironment to complete the senescence transcription program. We would expect our scRNA-seq might also shed some light on this perspective regarding the difference between in vitro and in vivo and also the heterogeneity lying amount the senescent cells themselves. Another interesting question arises from our work: what are the underlying molecular mechanisms of differential sensitivity towards IFNγ between senescent and proliferating tumor cells? Coincidentally, a recent preprint study from Julian Downward group has documented a relevant finding that KrasG12C inhibition through drug increased the tumor sensitivity towards both type I and II IFN signaling in a lung cancer model. They linked this increased sensitivity towards to the downregulation of Myc when Ras is inhibited. Interesting, senescence is also known to downregulate Myc transcriptional output, and thus this might also serve as a plausible explanation for our observation. The transcription factor analysis on those IFN sensing genes might be us some more clues how this pathway is concomitantly regulated during senescence. And these findings will be relevant for understanding the underlying mechanisms to overcome the resistance to immunotherapy by re-engaging IFNγ signaling in tumor cells.

APPENDIX

Identification of cell surface factors as novel targets for senolytics

Here, I will briefly discuss the ongoing work performing an in vitro shRNA pooled screen using the aforementioned Nras-shp53 liver tumor cells lines. As p53-restored senescent cells have undergone substantial transcriptional and proteomic changes, we hypothesized that some factors may be critical for maintaining the survival of those cells. We have thus selected the differentially expressed genes from the RNA-seq and also PM-enriched MS analyses to assemble the gene list for functional genetic screen. We have divided those genes into several subgroups based on the subcellular compartments, including cytoplasmic, nucleus, plasma membrane, and extracellular region.

Based on our previous finding that senescent cells exhibit a drastic change on the cell surfaceome, we decided to focus on those factors to identify potential targets for senolytics. We have thus used a library containing 147 genes chosen from the DEGs in our MS analysis. With 6 shRNA replicates targeting individual genes, we have about 1000 shRNA in total, including the essential gene and neutral control, in our library. As our initial proposal is to have a focused library with small size so that we can simultaneously perform in vitro and in vivo screen, we estimated how many clones that can be recovered from our Nras-shp53 liver cancer model. Our preliminary results showed that from a library of 3000 barcodes, an average of 700-800 barcodes can be well recovered with good representation (Fig. 11A). Thus, we decided to divide our initial library into 2 sub-libraries

containing about 500 shRNA each to make it more feasible for the in vivo screen. Due to the limited time, we have so far only performed the in vitro screen.

As shown in Fig. 11B, we used three orthogonal Nras-p53 liver cell lines for screening and collected the cells at 4 indicated timepoints for comparison. That is the initial timepoint (T0D), at least 15 doublings in the proliferating condition (T9G), early senescent timepoint (T10S) and also late senescent timepoint where the bypasser cells might ourgrow (T15S). The goal of study can be divided into three arms based on the comparison we can make: 1) Identify targets eliciting tumor suppressive effect in the proliferating cells (T9G vs. T0D, Fig. 11C). 2) Identify targets eliciting senolytic effect in the senescent cells (T10S vs. T0D, Fig. 10D right red box). We further make the criteria stricter by comparing (T10S vs. T9G) to eliminate targets that have effects on both proliferating and senescent cells. 3) Identify targets that may help bypass senescence (T15S vs. T10s, Fig. 10D left red box). By intersecting the hits between 3 cell lines, we have found two putative targets shown in figure 12. The rest of the other candidates are still under analysis. As it is still at the early stage of the screen, the functional validation is currently still ongoing, and we haven't looked into any specific biology behind yet so far. Given the beneficial effect of eliminating senescent cells in a timely manner, our ultimate goal is to identify novel senolytic targets that can be exploited in cancer therapeutics as well as in treatment for other aging-related pathologies.

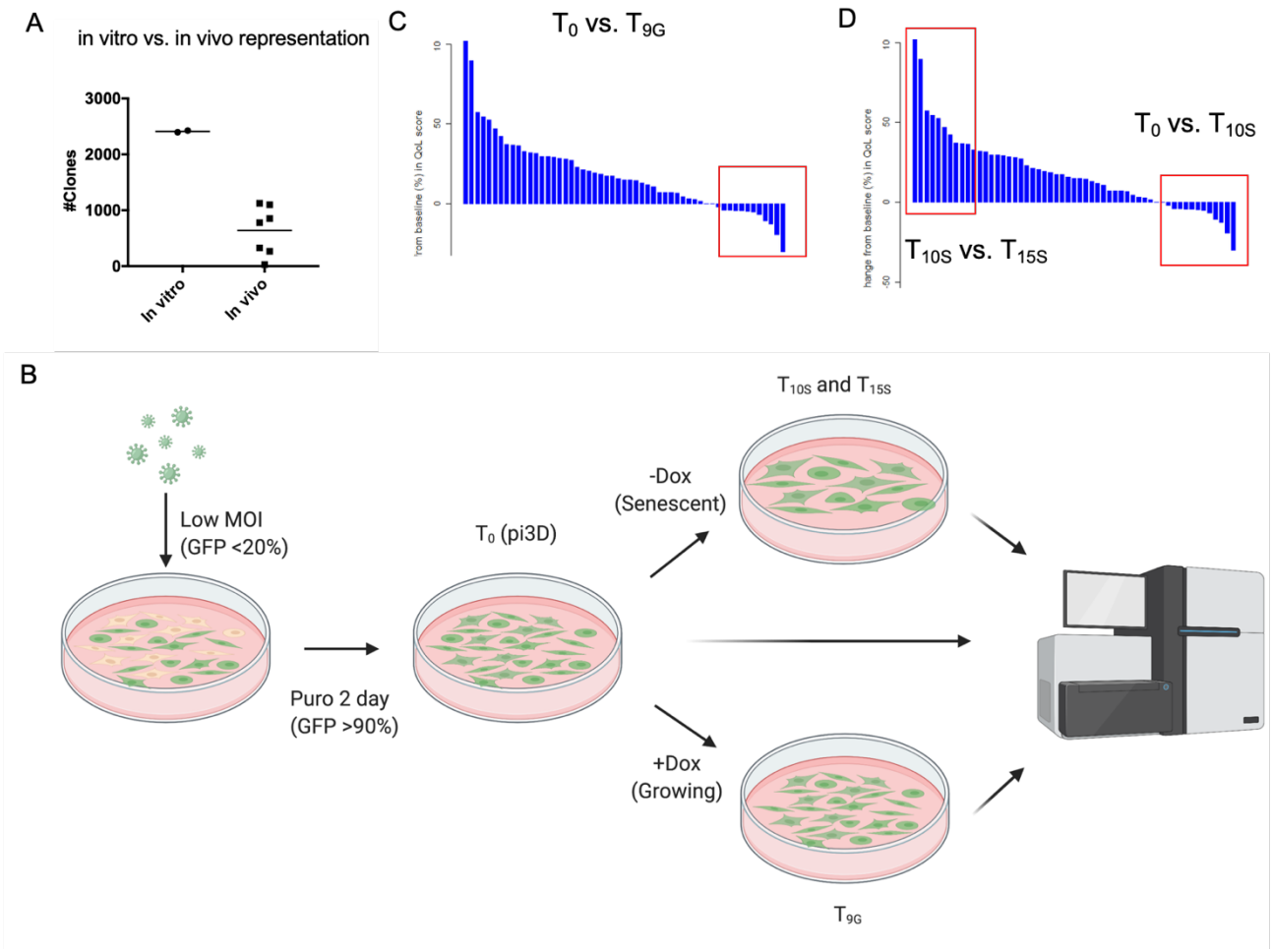

Figure 11. Experimental setup of shRNA pooled screen to identify novel senolytic targets.

A, Comparison between in vitro vs. in vivo barcode recovery as a strategy to identify optimal number of shRNA used for in vivo study. **B**, experimental design of the screen setup. **C**, waterfall plot for identifying targets depleted in the proliferating setting. **D**, waterfall plot for identifying targets depleted and enriched in the senescent setting.

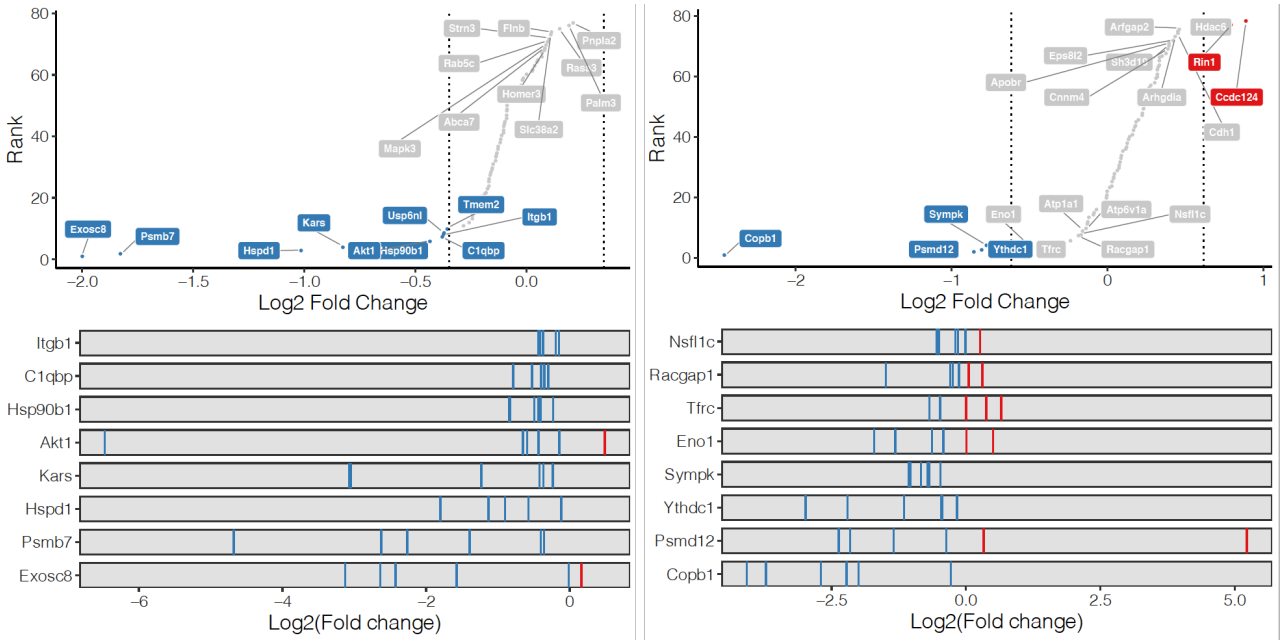

Figure 12. Putative targets in the proliferating group comparsion from two sub-libraries.

By comparing T9G vs. T0D: blue dots indicated depleted hits whereas rot dots indicated enriched hits. Noted some of the top targets are listed as essential genes in our library, thus could be excluded for further study.

BIBLIOGRAPHY

1. Hayflick L, Moorhead PS. The serial cultivation of human diploid cell strains. Experimental cell research **1961**;25:585-621 doi 10.1016/0014-4827(61)90192-6.
2. d'Adda di Fagagna F, Reaper PM, Clay-Farrace L, Fiegler H, Carr P, Von Zglinicki T*, et al.* A DNA damage checkpoint response in telomere-initiated senescence. Nature **2003**;426(6963):194-8 doi 10.1038/nature02118.
3. Herbig U, Jobling WA, Chen BP, Chen DJ, Sedivy JM. Telomere shortening triggers senescence of human cells through a pathway involving ATM, p53, and p21(CIP1), but not p16(INK4a). Mol Cell **2004**;14(4):501-13 doi 10.1016/s1097-2765(04)00256-4.
4. Di Micco R, Fumagalli M, Cicalese A, Piccinin S, Gasparini P, Luise C*, et al.* Oncogene-induced senescence is a DNA damage response triggered by DNA hyper-replication. Nature **2006**;444(7119):638-42 doi 10.1038/nature05327.
5. Bartkova J, Rezaei N, Liontos M, Karakaidos P, Kletsas D, Issaeva N*, et al.* Oncogene-induced senescence is part of the tumorigenesis barrier imposed by DNA damage checkpoints. Nature **2006**;444(7119):633-7 doi 10.1038/nature05268.
6. Ewald JA, Desotelle JA, Wilding G, Jarrard DF. Therapy-induced senescence in cancer. Journal of the National Cancer Institute **2010**;102(20):1536-46 doi 10.1093/jnci/djq364.
7. Halazonetis TD, Gorgoulis VG, Bartek J. An oncogene-induced DNA damage model for cancer development. Science **2008**;319(5868):1352-5 doi 10.1126/science.1140735.
8. Serrano M, Lin AW, McCurrach ME, Beach D, Lowe SW. Oncogenic ras provokes premature cell senescence associated with accumulation of p53 and p16INK4a. Cell **1997**;88(5):593-602 doi 10.1016/s0092-8674(00)81902-9.
9. Fumagalli M, Rossiello F, Clerici M, Barozzi S, Cittaro D, Kaplunov JM*, et al.* Telomeric DNA damage is irreparable and causes persistent DNA-damage-response activation. Nature cell biology **2012**;14(4):355-65 doi 10.1038/ncb2466.
10. Neurohr GE, Terry RL, Lengefeld J, Bonney M, Brittingham GP, Moretto F*, et al.* Excessive Cell Growth Causes Cytoplasm Dilution And Contributes to Senescence. Cell **2019**;176(5):1083-97 e18 doi 10.1016/j.cell.2019.01.018.
11. Dimri GP, Lee X, Basile G, Acosta M, Scott G, Roskelley C*, et al.* A biomarker that identifies senescent human cells in culture and in aging skin in vivo. Proc Natl Acad Sci U S A **1995**;92(20):9363-7 doi 10.1073/pnas.92.20.9363.
12. Yang NC, Hu ML. The limitations and validities of senescence associated-beta-galactosidase activity as an aging marker for human foreskin fibroblast Hs68 cells. Exp Gerontol **2005**;40(10):813-9 doi 10.1016/j.exger.2005.07.011.

13. Chapman J, Fielder E, Passos JF. Mitochondrial dysfunction and cell senescence: deciphering a complex relationship. FEBS Lett **2019**;593(13):1566-79 doi 10.1002/1873-3468.13498.
14. Beausejour CM, Krtolica A, Galimi F, Narita M, Lowe SW, Yaswen P*, et al.* Reversal of human cellular senescence: roles of the p53 and p16 pathways. The EMBO journal **2003**;22(16):4212-22 doi 10.1093/emboj/cdg417.
15. Dulic V, Beney GE, Frebourg G, Drullinger LF, Stein GH. Uncoupling between phenotypic senescence and cell cycle arrest in aging p21-deficient fibroblasts. Molecular and cellular biology **2000**;20(18):6741-54 doi 10.1128/MCB.20.18.6741-6754.2000.
16. Coppe JP, Patil CK, Rodier F, Sun Y, Munoz DP, Goldstein J*, et al.* Senescence-associated secretory phenotypes reveal cell-nonautonomous functions of oncogenic RAS and the p53 tumor suppressor. PLoS biology **2008**;6(12):2853-68 doi 10.1371/journal.pbio.0060301.
17. Coppe JP, Rodier F, Patil CK, Freund A, Desprez PY, Campisi J. Tumor suppressor and aging biomarker p16(INK4a) induces cellular senescence without the associated inflammatory secretory phenotype. J Biol Chem **2011**;286(42):36396-403 doi 10.1074/jbc.M111.257071.
18. Yosef R, Pilpel N, Tokarsky-Amiel R, Biran A, Ovadya Y, Cohen S*, et al.* Directed elimination of senescent cells by inhibition of BCL-W and BCL-XL. Nature communications **2016**;7:11190 doi 10.1038/ncomms11190.
19. Sanchez-Rivera FJ, Ryan J, Soto-Feliciano YM, Clare Beytagh M, Xuan L, Feldser DM*, et al.* Mitochondrial apoptotic priming is a key determinant of cell fate upon p53 restoration. Proc Natl Acad Sci U S A **2021**;118(23) doi 10.1073/pnas.2019740118.
20. Sagiv A, Krizhanovsky V. Immunosurveillance of senescent cells: the bright side of the senescence program. Biogerontology **2013**;14(6):617-28 doi 10.1007/s10522-013-9473-0.
21. Chang J, Wang Y, Shao L, Laberge RM, Demaria M, Campisi J*, et al.* Clearance of senescent cells by ABT263 rejuvenates aged hematopoietic stem cells in mice. Nat Med **2016**;22(1):78-83 doi 10.1038/nm.4010.
22. Zhang R, Chen W, Adams PD. Molecular dissection of formation of senescence-associated heterochromatin foci. Molecular and cellular biology **2007**;27(6):2343-58 doi 10.1128/MCB.02019-06.
23. Di Micco R, Sulli G, Dobreva M, Liontos M, Botrugno OA, Gargiulo G*, et al.* Interplay between oncogene-induced DNA damage response and heterochromatin in senescence and cancer. Nature cell biology **2011**;13(3):292-302 doi 10.1038/ncb2170.
24. Samaraweera L, Adomako A, Rodriguez-Gabin A, McDaid HM. A Novel Indication for Panobinostat as a Senolytic Drug in NSCLC and HNSCC. Scientific reports **2017**;7(1):1900 doi 10.1038/s41598-017-01964-1.
25. Swanson EC, Manning B, Zhang H, Lawrence JB. Higher-order unfolding of satellite heterochromatin is a consistent and early event in cell senescence. The Journal of cell biology **2013**;203(6):929-42 doi 10.1083/jcb.201306073.

26. Dou Z, Xu C, Donahue G, Shimi T, Pan JA, Zhu J*, et al.* Autophagy mediates degradation of nuclear lamina. Nature **2015**;527(7576):105-9 doi 10.1038/nature15548.
27. Dou Z, Ghosh K, Vizioli MG, Zhu J, Sen P, Wangensteen KJ*, et al.* Cytoplasmic chromatin triggers inflammation in senescence and cancer. Nature **2017**;550(7676):402-6 doi 10.1038/nature24050.
28. Yang H, Wang H, Ren J, Chen Q, Chen ZJ. cGAS is essential for cellular senescence. Proc Natl Acad Sci U S A **2017**;114(23):E4612-E20 doi 10.1073/pnas.1705499114.
29. Gluck S, Guey B, Gulen MF, Wolter K, Kang TW, Schmacke NA*, et al.* Innate immune sensing of cytosolic chromatin fragments through cGAS promotes senescence. Nature cell biology **2017**;19(9):1061-70 doi 10.1038/ncb3586.
30. Kuilman T, Michaloglou C, Mooi WJ, Peeper DS. The essence of senescence. Genes & development **2010**;24(22):2463-79 doi 10.1101/gad.1971610.
31. Wajapeyee N, Serra RW, Zhu X, Mahalingam M, Green MR. Oncogenic BRAF induces senescence and apoptosis through pathways mediated by the secreted protein IGFBP7. Cell **2008**;132(3):363-74 doi 10.1016/j.cell.2007.12.032.
32. Xu M, Pirtskhalava T, Farr JN, Weigand BM, Palmer AK, Weivoda MM*, et al.* Senolytics improve physical function and increase lifespan in old age. Nat Med **2018**;24(8):1246-56 doi 10.1038/s41591-018-0092-9.
33. Basisty N, Kale A, Jeon OH, Kuehnemann C, Payne T, Rao C*, et al.* A proteomic atlas of senescence-associated secretomes for aging biomarker development. PLoS biology **2020**;18(1):e3000599 doi 10.1371/journal.pbio.3000599.
34. Hernandez-Segura A, de Jong TV, Melov S, Guryev V, Campisi J, Demaria M. Unmasking Transcriptional Heterogeneity in Senescent Cells. Curr Biol **2017**;27(17):2652-60 e4 doi 10.1016/j.cub.2017.07.033.
35. Hoare M, Ito Y, Kang TW, Weekes MP, Matheson NJ, Patten DA*, et al.* NOTCH1 mediates a switch between two distinct secretomes during senescence. Nature cell biology **2016**;18(9):979-92 doi 10.1038/ncb3397.
36. Chien Y, Scuoppo C, Wang X, Fang X, Balgley B, Bolden JE*, et al.* Control of the senescence-associated secretory phenotype by NF-kappaB promotes senescence and enhances chemosensitivity. Genes & development **2011**;25(20):2125-36 doi 10.1101/gad.17276711.
37. Kuilman T, Michaloglou C, Vredeveld LC, Douma S, van Doorn R, Desmet CJ*, et al.* Oncogene-induced senescence relayed by an interleukin-dependent inflammatory network. Cell **2008**;133(6):1019-31 doi 10.1016/j.cell.2008.03.039.
38. Tasdemir N, Banito A, Roe JS, Alonso-Curbelo D, Camiolo M, Tschaharganeh DF*, et al.* BRD4 Connects Enhancer Remodeling to Senescence Immune Surveillance. Cancer discovery **2016**;6(6):612-29 doi 10.1158/2159-8290.CD-16-0217.

39. Ito T, Teo YV, Evans SA, Neretti N, Sedivy JM. Regulation of Cellular Senescence by Polycomb Chromatin Modifiers through Distinct DNA Damage- and Histone Methylation-Dependent Pathways. Cell reports **2018**;22(13):3480-92 doi 10.1016/j.celrep.2018.03.002.
40. Rodier F, Coppe JP, Patil CK, Hoeijmakers WA, Munoz DP, Raza SR*, et al.* Persistent DNA damage signalling triggers senescence-associated inflammatory cytokine secretion. Nature cell biology **2009**;11(8):973-9 doi 10.1038/ncb1909.
41. Yu Q, Katlinskaya YV, Carbone CJ, Zhao B, Katlinski KV, Zheng H*, et al.* DNA-damage-induced type I interferon promotes senescence and inhibits stem cell function. Cell reports **2015**;11(5):785-97 doi 10.1016/j.celrep.2015.03.069.
42. De Cecco M, Ito T, Petrashen AP, Elias AE, Skvir NJ, Criscione SW*, et al.* L1 drives IFN in senescent cells and promotes age-associated inflammation. Nature **2019**;566(7742):73-8 doi 10.1038/s41586-018-0784-9.
43. Jochems F, Thijssen B, De Conti G, Jansen R, Pogacar Z, Groot K*, et al.* The Cancer SENESCopedia: A delineation of cancer cell senescence. Cell reports **2021**;36(4):109441 doi 10.1016/j.celrep.2021.109441.
44. Rhinn M, Ritschka B, Keyes WM. Cellular senescence in development, regeneration and disease. Development **2019**;146(20) doi 10.1242/dev.151837.
45. Storer M, Mas A, Robert-Moreno A, Pecoraro M, Ortells MC, Di Giacomo V*, et al.* Senescence is a developmental mechanism that contributes to embryonic growth and patterning. Cell **2013**;155(5):1119-30 doi 10.1016/j.cell.2013.10.041.
46. Munoz-Espin D, Canamero M, Maraver A, Gomez-Lopez G, Contreras J, Murillo-Cuesta S*, et al.* Programmed cell senescence during mammalian embryonic development. Cell **2013**;155(5):1104-18 doi 10.1016/j.cell.2013.10.019.
47. Krizhanovsky V, Yon M, Dickins RA, Hearn S, Simon J, Miething C*, et al.* Senescence of activated stellate cells limits liver fibrosis. Cell **2008**;134(4):657-67 doi 10.1016/j.cell.2008.06.049.
48. Lujambio A, Akkari L, Simon J, Grace D, Tschaharganeh DF, Bolden JE*, et al.* Non-cell-autonomous tumor suppression by p53. Cell **2013**;153(2):449-60 doi 10.1016/j.cell.2013.03.020.
49. Demaria M, Ohtani N, Youssef SA, Rodier F, Toussaint W, Mitchell JR*, et al.* An essential role for senescent cells in optimal wound healing through secretion of PDGF-AA. Developmental cell **2014**;31(6):722-33 doi 10.1016/j.devcel.2014.11.012.
50. Acosta JC, O'Loghlen A, Banito A, Guijarro MV, Augert A, Raguz S*, et al.* Chemokine signaling via the CXCR2 receptor reinforces senescence. Cell **2008**;133(6):1006-18 doi 10.1016/j.cell.2008.03.038.
51. Kang TW, Yevsa T, Woller N, Hoenicke L, Wuestefeld T, Dauch D*, et al.* Senescence surveillance of pre-malignant hepatocytes limits liver cancer development. Nature **2011**;479(7374):547-51 doi 10.1038/nature10599.

52. Xue W, Zender L, Miething C, Dickins RA, Hernando E, Krizhanovsky V*, et al.* Senescence and tumour clearance is triggered by p53 restoration in murine liver carcinomas. Nature **2007**;445(7128):656-60 doi 10.1038/nature05529.
53. Ruscetti M, Leibold J, Bott MJ, Fennell M, Kulick A, Salgado NR*, et al.* NK cell-mediated cytotoxicity contributes to tumor control by a cytostatic drug combination. Science **2018**;362(6421):1416-22 doi 10.1126/science.aas9090.
54. Ruscetti M, Morris JPt, Mezzadra R, Russell J, Leibold J, Romesser PB*, et al.* Senescence-Induced Vascular Remodeling Creates Therapeutic Vulnerabilities in Pancreas Cancer. Cell **2020**;181(2):424-41 e21 doi 10.1016/j.cell.2020.03.008.
55. Coppe JP, Desprez PY, Krtolica A, Campisi J. The senescence-associated secretory phenotype: the dark side of tumor suppression. Annual review of pathology **2010**;5:99-118 doi 10.1146/annurev-pathol-121808-102144.
56. Childs BG, Baker DJ, Wijshake T, Conover CA, Campisi J, van Deursen JM. Senescent intimal foam cells are deleterious at all stages of atherosclerosis. Science **2016**;354(6311):472-7 doi 10.1126/science.aaf6659.
57. Bird TG, Muller M, Boulter L, Vincent DF, Ridgway RA, Lopez-Guadamillas E*, et al.* TGFbeta inhibition restores a regenerative response in acute liver injury by suppressing paracrine senescence. Science translational medicine **2018**;10(454) doi 10.1126/scitranslmed.aan1230.
58. Childs BG, Durik M, Baker DJ, van Deursen JM. Cellular senescence in aging and age-related disease: from mechanisms to therapy. Nat Med **2015**;21(12):1424-35 doi 10.1038/nm.4000.
59. Franceschi C, Garagnani P, Parini P, Giuliani C, Santoro A. Inflammaging: a new immune-metabolic viewpoint for age-related diseases. Nat Rev Endocrinol **2018**;14(10):576-90 doi 10.1038/s41574-018-0059-4.
60. Baker DJ, Wijshake T, Tchkonia T, LeBrasseur NK, Childs BG, van de Sluis B*, et al.* Clearance of p16Ink4a-positive senescent cells delays ageing-associated disorders. Nature **2011**;479(7372):232-6 doi 10.1038/nature10600.
61. Baker DJ, Childs BG, Durik M, Wijers ME, Sieben CJ, Zhong J*, et al.* Naturally occurring p16(Ink4a)-positive cells shorten healthy lifespan. Nature **2016**;530(7589):184-9 doi 10.1038/nature16932.
62. Ortiz-Montero P, Londono-Vallejo A, Vernot JP. Senescence-associated IL-6 and IL-8 cytokines induce a self- and cross-reinforced senescence/inflammatory milieu strengthening tumorigenic capabilities in the MCF-7 breast cancer cell line. Cell Commun Signal **2017**;15(1):17 doi 10.1186/s12964-017-0172-3.
63. Davalos AR, Coppe JP, Campisi J, Desprez PY. Senescent cells as a source of inflammatory factors for tumor progression. Cancer metastasis reviews **2010**;29(2):273-83 doi 10.1007/s10555-010-9220-9.
64. Eggert T, Wolter K, Ji J, Ma C, Yevsa T, Klotz S*, et al.* Distinct Functions of Senescence-Associated Immune Responses in Liver Tumor Surveillance

and Tumor Progression. Cancer cell **2016**;30(4):533-47 doi 10.1016/j.ccell.2016.09.003.
65. Di Mitri D, Toso A, Chen JJ, Sarti M, Pinton S, Jost TR*, et al.* Tumour-infiltrating Gr-1+ myeloid cells antagonize senescence in cancer. Nature **2014**;515(7525):134-7 doi 10.1038/nature13638.
66. Parrinello S, Coppe JP, Krtolica A, Campisi J. Stromal-epithelial interactions in aging and cancer: senescent fibroblasts alter epithelial cell differentiation. Journal of cell science **2005**;118(Pt 3):485-96 doi 10.1242/jcs.01635.
67. Laberge RM, Awad P, Campisi J, Desprez PY. Epithelial-mesenchymal transition induced by senescent fibroblasts. Cancer Microenviron **2012**;5(1):39-44 doi 10.1007/s12307-011-0069-4.
68. Demaria M, O'Leary MN, Chang J, Shao L, Liu S, Alimirah F*, et al.* Cellular Senescence Promotes Adverse Effects of Chemotherapy and Cancer Relapse. Cancer discovery **2017**;7(2):165-76 doi 10.1158/2159-8290.CD-16-0241.
69. Wiley CD, Liu S, Limbad C, Zawadzka AM, Beck J, Demaria M*, et al.* SILAC Analysis Reveals Increased Secretion of Hemostasis-Related Factors by Senescent Cells. Cell reports **2019**;28(13):3329-37 e5 doi 10.1016/j.celrep.2019.08.049.
70. Zhu Y, Tchkonia T, Pirtskhalava T, Gower AC, Ding H, Giorgadze N*, et al.* The Achilles' heel of senescent cells: from transcriptome to senolytic drugs. Aging Cell **2015**;14(4):644-58 doi 10.1111/acel.12344.
71. Hickson LJ, Langhi Prata LGP, Bobart SA, Evans TK, Giorgadze N, Hashmi SK*, et al.* Senolytics decrease senescent cells in humans: Preliminary report from a clinical trial of Dasatinib plus Quercetin in individuals with diabetic kidney disease. EBioMedicine **2019**;47:446-56 doi 10.1016/j.ebiom.2019.08.069.
72. Fuhrmann-Stroissnigg H, Ling YY, Zhao J, McGowan SJ, Zhu Y, Brooks RW*, et al.* Identification of HSP90 inhibitors as a novel class of senolytics. Nature communications **2017**;8(1):422 doi 10.1038/s41467-017-00314-z.
73. Wang L, Leite de Oliveira R, Wang C, Fernandes Neto JM, Mainardi S, Evers B*, et al.* High-Throughput Functional Genetic and Compound Screens Identify Targets for Senescence Induction in Cancer. Cell reports **2017**;21(3):773-83 doi 10.1016/j.celrep.2017.09.085.
74. Wang C, Vegna S, Jin H, Benedict B, Lieftink C, Ramirez C*, et al.* Inducing and exploiting vulnerabilities for the treatment of liver cancer. Nature **2019**;574(7777):268-72 doi 10.1038/s41586-019-1607-3.
75. Amor C, Feucht J, Leibold J, Ho YJ, Zhu C, Alonso-Curbelo D*, et al.* Senolytic CAR T cells reverse senescence-associated pathologies. Nature **2020**;583(7814):127-32 doi 10.1038/s41586-020-2403-9.
76. Llovet JM, Kelley RK, Villanueva A, Singal AG, Pikarsky E, Roayaie S*, et al.* Hepatocellular carcinoma. Nat Rev Dis Primers **2021**;7(1):6 doi 10.1038/s41572-020-00240-3.
77. Sia D, Villanueva A, Friedman SL, Llovet JM. Liver Cancer Cell of Origin, Molecular Class, and Effects on Patient Prognosis. Gastroenterology **2017**;152(4):745-61 doi 10.1053/j.gastro.2016.11.048.

78. Suda T, Liu D. Hydrodynamic gene delivery: its principles and applications. Mol Ther **2007**;15(12):2063-9 doi 10.1038/sj.mt.6300314.
79. Deng J, Wang ES, Jenkins RW, Li S, Dries R, Yates K*, et al.* CDK4/6 Inhibition Augments Antitumor Immunity by Enhancing T-cell Activation. Cancer discovery **2018**;8(2):216-33 doi 10.1158/2159-8290.CD-17-0915.
80. Verma V, Jafarzadeh N, Boi S, Kundu S, Jiang Z, Fan Y*, et al.* MEK inhibition reprograms CD8(+) T lymphocytes into memory stem cells with potent antitumor effects. Nature immunology **2021**;22(1):53-66 doi 10.1038/s41590-020-00818-9.
81. Charni-Natan M, Goldstein I. Protocol for Primary Mouse Hepatocyte Isolation. STAR Protoc **2020**;1(2):100086 doi 10.1016/j.xpro.2020.100086.
82. Adrover JM, Aroca-Crevillen A, Crainiciuc G, Ostos F, Rojas-Vega Y, Rubio-Ponce A*, et al.* Programmed 'disarming' of the neutrophil proteome reduces the magnitude of inflammation. Nature immunology **2020**;21(2):135-44 doi 10.1038/s41590-019-0571-2.
83. Susaki EA, Tainaka K, Perrin D, Yukinaga H, Kuno A, Ueda HR. Advanced CUBIC protocols for whole-brain and whole-body clearing and imaging. Nature protocols **2015**;10(11):1709-27 doi 10.1038/nprot.2015.085.
84. Perna F, Berman SH, Soni RK, Mansilla-Soto J, Eyquem J, Hamieh M*, et al.* Integrating Proteomics and Transcriptomics for Systematic Combinatorial Chimeric Antigen Receptor Therapy of AML. Cancer cell **2017**;32(4):506-19 e5 doi 10.1016/j.ccell.2017.09.004.
85. Bolger AM, Lohse M, Usadel B. Trimmomatic: a flexible trimmer for Illumina sequence data. Bioinformatics **2014**;30(15):2114-20 doi 10.1093/bioinformatics/btu170.
86. Dobin A, Davis CA, Schlesinger F, Drenkow J, Zaleski C, Jha S*, et al.* STAR: ultrafast universal RNA-seq aligner. Bioinformatics **2013**;29(1):15-21 doi 10.1093/bioinformatics/bts635.
87. Anders S, Pyl PT, Huber W. HTSeq--a Python framework to work with high-throughput sequencing data. Bioinformatics **2015**;31(2):166-9 doi 10.1093/bioinformatics/btu638.
88. Love MI, Huber W, Anders S. Moderated estimation of fold change and dispersion for RNA-seq data with DESeq2. Genome Biol **2014**;15(12):550 doi 10.1186/s13059-014-0550-8.
89. Chen EY, Tan CM, Kou Y, Duan Q, Wang Z, Meirelles GV*, et al.* Enrichr: interactive and collaborative HTML5 gene list enrichment analysis tool. BMC Bioinformatics **2013**;14:128 doi 10.1186/1471-2105-14-128.
90. Chiang DY, Villanueva A, Hoshida Y, Peix J, Newell P, Minguez B*, et al.* Focal gains of VEGFA and molecular classification of hepatocellular carcinoma. Cancer research **2008**;68(16):6779-88 doi 10.1158/0008-5472.CAN-08-0742.
91. Hoekstra ME, Bornes L, Dijkgraaf FE, Philips D, Pardieck IN, Toebes M*, et al.* Long-distance modulation of bystander tumor cells by CD8(+) T cell-secreted IFNgamma. Nat Cancer **2020**;1(3):291-301 doi 10.1038/s43018-020-0036-4.

92. Hoshida Y, Nijman SM, Kobayashi M, Chan JA, Brunet JP, Chiang DY*, et al.* Integrative transcriptome analysis reveals common molecular subclasses of human hepatocellular carcinoma. Cancer research **2009**;69(18):7385-92 doi 10.1158/0008-5472.CAN-09-1089.
93. Morris JPt, Yashinskie JJ, Koche R, Chandwani R, Tian S, Chen CC*, et al.* alpha-Ketoglutarate links p53 to cell fate during tumour suppression. Nature **2019**;573(7775):595-9 doi 10.1038/s41586-019-1577-5.
94. Bruix J, Cheng AL, Meinhardt G, Nakajima K, De Sanctis Y, Llovet J. Prognostic factors and predictors of sorafenib benefit in patients with hepatocellular carcinoma: Analysis of two phase III studies. Journal of hepatology **2017**;67(5):999-1008 doi 10.1016/j.jhep.2017.06.026.
95. Amanzada A, Malik IA, Nischwitz M, Sultan S, Naz N, Ramadori G. Myeloperoxidase and elastase are only expressed by neutrophils in normal and in inflamed liver. Histochem Cell Biol **2011**;135(3):305-15 doi 10.1007/s00418-011-0787-1.
96. Simon S, Labarriere N. PD-1 expression on tumor-specific T cells: Friend or foe for immunotherapy? Oncoimmunology **2017**;7(1):e1364828 doi 10.1080/2162402X.2017.1364828.
97. Kaech SM, Hemby S, Kersh E, Ahmed R. Molecular and functional profiling of memory CD8 T cell differentiation. Cell **2002**;111(6):837-51 doi 10.1016/s0092-8674(02)01139-x.
98. Zeisberger SM, Odermatt B, Marty C, Zehnder-Fjallman AH, Ballmer-Hofer K, Schwendener RA. Clodronate-liposome-mediated depletion of tumour-associated macrophages: a new and highly effective antiangiogenic therapy approach. Br J Cancer **2006**;95(3):272-81 doi 10.1038/sj.bjc.6603240.
99. Milanovic M, Fan DNY, Belenki D, Dabritz JHM, Zhao Z, Yu Y*, et al.* Senescence-associated reprogramming promotes cancer stemness. Nature **2018**;553(7686):96-100 doi 10.1038/nature25167.
100. Manguso RT, Pope HW, Zimmer MD, Brown FD, Yates KB, Miller BC*, et al.* In vivo CRISPR screening identifies Ptpn2 as a cancer immunotherapy target. Nature **2017**;547(7664):413-8 doi 10.1038/nature23270.
101. Alexander WS, Starr R, Fenner JE, Scott CL, Handman E, Sprigg NS*, et al.* SOCS1 is a critical inhibitor of interferon gamma signaling and prevents the potentially fatal neonatal actions of this cytokine. Cell **1999**;98(5):597-608 doi 10.1016/s0092-8674(00)80047-1.
102. Song MM, Shuai K. The suppressor of cytokine signaling (SOCS) 1 and SOCS3 but not SOCS2 proteins inhibit interferon-mediated antiviral and antiproliferative activities. J Biol Chem **1998**;273(52):35056-62 doi 10.1074/jbc.273.52.35056.
103. Clapham DE. Calcium signaling. Cell **2007**;131(6):1047-58 doi 10.1016/j.cell.2007.11.028.
104. Kulaeva OI, Draghici S, Tang L, Kraniak JM, Land SJ, Tainsky MA. Epigenetic silencing of multiple interferon pathway genes after cellular immortalization. Oncogene **2003**;22(26):4118-27 doi 10.1038/sj.onc.1206594.

105. Fridman AL, Tang L, Kulaeva OI, Ye B, Li Q, Nahhas F*, et al.* Expression profiling identifies three pathways altered in cellular immortalization: interferon, cell cycle, and cytoskeleton. J Gerontol A Biol Sci Med Sci **2006**;61(9):879-89 doi 10.1093/gerona/61.9.879.
106. Subramaniam PS, Cruz PE, Hobeika AC, Johnson HM. Type I interferon induction of the Cdk-inhibitor p21WAF1 is accompanied by ordered G1 arrest, differentiation and apoptosis of the Daudi B-cell line. Oncogene **1998**;16(14):1885-90 doi 10.1038/sj.onc.1201712.
107. Moiseeva O, Mallette FA, Mukhopadhyay UK, Moores A, Ferbeyre G. DNA damage signaling and p53-dependent senescence after prolonged beta-interferon stimulation. Mol Biol Cell **2006**;17(4):1583-92 doi 10.1091/mbc.e05-09-0858.
108. Takaoka A, Hayakawa S, Yanai H, Stoiber D, Negishi H, Kikuchi H*, et al.* Integration of interferon-alpha/beta signalling to p53 responses in tumour suppression and antiviral defence. Nature **2003**;424(6948):516-23 doi 10.1038/nature01850.
109. Platanias LC. Mechanisms of type-I- and type-II-interferon-mediated signalling. Nature reviews Immunology **2005**;5(5):375-86 doi 10.1038/nri1604.
110. Ayers M, Lunceford J, Nebozhyn M, Murphy E, Loboda A, Kaufman DR*, et al.* IFN-gamma-related mRNA profile predicts clinical response to PD-1 blockade. The Journal of clinical investigation **2017**;127(8):2930-40 doi 10.1172/JCI91190.
111. Gao J, Shi LZ, Zhao H, Chen J, Xiong L, He Q*, et al.* Loss of IFN-gamma Pathway Genes in Tumor Cells as a Mechanism of Resistance to Anti-CTLA-4 Therapy. Cell **2016**;167(2):397-404 e9 doi 10.1016/j.cell.2016.08.069.
112. Benci JL, Johnson LR, Choa R, Xu Y, Qiu J, Zhou Z*, et al.* Opposing Functions of Interferon Coordinate Adaptive and Innate Immune Responses to Cancer Immune Checkpoint Blockade. Cell **2019**;178(4):933-48 e14 doi 10.1016/j.cell.2019.07.019.
113. Benci JL, Xu B, Qiu Y, Wu TJ, Dada H, Twyman-Saint Victor C*, et al.* Tumor Interferon Signaling Regulates a Multigenic Resistance Program to Immune Checkpoint Blockade. Cell **2016**;167(6):1540-54 e12 doi 10.1016/j.cell.2016.11.022.
114. De Simone G, Andreata F, Bleriot C, Fumagalli V, Laura C, Garcia-Manteiga JM*, et al.* Identification of a Kupffer cell subset capable of reverting the T cell dysfunction induced by hepatocellular priming. Immunity **2021**;54(9):2089-100 e8 doi 10.1016/j.immuni.2021.05.005.